HIGH GRADE METAMORPHIC REACTIONS AND PARTIAL MELTING IN PELITIC SCHIST, QUABBIN RESERVOIR AREA, MASSACHUSETTS

BY ROBERT J. TRACY

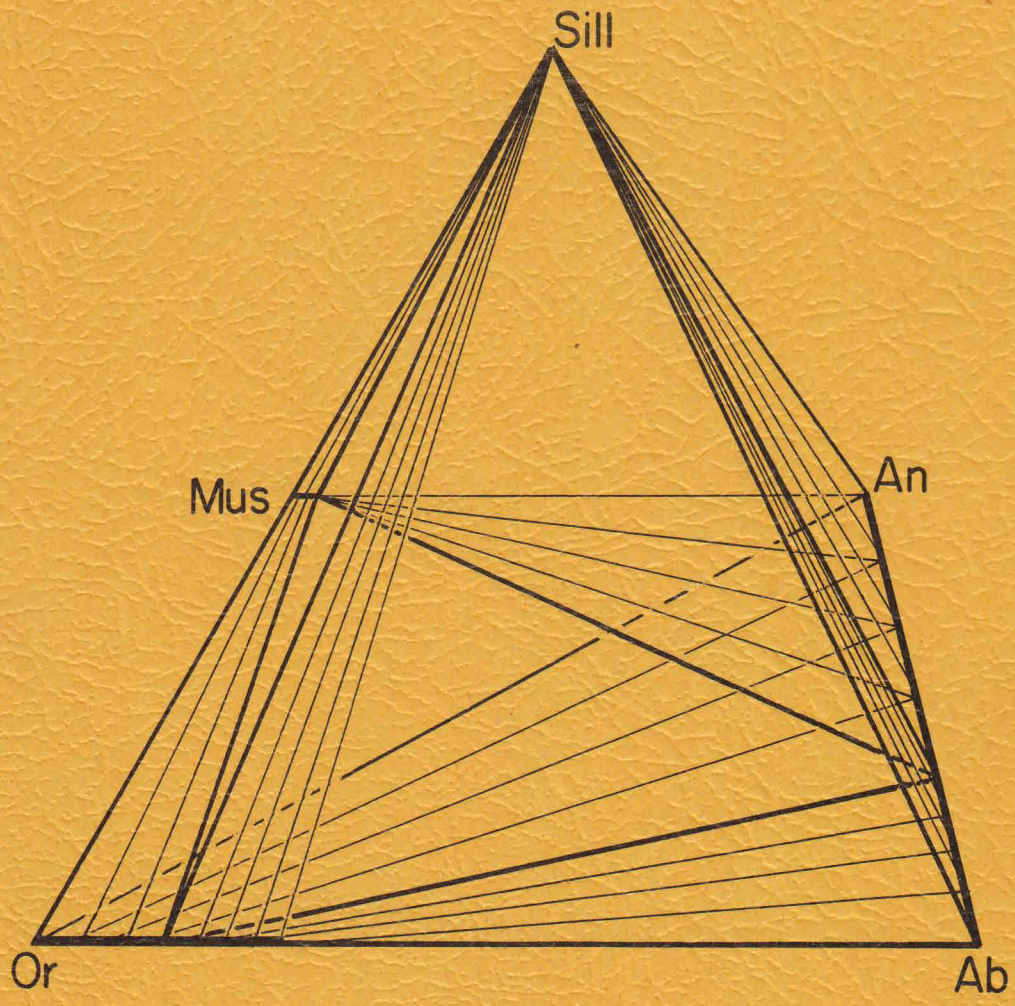

CONTRIBUTION NO. 20
GEOLOGY DEPARTMENT
UNIVERSITY OF MASSACHUSETTS
AMHERST, MASSACHUSETTS

HIGH GRADE METAMORPHIC REACTIONS AND PARTIAL MELTING IN PELITIC SCHIST, QUABBIN RESERVOIR AREA, MASSACHUSETTS

by

Robert J. Tracy

Contribution No. 20

Department of Geology
University of Massachusetts
Amherst, Massachusetts

April, 1975

TABLE OF CONTENTS

FIGURES

TABLES

ABSTRACT

Pelitic schists in a narrow belt of Middle Ordovician Partridge Formation near Quabbin Reservoir, west-central Massachusetts, display the transition from sillimanite-muscovite to sillimanite-orthoclase assemblages, which represents the sillimanite-orthoclase "isograd" as mapped in other areas. Sillimanite-muscovite-orthoclase assemblages crop out over a 10 km zone in which migmatites are common. Partial melting and muscovite dehydration reactions are interpreted to have been nearly simultaneous on the basis of structure, field observations and petrography.

Of the many samples of sulfidic and graphitic schist collected and examined, twenty were selected for electron microprobe analysis of muscovite, biotite, garnet, plagioclase, orthoclase and ilmenite. Muscovites contain approximately 6 mol. percent paragonite, about 1 wt.% FeO and MgO, and up to 1.7 wt.% TiO_2. Biotites have up to 4 wt.% TiO_2, Fe/Fe+Mg of about 0.5, and 10 to 15 percent of octahedral sites filled by Al. Muscovites have 1 or 2 percent trioctahedral character while biotites are 5 to 10 percent dioctahedral. Garnet of variable composition averages $Alm_{71}\ Py_{15}\ Sp_{10}\ Gr_4$ with rims enriched in Fe and Mn. Plagioclase ranges from An_{17} to An_{40} and is unzoned. Orthoclases range from Or_{83} to Or_{90} and contain up to 1.1 wt.% BaO. X-ray powder diffraction data on the structural state of orthoclase indicates an average Δbc of .77. Ilmenite is rare in schists and appears to be nearly pure $FeTiO_3$.

Systematic compositional behavior of minerals, particularly of

plagioclase in the assemblage qz-mus-or-sill-plag, strongly suggests regional rather than local variation of intensive variables P, T and μH_2O. The An content of plagioclase in this assemblage, ideally a function of metamorphic grade, has been mapped and contoured for the Quabbin Reservoir field area. These contours are contours of metamorphic grade and are a very sensitive indicator of metamorphic gradient. The contours trend NNE-SSW and suggest an ESE direction of temperature increase. Based on published experiments, they indicate a temperature range for the mus-or transition zone at Quabbin of about 10^{o} C. The nearby transition from kyanite to sillimanite suggests pressures in excess of 5.5 Kbar. Near coincidence of melting and dehydration reactions at this pressure allows estimation of metamorphic temperatures of 650 - 700^{o} C, based on published experimental studies. Fe/Mg fractionation between garnet and biotite independently indicates temperatures in the same range, while also suggesting minor retrograde compositional readjustment, particularly in garnet rims. Structural features demonstrate a transition from plastic to more brittle behavior which is interpreted as an effect of the rocks "drying out". This dehydration can be ascribed to strong fractionation of H_2O from the fluid phase into newly-formed melts and possibly to establishment of a fissure-type equilibrium ($P_f < P_t$) if the melt network connects to higher levels in the crust.

INTRODUCTION

In many regionally metamorphosed terranes, an isograd has been recognized marking the disappearance of muscovite or the first appearance of alkali feldspar in aluminous rocks. It was noted by Heald (1950) in southern New Hampshire, but the first detailed petrologic studies of this isograd were those of Evans and Guidotti (1966) in Maine and Lundgren (1966) in southeastern Connecticut. Robinson (1967b) has described the isograd in west-central Massachusetts, in the vicinity of Quabbin Reservoir, where it forms the transition between the lower grade rocks of the Orange area (Robinson, 1963; Hall, 1970) and the sillimanite-orthoclase-cordierite terrane of central Massachusetts (Barker, 1962; Hess, 1969). The present study was undertaken to provide more detailed information on the chemistry of the transition from the sillimanite-muscovite to the sillimanite-orthoclase zone in west-central Massachusetts. In addition, structural analysis of the area (Robinson, 1967b) makes it feasible to correlate the timing of metamorphic and structural events. The Quabbin Reservoir area provides an excellent locale for doing detailed structural and petrologic studies, because of the abundance of large fresh, wave-washed outcrops along the shores of the reservoir.

The area lies within the Bronson Hill anticlinorium in west-central Massachusetts. The geology, discussed by Thompson, Robinson, Clifford and Trask (1968), consists of gneiss domes mantled by steeply-dipping Paleozoic metamorphic rocks. The dome gneisses are of uncertain age but are at least in part pre-middle Ordovician (Naylor, Boone, Boudette, Ashenden and Robinson, 1973). Mantling rocks include the Middle

Ordovician Ammonoosuc Volcanics and Partridge Formation, the Silurian Clough and Fitch Formations and the Devonian Littleton and Erving Formations. There is a steep metamorphic gradient across the region with grade increasing from west to east (Fig. 1).

The specific area studied is a syncline of Partridge Formation completely surrounded by Monson Gneiss. The syncline was mapped by Emerson (1898) and named by him the East Greenwich-Enfield Syncline. The north end has been mapped by Robinson (1967b and unpublished data), in part assisted by the author. The south end was mapped by Peper (1967). Rock types which crop out in the belt include pelitic schist, felsic gneiss, amphibolite and calc-silicate granulite. Figure 2 is a detailed map of the Quabbin Reservoir area showing the distribution of assemblages found in pelitic schists. The northern end of the syncline is characterized by the assemblage sillimanite-muscovite, the middle part by sillimanite-muscovite-orthoclase and the southern end by sillimanite-orthoclase. The considerable width of the central zone (about 5 km) reflects the non-univariant behavior of the muscovite dehydration reaction, as noted by other investigators (Evans and Guidotti, 1966; Lundgren, 1966).

Field work for this project was done during the period 1971-1974. Most of the field work involved sample collection, although some mapping was done (with Robinson). Samples were studied using standard petrographic techniques, and selected specimens were analyzed using the electron microprobe and X-ray diffraction. A considerable part of the chemical data reported was obtained to document the compositional variables involved in the muscovite dehydration reaction. In addition, many outcrops contain migmatites which are interpreted as the result of

partial melting of schists. An attempt is made to relate the partial melting and muscovite dehydration and to assess their dependence and potential effects on the physical conditions during metamorphism.

Acknowledgments

This paper was submitted in partial fulfillment of the requirements for the Ph.D. at the University of Massachusetts, Amherst, in April, 1975. The writer expresses considerable appreciation to Peter Robinson for his great help in designing and executing this project, and to S.A. Morse, S.E. Haggerty and L.M. Hall for advice and guidance. Thanks are due to Alan B. Thompson of Harvard University for numerous discussions and for his calibration of temperature dependence of Fe-Mg fractionation in garnet-biotite pairs. Patricia Tracy is thanked for help in the typing and preparation of this manuscript. Field work and microprobe analyses were supported by NSF Grant GA-33857A1 (to Robinson) GA-31989 (to Robinson and H.W. Jaffe), which also provided a research assistantship for the author. A sigma Xi Grant-in-Aid supported purchase of thin sections.

Fig. 1. Generalized geologic map of the central part of the Bronson Hill anticlinorium, west-central Massachusetts, showing the Quabbin Reservoir, Orange and Ware areas.

Rock Types:


Triassic-Jurassic sedimentary rocks.


Syntectonic intrusions.


Ordovician and Devonian pelitic schist.


Dome gneisses and Ammonoosuc Volcanics.

Metamorphic Zones with Characteristic Assemblages in Pelitic Schist.

C-G. Chlorite, biotite and garnet zones.

I. Kyanite-muscovite-staurolite-garnet-biotite.

II. Sillimanite-muscovite-staurolite-garnet-biotite.

III. Sillimanite-muscovite-garnet-biotite.

IV. Sillimanite-muscovite-orthoclase-garnet-biotite.

V. Sillimanite-orthoclase-garnet-biotite.

VI. Sillimanite-orthoclase-cordierite-garnet-biotite.

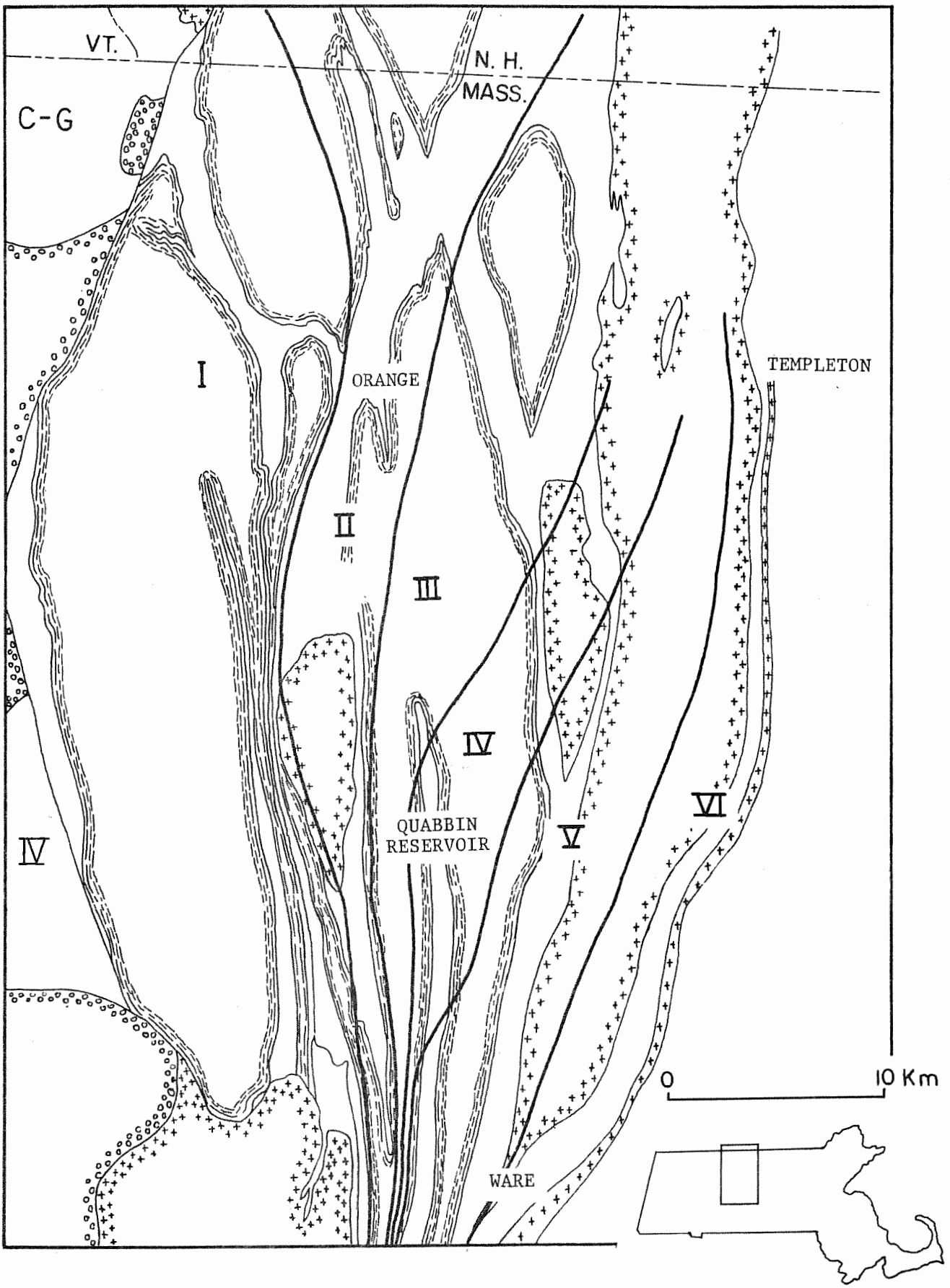
VT.
N. H.
MASS.
C-G
I
ORANGE
II
III
IV
QUABBIN
RESERVOIR
V
VI
TEMPLETON
IV
WARE
0
10 Km

Fig. 2. Geologic map of the Quabbin Reservoir area, showing distribution of assemblages in pelitic schists.

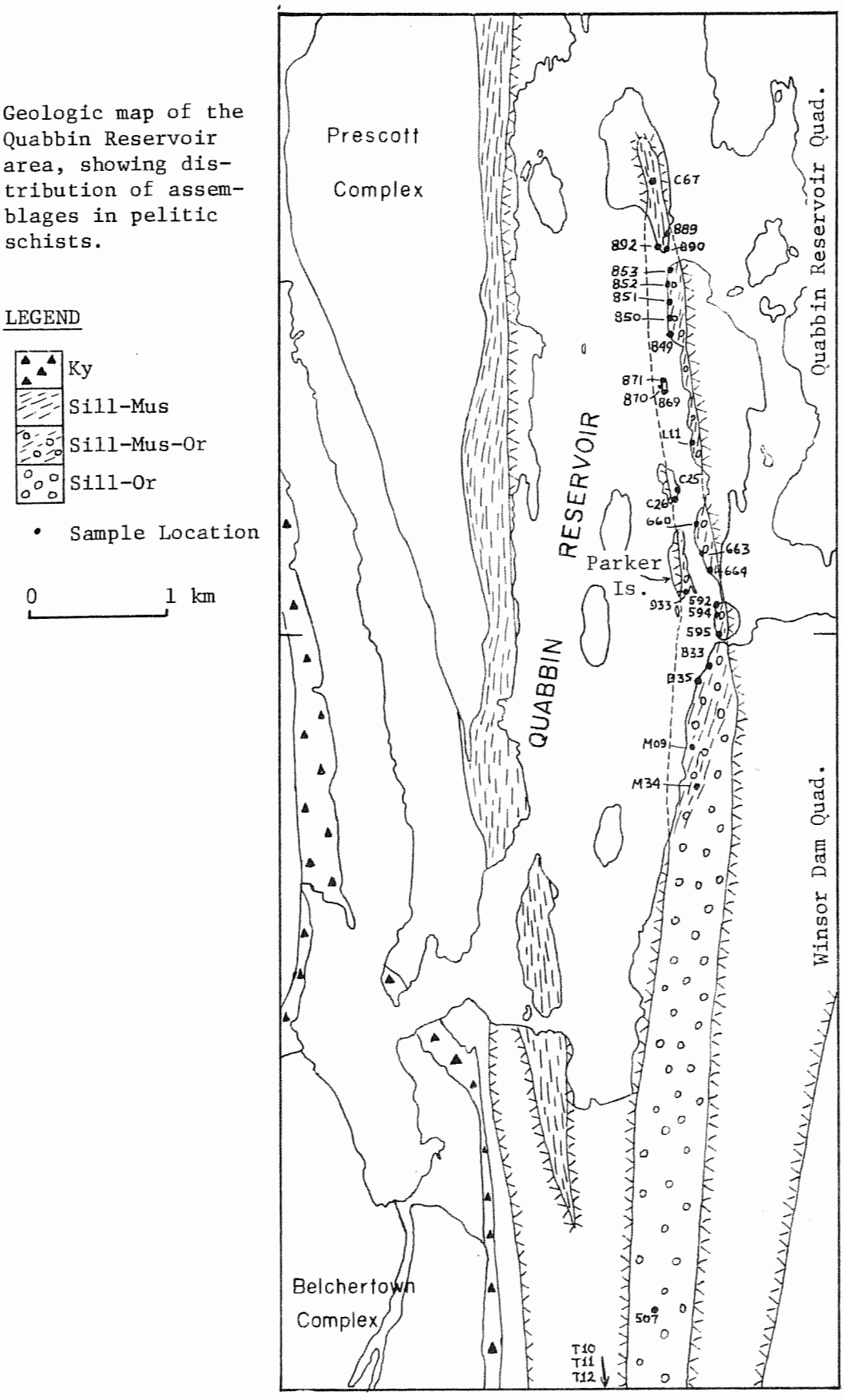

STRUCTURAL GEOLOGY

The structural geology of this part of the Bronson Hill anticlinorium has been studied and reported by Robinson and co-workers (Robinson, 1963, 1967a, 1967b; Thompson, Robinson, Clifford and Trask, 1968). The regional structural history includes the development of at least three levels of large-scale nappes with east to west transport; an episode of west to east, or southwest to northeast, overfolding associated with early stages in the rise of gneiss domes; and final emplacement of gneiss domes with associated north-south trending isoclinal anticlines and synclines. The earlier parts of the sequence are undoubtedly Acadian (Early to Middle Devonian) in age, and the whole sequence is probably Devonian. The regional structural features, worked out on a quadrangle or regional scale, are represented by smaller structures which can be recognized in individual outcrops and whose time relations can be established. In outcrops in the Quabbin Reservoir area (Robinson, 1967b) three phases of folding, an episode of shearing and cataclasis and two igneous phases have been recognized. The tentative correlation between these local features and regional structural features, as suggested by Robinson (1967a, b), is given in Table 1.

The relative timing of structural features seen in outcrops is fairly clear. The early first folds are only recognized in rare exposures of hinges which occur within second-generation folds. Foliation appears to crosscut compositional layering in these hinges, suggesting that the regional foliation, which is generally parallel to compositional layering, formed as axial plane foliation in the early folding.

TABLE 1. CORRELATION AND SEQUENCE OF STRUCTURAL FEATURES.

Regional Structural Features	Minor Structural and Igneous Features (Outcrop Scale at Parker Island)
Cornish, Skitchewaug and Fall Mountain Nappes -- east to west overfolding	First isoclinal folding -- Development of foliation
	Fractional fusion -- formation and solidification of migmatite layers parallel to foliation
Southwest to northeast overfolding and northeastward flowage of main body of Monson Gneiss	Second isoclinal folding (axes steeply plunging north to vertical)
	Intrusion of pegmatite dikes along second fold axial surfaces
	Shearing and cataclasis in thin zones crossing all previous features
Final rise and emplacement of gneiss domes with associated N - S isoclinal folds	Third folding (open to isoclinal) with axes gently plunging north or south. Development of moderate to strong mineral lineation in most rocks, roughly parallel to third fold axes. Recrystallization of cataclastic rocks.

Second-generation folds are quite common and are almost always isoclinal. In the reservoir area, they display steep north-plunging to vertical axes. In outcrops containing migmatitic rocks, the leucocratic and restite layers are involved in the second folds and the leucocratic layers appear to have been competent during the folding (Fig. 3). These rocks are interpreted as internally derived partial melts and their structure requires that they were largely crystalline and competent by the time of the second folding (Robinson, 1967b). The axial planes of some second folds are cut by pegmatite dikes which appear to be genetically unrelated to the migmatites. These pegmatites and all other rocks are cut by cataclastic shear zones which consist of thoroughly recrystallized mylonites and which show displacements in outcrop of up to 28 feet.

The third generation of folding is much more open in character and third fold axes plunge gently either north or south. All previous structural features can be found to have been folded by this generation of folding. A prominent sillimanite lineation in highly aluminous schists is aligned parallel to third fold axes; other rock types show a similarly aligned mineral lineation.

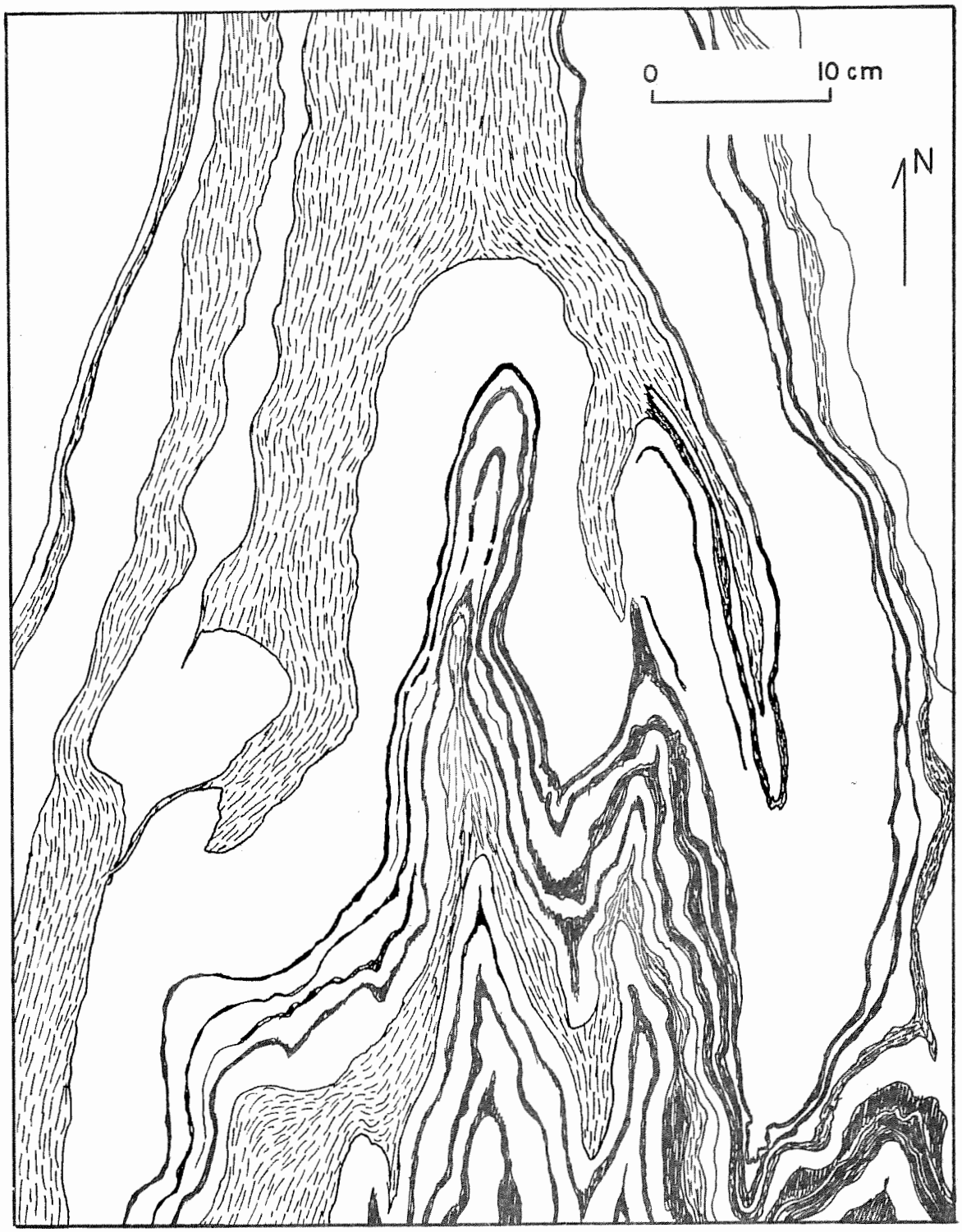

Fig. 3. Sketch of a horizontal outcrop surface in Partridge Formation, Parker Island, showing interlayered schist and leucocratic layers in typical migmatite. The prominent folds are phase 2 folds; note that the leucocratic layers appear to have been more competent than the schist during folding.

PETROGRAPHY

This study was limited to examination of assemblages in aluminous schists and in interlayered migmatitic rocks. Nearly all the schists examined contained both iron sulfide (pyrrhotite ± pyrite) and graphite, typical of the rusty-weathering Partridge Formation. In the Quabbin Reservoir area, three main assemblage types were recognized. In addition to the universal phases quartz, plagioclase, biotite and sillimanite, schists contained either muscovite alone, muscovite plus potassic feldspar, or potassic feldspar alone. Table 2 lists the assemblages found in the pelitic rocks and in several gneisses. Petrography was done on standard petrographic thin sections; determination of opaque minerals was made in polished sections by reflected-light microscopy. Samples marked with an asterisk in Table 2 were selected for probe analysis on the basis of freshness, geographic location and assemblage. Many of the samples chosen for probe analysis were point-counted (500 counts per sample) to obtain approximate modal compositions. These modes were used in conjunction with the actual mineral compositions determined by microprobe to calculate bulk compositions. Bulk compositions are useful both for plotting purposes and for comparison with published analyses of shales and schists. Table 3 tabulates modes and calculated bulk compositions for Quabbin area rocks.

An important feature of these schists is the apparent attainment of textural equilibrium, which is a necessary adjunct of chemical equilibrium. The rocks are strongly foliated, the folia consisting of aligned plates of biotite, muscovite, and graphite, needles of sillimanite and interspersed grains of other phases. Within very small areas,

TABLE 2. MINERAL ASSEMBLAGES IN PELITIC SCHISTS AND OTHER ROCKS FROM THE PARTRIDGE FORMATION, GREENWICH SYNCLINE, QUABBIN RESERVOIR AREA.

	Qz	Plag	Mus	Bio	Sill	Ksp	Gar	Graph	Ilm	Po	Py
892U*	x	x	x	x	x		x	x		x	
C67*	x	x	x	x	x		x	x	x	x	
890*	x	x	x	x	x		x	x	x	x	
853A*	x	x	x	x	x	x		x		x	
849A*	x	x	x	x	x	x		x		x	x
849C	x	x	x	x	x			x	x	x	
852C	x	x	x	x	x	x		x	x	x	
869*	x	x	x	x	x	x	x	x	x	x	
871*	x	x	x	x	x	x	x	x		x	
C25	x	x	x	x	x	x	x	x		x	
C26*	x	x	x	x	x	x	x	x		x	
C26A	x	x	x	x	x	x	x	x			
663A	x	x		x	x	x		x			
L11Y*	x	x		x	x	x	x	x			
933A*	x	x		x	x	x	x	x		x	
933B*	x	x		x	x	x	x	x		x	
592B*	x	x	x	x	x	x		x		x	
594B*	x	x	x	x	x	x		x		x	
594Z	x	x	x	x	x	x		x		x	
595A	x	x	x	x	x	x		x			
595B	x	x	x	x	x	x	x	x		x	
595C*	x	x	x	x	x	x	x	x	x	x	
B35*	x	x	x	x	x	x		x	x	x	x
M09*	x	x		x	x	x	x	x			
M34*	x	x	x	x	x	x	x	x	x	x	
507B*	x	x		x	x	x	x	x	x	x	
T10B*	x	x		x	x	x	x	x		x	
T11F	x	x		x	x	x	x	x		x	
T12A	x	x		x	x	x	x	x	x	x	
870B[1]	x	x		x	x	x					
851Z[1]	x	x			x	x					
L11X[1]	x	x			x	x					
507[2]	x	x		x		x	x				
T11E[2]	x	x		x		x	x				
T12B[2]	x	x		x		x	x				

*Designates samples chosen for probe analysis.

[1]Concordant fine-grained leucocratic layers, apparently not intrusive, possibly derived from pyroclastic material.

[2]Gray garnet-gneisses, probably derived from felsic volcanics.

all phases are in contact with each other. The only phases of variable composition within single specimens are garnet and plagioclase, although plagioclase zoning is uncommon. Garnet is always at least slightly zoned, and it can be assumed that only the rim composition is in chemical equilibrium with the rest of the rock. It can be difficult to decide whether this equilibrium is prograde or retrograde; this problem will be discussed in detail in a later section.

Medium grain size is typical in the schists, with the exception of porphyroblasts of garnet or potassic feldspar. Muscovite (when present) and biotite are strongly aligned in a planar fabric which is a pervasive regional foliation. Sillimanite occurs in several forms--as fibrolitic mats, as needles and as larger prismatic crystals, all of which lie within the plane of foliation. Fibrolite, which is apparently a fine-grained intergrowth of sillimanite and quartz (and possibly also biotite) (Bell and Nord, 1974), is more common in the lower-grade end of the area and rather rare in the higher-grade end. It is usual for fibrolite and coarser sillimanite to coexist, however. The disappearance of fibrolite at higher grade is strongly suggestive of its presence as a metastable texture. With its considerably larger surface free energy, it is almost certainly metastable with respect to a coarser quartz-sillimanite intergrowth. Other authors have proposed numerous explanations for the existence of both forms of sillimanite, including order-disorder relations, metastable overstepping of equilibrium phase boundaries and various reaction mechanisms (Zen, 1969; Cameron and Ashworth, 1972; Carmichael, 1969). Petrographic and petrologic evidence from Quabbin suggests that the most likely mechanism for producing fibrolite is as a reaction product in the lower part of the sillimanite zone from a reaction producing both sillimanite and quartz. A possible reaction is:

TABLE 3. POINT-COUNTED MODES AND CALCULATED BULK COMPOSITIONS.

	C67	890	892U	853A	849A	869	871	C26	933A
Qz	27.6	34.6	34.0	35.8	28.8	26.9	38.9	27.9	31.6
Plag	15.2	14.6	17.6	8.0	8.0	10.2	7.4	24.7	9.6
Biot	37.2	33.3	35.8	28.2	25.0	31.6	29.3	28.7	31.8
Musc	4.0	2.5	3.4	5.8	13.8	4.9	8.8	2.3	--
Sill	13.4	13.8	7.0	15.0	11.6	17.6	5.6	3.0	13.6
Kspar	--	--	--	3.2	5.0	6.3	8.8	8.5	5.0
Gar	0.2	0.2	0.2	--	--	0.9	0.2	0.8	6.6
Graph	1.9	1.2	1.0	3.0	6.0	1.0	0.4	3.0	1.5
Sulf	0.5	1.0	1.0	1.0	1.8	0.6	0.6	1.1	0.3
	100.0	100.0	100.0	100.0	100.0	100.0	100.0	100.0	100.0
SiO_2	55.41	60.19	59.87	59.61	55.09	55.46	63.60	60.04	57.74
TiO_2	1.21	1.16	1.16	1.09	.91	1.07	1.17	.82	1.12
Al_2O_3	21.99	20.70	17.71	20.37	21.03	24.62	17.10	16.52	20.31
Cr_2O_3	0	.05	.05	0	0	.03	.04	.04	.02
FeO	8.26	6.78	8.29	5.80	5.70	6.89	6.75	6.72	8.97
MnO	.13	.10	.07	.10	.10	.14	.07	.12	.29
MgO	3.33	3.48	3.72	3.24	3.45	3.11	2.83	3.02	3.38
CaO	.53	.79	.84	.48	.46	.44	.45	1.25	.51
BaO	.15	.15	.14	.12	.15	.12	.22	.11	.15
Na_2O	1.37	1.12	1.43	.72	.75	1.00	.69	2.34	.91
K_2O	3.86	3.55	3.87	3.80	4.73	4.23	5.17	4.40	3.77
H_2O	1.94	1.69	1.85	1.60	1.81	1.61	1.81	1.51	1.49
C	1.60	1.00	.80	2.40	4.80	.80	.30	2.40	1.20
S	.23	.10	.64	.64	1.10	.38	.50	.90	.19
Total	100.01	100.86	100.44	99.97	100.08	99.90	100.70	100.16	100.05
fe*	.581	.522	.556	.503	.479	.555	.573	.556	.598
na**	.349	.321	.359	.224	.193	.262	.167	.447	.273

* fe = Fe/Fe + Mg (Atomic ratios)

** na = Na/Na + K

	595C	B35	M34	507B	A[1]	B[2]	C[3]	
Qz	28.0	27.8	33.8	28.9		34.4	40.5	
Plag	25.5	13.4	14.2	11.6		0.2	5.2	
Biot	31.1	27.8	28.2	37.9		20.8	25.1	
Musc	1.6	3.2	2.2	--		28.0	--	
Sill	4.8	8.6	17.0	8.2		10.9	11.5	
Kspar	4.4	12.8	3.6	7.6		--	3.0	
Gar	Tr	--	0.2	1.7		3.3	7.0	
Graph	3.6	6.0	0.6	3.3		1.9	0.5	Opaques
Sulf	1.0	0.4	0.2	0.8		--	2.0	Cordierite
	100.0	100.0	100.0	100.0		99.5	94.8	
SiO_2	57.81	57.99	60.24	57.00	59.01	62.51	62.04	
TiO_2	1.20	1.11	1.21	1.51	1.00	1.06	1.11	
Al_2O_3	17.93	18.67	22.45	17.69	18.93	18.91	18.29	
Cr_2O_3	.03	0	.01	0	-	-	-	
FeO	6.69	5.63	5.80	8.83	7.17	6.91	8.75	
MnO	.09	.06	.06	.05	.06	.10	.22	
MgO	3.61	3.03	2.46	3.67	3.08	1.66	3.23	
CaO	1.73	.88	.85	.42	.24	.33	.45	
BaO	.04	.14	.12	.16	.05	.07	.01	
Na_2O	2.01	1.16	1.19	1.16	.77	1.13	.77	
K_2O	4.12	4.65	3.53	4.72	4.42	3.94	3.54	
H_2O	1.57	1.48	1.44	1.80	4.26	2.58	.99	
C	2.90	4.80	.50	2.80	.31	.33	-	
S	.65	.27	.12	.38	.02	.03	.03	
Total	100.38	99.87	99.98	100.19	99.32	99.56	99.43	
fe*	.508	.510	.570	.575	.568	.701	.604	
na**	.421	.279	.288	.270	.210	.300	.250	

[1]Littleton "shale", Lyman Twp., N.H. (Shaw, 1956, Sample #L-9) (Wet chemical analysis)

[2]Littleton garnet-sillimanite gneiss, Rumney, N.H. (Shaw, sample #L-29) (Wet chemical analysis)

[3]Littleton orthoclase-sillimanite gneiss, Marlow, N.H. (Heald, 1950) (Wet chemical analysis, L.C. Peck, Analyst)

Gar + Mus = Sill + Qz + Bio.

Quartz and plagioclase grains occur interspersed with the micaceous folia. Quartz commonly shows fracturing and undulatory extinction induced by strain. While albite twinning is common in plagioclase, it is not universal. There is no apparent correlation between plagioclase composition and extent of twinning. Potassic feldspar occurs both as small groundmass grains and as larger porphyroblasts. Neither groundmass nor porphyroblastic potassic feldspar has been found to show exsolution textures, though some is quite sodic (see detailed discussion in next section). Garnet occurs in many samples as porphyroblasts, commonly rounded but only rarely euhedral. Inclusions in garnet are quite uncommon and are almost exclusively quartz. Modal garnet increases in the higher-grade part of the area, probably because of the following reaction:

Bio + Sill + Qz = Gar + Ksp + V.

This reaction is further suggested by patchy Ksp rims which occur around garnets in the sillimanite-Kspar zone.

The schists studied are quite reduced since all contain graphite and pyrrhotite. Graphite is interleaved with muscovite and biotite. Pyrrhotite occurs both as rounded and tabular grains and is commonly intergrown with graphite and biotite. The other opaque phase is ilmenite, which is not abundant (Table 2) and is very fine-grained when it does occur. This is in contrast to lower and higher-grade schists from central Massachusetts (Hall, 1970; Field, 1975), in which ilmenite is

common. It appears that there may be reactions involving silicates, ilmenite and possibly also pyrrhotite which are continuously changing the modal proportions of the minor phases. Low oxygen fugacity is also suggested by the fact that no magnetite has been identified in any of the schists.

Migmatites consist of interlayered coarse leucocratic rocks and mafic and aluminous schist lenses. The leucocratic layers contain quartz, alkali feldspar and plagioclase in amounts approximating the melt composition in a Ca-bearing granite system, approximately 30% quartz, 40% plagioclase (oligoclase) and 20% orthoclase with minor amounts of biotite, garnet and sillimanite. The dark restite layers commonly contain minor quartz and plagioclase with concentrated amounts of biotite, garnet and sillimanite, although some are completely depleted in quartzo-feldspathic constituents. Typical appearance of migmatitic rocks is illustrated in Figure 4 showing a sawed slab from Parker Island.

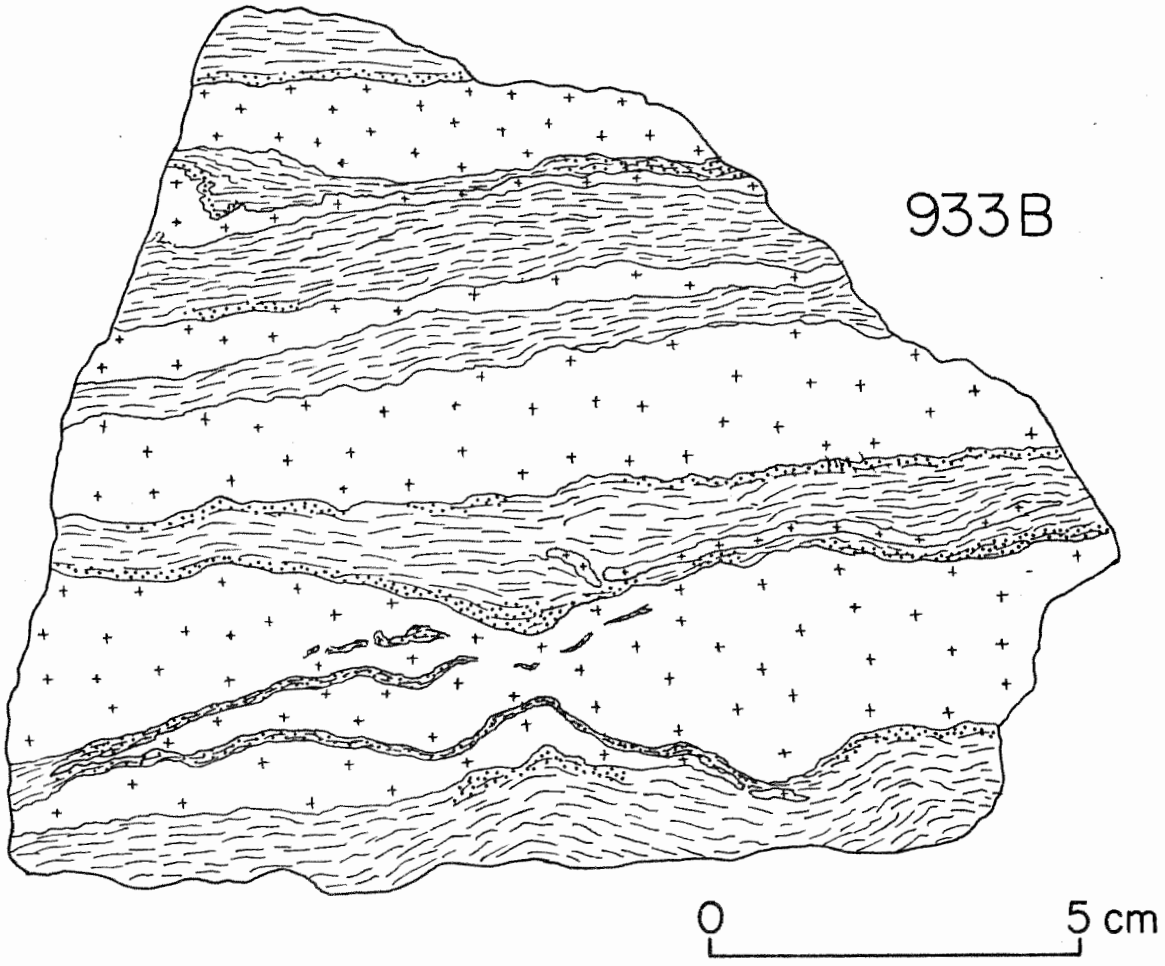

Fig. 4. Sketch of a sawed slab of migmatite from Parker Island, Quabbin Reservoir. The cross pattern indicates leucocratic layers composed of quartz, plagioclase and orthoclase. The line pattern represents schist which is enriched in garnet, biotite and sillimanite, especially in the stippled areas adjacent to leucocratic layers.

SYSTEMATIC MINERALOGY

The following section is a detailed discussion of the chemistry of individual minerals. Analyses were made on polished thin sections and grain mounts using a MAC Model 400 electron microprobe at the Department of Earth and Planetary Sciences, Massachusetts Institute of Technology. Operating conditions were 15Kv accelerating potential and .03 microamps beam current. Spot size was in the range of 2 - 5 microns. The silicate and oxide standards used are listed in Table 4. Mineral analyses were corrected using the method of Bence and Albee (1968) and the correction factors of Albee and Ray (1970).

TABLE 4. MICROPROBE STANDARDS

Oxide	Standard
SiO_2	JD 35 (jadeitic diopside)
	Orthoclase
TiO_2	Ilmenite
Al_2O_3	JD 35
	An 60 (plagioclase)
Cr_2O_3	Cr CaTs
FeO	Ilmenite
MnO	Ilmenite
MgO	JD 35
	P-140 (olivine)
CaO	JD 35
BaO	Barium glass
Na_2O	JD 35
K_2O	Orthoclase

Muscovite

Muscovite occurs in a majority of the rocks examined in this study, and in rocks where it is absent, it has been replaced in the assemblage by alkali feldspar. It constitutes about 1 to 15 modal percent of the schists in which it is found. It is commonly fine-grained and intimately intergrown with biotite, and the parallel alignment of muscovite and biotite defines the foliation in the rocks.

Discrimination between primary and secondary white mica is important for proper determination of mineral assemblages and phase chemistry. The following petrographic criteria were developed to identify rocks containing retrograde white mica:

1) Primary muscovite is predominantly fine-grained and shows strain features in thin section, while secondary muscovite commonly occurs in large unstrained flakes which crosscut the foliation.
2) Ragged edges are typical of primary muscovite, in contrast to the fresh, clean edges of secondary muscovite.
3) Much of the primary muscovite contains inclusions of sillimanite as swarms of minute crystals not found in secondary muscovite.
4) Hydrous alteration of feldspar appears to be a universal adjunct to production of secondary muscovite by rehydration.

One goal of this study is chemical characterization of muscovites in rocks which were undergoing the muscovite dehydration reaction. This includes compositional variations within the rocks of this restricted area, as well as contrasts with muscovite compositions in lower-grade rocks from western Massachusetts and in high-grade schists from other areas. Toward this end, electron microprobe analyses were made of muscovites from 12 carefully selected samples and are reported in

Table 5. Many analyses given are averages of probe analyses for the sample, as noted in the table. Table 6 illustrates this averaging procedure for sample 853A, giving individual analyses, average analysis and standard deviations. Included in Table 5 for comparison are analyses of kyanite and sillimanite zone muscovites from the Orange, Massachusetts, area and muscovite from sillimanite-muscovite-orthoclase schist of western Maine, as reported by Evans and Guidotti (1966).

Four principal dioctahedral mica end members which can be used to categorize natural muscovite are:

K-muscovite: $KAl_2Si_3AlO_{10}(OH)_2$

Paragonite: $NaAl_2Si_3AlO_{10}(OH)_2$

Margarite: $CaAl_2Si_2Al_2O_{10}(OH)_2$

Celadonite: $(K,Na)Al(Fe,Mg)Si_4O_{10}(OH)_2$.

These standard end members are derived by a combination of simple and coupled substitutions which preserve both charge balance and exactly two octahedral cations. Simple replacement substitutions include $Na^{+1} \rightarrow K^{+1}$, $Fe^{+3} \rightarrow Al^{+3}$, and $Cr^{+3} \rightarrow Al^{+3}$. Coupled substitutions involve simultaneous replacement of more than one cation, such as the margarite substitution:

$$Ca^{+2} + {}^{IV}Al^{+3} \rightarrow K^{+1} + {}^{IV}Si^{+4}.$$

Muscovites of this study show a variety of such compositional variations. There is appreciable replacement of K by Na in the interlayer site, some Ba, but virtually no Ca, which is typical of high-grade muscovite (Guidotti, 1973). Since Ba is divalent, coupled substitutions are needed to explain its presence. Three alternative schemes are:

$$Ba^{+2} + \square \rightarrow 2\ K^{+1}$$

TABLE 5. MICROPROBE ANALYSES OF MUSCOVITES.

	C67	890	892U	853A	849A	869	C26	871
SiO_2	47.68	46.21	46.06	46.73	47.46	47.14	46.34	45.84
TiO_2	.89	.95	.97	1.46	1.67	1.10	.91	.98
Al_2O_3	34.93	35.44	36.00	35.02	34.08	35.16	36.55	36.18
Cr_2O_3	.03	.11	.08	.01	.08	.09	.02	.11
FeO	1.27	1.20	1.28	1.02	1.01	1.21	1.27	1.26
MnO	.00	.04	.02	.00	.05	.06	.06	.01
MgO	.65	.84	.74	.86	1.04	.67	.69	.71
CaO	.00	.00	.00	.00	.03	.04	.00	.00
BaO	.25	.20	.23	.23	.34	.09	.09	.30
Na_2O	.37	.42	.33	.33	.34	.35	.33	.32
K_2O	9.88	10.31	10.26	10.01	10.12	10.00	10.31	10.66
Total	95.94	95.71	95.97	95.67	96.22	95.91	96.57	96.37
N*	1:3	1:3	5	9	9	9	4	1:3
Formulas based on 11 oxygens								
Si	3.135	3.062	3.043	3.087	3.123	3.104	3.039	3.026
Al	.865	.938	.957	.913	.877	.896	.961	.974
	4.000	4.000	4.000	4.000	4.000	4.000	4.000	4.000
Al	1.842	1.831	1.847	1.814	1.767	1.834	1.863	1.842
Ti	.043	.047	.048	.073	.083	.054	.045	.049
Cr	.000	.006	.004	.001	.004	.005	.001	.006
Fe	.069	.067	.071	.056	.056	.067	.070	.070
Mn	.000	.002	.001	.000	.003	.003	.003	.001
Mg	.060	.083	.073	.085	.102	.066	.067	.070
	2.014	2.036	2.044	2.029	2.015	2.029	2.045	2.038
Ca	.000	.000	.000	.000	.002	.003	.000	.000
Ba	.006	.005	.006	.006	.009	.001	.002	.008
Na	.045	.054	.042	.042	.043	.045	.042	.041
K	.828	.872	.865	.844	.850	.840	.863	.898
	.879	.931	.913	.892	.904	.889	.907	.947
Mol % Mus	94.8	94.2	95.4	95.3	95.2	94.9	95.4	95.6
Mol % Par	5.2	5.8	4.6	4.7	4.8	5.1	4.6	4.4
Fe/Fe+Mg	.535	.447	.493	.397	.354	.504	.511	.500

* Number of analyses averaged; 1:N indicates a selected analysis.

Samples from Orange, Mass. (Robinson, 1963; Hall, 1970)
4F5AY - Kyanite Zone
36Y - Sillimanite Zone

$ Sample from Sillimanite-Orthoclase Zone, Maine (Evans and Guidotti, 1966)

594Y	595C	B35	M34	4F5AY[#]	36Y[#]	11[$]
46.39	46.11	46.16	46.36	46.36	44.24	45.6
1.73	1.38	1.64	1.51	.77	.65	1.25
35.16	35.82	35.37	35.29	37.30	36.72	35.4
.04	.05	.04	.00	.00	.00	n.a.
.86	1.14	1.03	1.05	1.04	.97	1.10
.00	.03	.03	.00	.00	.03	n.a.
.97	.88	.88	.63	.64	.50	1.11
.00	.01	.02	.01	.01	.00	.02
n.a.	n.a.	.14	.12	n.a.	n.a.	.21
.33	.26	.23	.18	1.16	.81	.63
10.57	10.06	10.35	10.50	8.14	9.26	10.38
96.05	95.74	95.89	95.65	95.42	93.19	95.70
1:3	7	9	6			
3.056	3.043	3.051	3.070	3.036	2.992	3.025
.944	.957	.949	.930	.964	1.008	.975
4.000	4.000	4.000	4.000	4.000	4.000	4.000
1.731	1.830	1.807	1.825	1.915	1.918	1.790
.084	.068	.082	.075	.037	.032	.060
.002	.003	.002	.001	.000	.000	---
.046	.063	.057	.058	.056	.054	.055
.000	.002	.002	.000	.000	.000	---
.093	.087	.087	.062	.061	.049	.110
1.956	2.053	2.037	2.020	2.069	2.053	2.015
.000	.001	.001	.001	.000	.000	.000
---	---	.004	.001	---	---	.005
.040	.033	.029	.023	.146	.105	.080
.887	.847	.873	.887	.678	.797	.880
.927	.881	.907	.912	.824	.902	.965
95.7	96.2	96.8	97.5	82.3	88.3	91.5
4.3	3.8	3.2	2.5	17.7	11.7	8.5
.331	.420	.396	.483	.479	.524	.333

TABLE 6. MUSCOVITE ANALYSES WITH AVERAGE AND STANDARD DEVIATION FOR SAMPLE 853A.

	1	2	3	4	5	6	7	8	9	Mean	σ *
SiO_2	45.44	46.73	47.09	46.89	46.50	46.74	47.35	46.78	47.03	46.73	.54
TiO_2	1.44	1.18	1.15	1.25	1.57	1.71	1.58	1.49	1.79	1.46	.23
Al_2O_3	35.36	34.96	34.90	35.11	35.16	35.21	35.02	34.98	34.52	35.02	.24
Cr_2O_3	.02	.00	.01	.01	.03	.04	.00	.00	.00	.01	.01
FeO	1.06	.97	.96	.90	1.11	1.09	1.08	.98	1.00	1.02	.07
MnO	.05	.00	.00	.00	.00	.00	.00	.00	.00	.00	--
MgO	.87	.90	.80	.83	.80	.93	.93	.86	.86	.86	.05
CaO	.00	.00	.00	.00	.00	.00	.00	.00	.00	.00	--
Na_2O	.37	.34	.28	.31	.27	.34	.37	.27	.43	.33	.05
K_2O	9.97	10.28	9.99	9.97	9.88	9.91	10.24	10.35	9.46	10.01	.27
Total	94.58	95.36	95.18	95.27	95.32	95.97	96.57	95.71	95.33	95.44	

* $\sigma = \sqrt{\text{variance}} = \sqrt{\sum_{i=1}^{N} (x_i - x_{mean})^2 / (N - 1)}$

$$Ba^{+2} + {}^{VI}(Fe,Mg)^{+2} \rightarrow K^{+1} + {}^{VI}Al^{+3}$$

$$Ba^{+2} + {}^{IV}Al^{+3} \rightarrow K^{+1} + {}^{IV}Si^{+4} \text{ (as in margarite).}$$

It is impossible to evaluate the extent of vacancy in the interlayer site because of substitution by such ions as H_3O^+ and Li^+ which cannot be analyzed with the microprobe. In fact, interlayer site vacancy might be considered as substitution toward pyrophyllite [$Al_2Si_4O_{10}(OH)_2$] by the substitution:

$$\square + {}^{IV}Si^{+4} \rightarrow K^{+1} + {}^{IV}Al^{+3}.$$

About 10 percent of the octahedral cations are Fe^{2+}, Mg^{2+}, Mn^{2+} and Ti^{+4}. All iron is considered Fe^{+2} rather than Fe^{+3} because of the extremely reduced character of the schists, which contain pyrrhotite + graphite. The principal substitution is a phengite-type coupled substitution which can be expressed as

$${}^{VI}(Fe,Mg,Mn)^{+2} + {}^{IV}Si^{+4} \rightarrow {}^{VI}Al^{+3} + {}^{IV}Al^{+3}.$$

The significant titanium content of these muscovites necessitates postulation of another substitution. Assuming that all Ti^{+4} is located in octahedral sites, the most likely substitution is

$${}^{VI}(Fe,Mg,Mn)^{+2} + {}^{VI}Ti^{+4} \rightarrow 2\ {}^{VI}Al^{+3},$$

which maintains both stoichiometry and charge balance. An alternative scheme is

$${}^{VI}Ti^{+4} + {}^{IV}Al^{+3} \rightarrow {}^{VI}Al^{+3} + {}^{IV}Si^{+4}.$$

This would seem less likely than the earlier scheme, in that it produces relatively unbalanced charge distribution between octahedral and tetrahedral layers. The two alternative schemes can also be weighed using Figure 5, which shows plots of Ti versus octahedral and tetrahedral Al. The correlation between Ti and octahedral Al (Fig. 5a) is much better than that between Ti and tetrahedral Al (Fig. 5b), making a convincing case that the first substitution is more probable.

It is quite difficult to evaluate the exact contribution of each substitution in analyzed natural muscovites. The principal difficulty arises from the large number of alternative substitution schemes which involve the same elements. Actually, however, there are only two substitutions involving octahedral and tetrahedral positions which are quantitatively important, the replacement of Al by Fe, Mg and Ti in octahedral sites, and the replacement of Al by Si in tetrahedral sites. Since both substitutions involve replacement of Al they can be combined to evaluate the substitutions graphically. The combined substitution is written:

$$Fe^{+2}_{VI} + Mg_{VI} + Ti_{VI} + (Si-3.0)_{IV} \rightarrow (2.0-Al)_{VI} + (1.0-Al)_{IV}.$$

A general plot of these parameters is shown in Figure 6, which illustrates both dioctahedral and trioctahedral composition trends and the distribution of analyzed muscovites and biotites of this study. There are distinct equations for dioctahedral and trioctahedral trends:

$$Fe^{+2} + Mg + Ti + (Si-3) = (2-Al)_{VI} + (1-Al)_{IV} \quad \text{DIOCTAHEDRAL}$$

$$Fe^{+2} + Mg + Ti + (Si-3) = (3-Al)_{VI} + (1-Al)_{IV} \quad \text{TRIOCTAHEDRAL.}$$

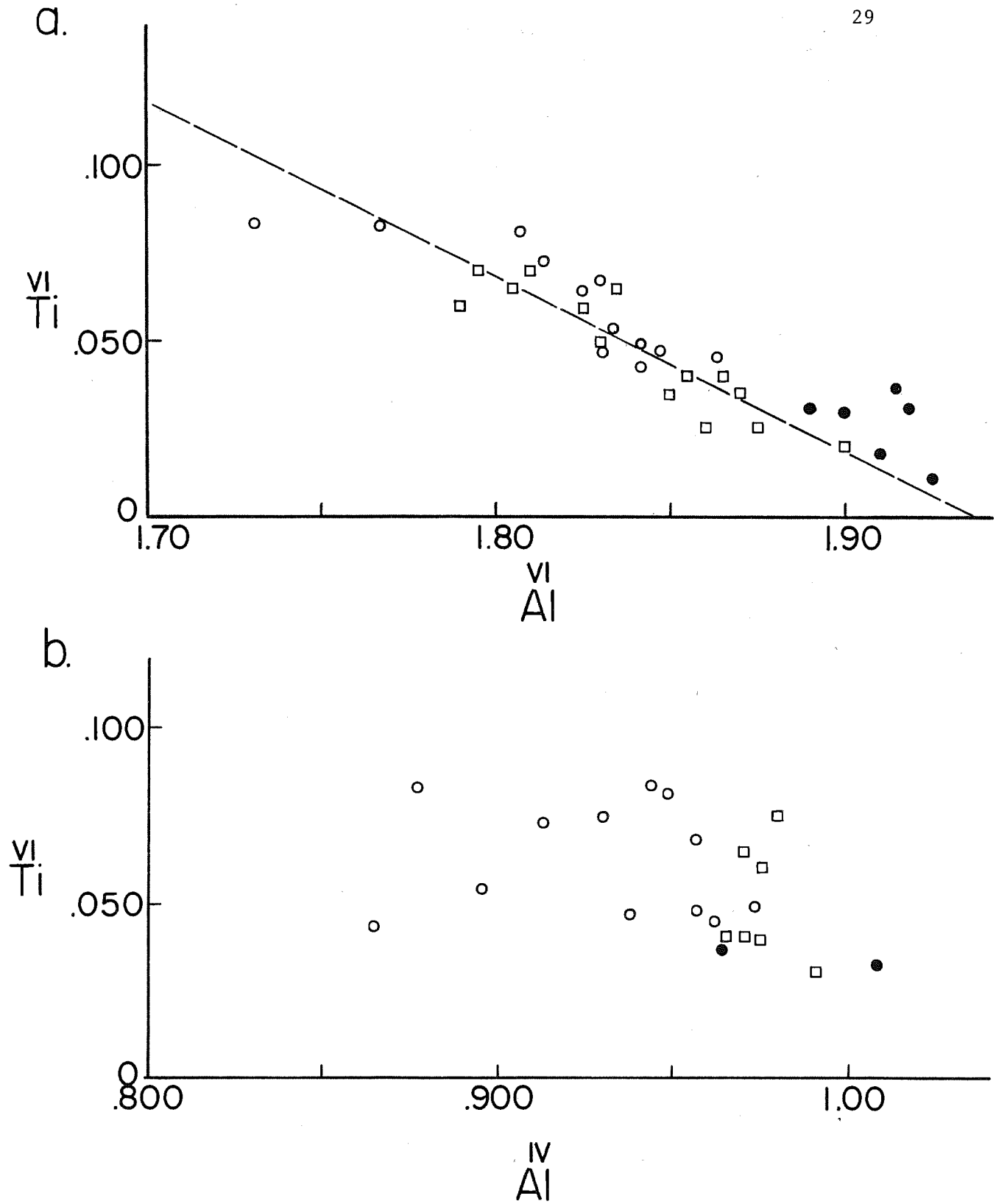

Fig. 5. a) Ti vs Al for analyzed muscovites; b) Ti vs Al for the same muscovites. Ti correlates much better with octahedral Al than with tetrahedral Al. Open circles are data from this study; closed circles are unpublished data from Orange, Mass.; squares are data from Evans and Guidotti (1966).

Table 7 lists a number of dioctahedral and trioctahedral mica compositions and gives their coordinates on Figure 6. Muscovite compositions are shown in more detail in the enlarged plot of Figure 7 which contains the "ideal" line for dioctahedral mica. Most of the muscovite analyses plotted fall above the line, indicating a slight excess of (Fe + Mg + Ti + Si-3) or deficiency of Al from ideal. There are several possible reasons for this deviation:

1) There are additional dioctahedral substitutions which are important but which have not been considered in the comprehensive scheme.
2) The analyses are in error.
3) There is an element of trioctahedral character in the muscovites, as suggested by their position on Figures 6 and 8, and by the sums of octahedral cations in the structural formulas of Table 5. This would involve a substitution scheme which maintains charge balance but not stoichiometry, such as the following:

$$3\ (Fe,Mg,Mn)^{+2} \rightarrow 2\ Al^{+3}.$$

The contribution of this substitution is minor but noticeable. The trioctahedral contribution of the Quabbin muscovites listed in Table 5 ranges from .7 to 2.7% while Fe+Mg+Mn/Total octahedral cations ranges from 5.9 to 8%, suggesting that the major part of the ferromagnesian constituents occurs as phengite (dioctahedral) substitution.

The consistency of muscovite analyses suggests that the first and third of the above explanations are the most likely, and that analytical problems are not indicated.

TABLE 7. PLOTTING PARAMETERS OF SOME SHEET SILICATE COMPOSITIONS.

	VI VI VI IV Fe + Mg + Ti + (Si-3)	VI IV (2-Al) + (1-Al)
Dioctahedral		
$KAl_2Si_3AlO_{10}(OH)_2$ (Muscovite)	0	0
$KFmAlSi_4O_{10}(OH)_2$ (Celadonite)	2	2
$KFm_{1.5}Ti_{1.5}Si_4O_{10}(OH)_2$	3	3
$KFmTiSi_3AlO_{10}(OH)_2$	2	2
$KTi_2SiAl_3O_{10}(OH)_2$	0	0
$\square\ Al_2Si_4O_{10}(OH)_2$ (Pyrophyllite)	1	1
Trioctahedral		
$KFm_3Si_3AlO_{10}(OH)_2$ (Biotite)	3	2
$KFm_{2.5}Al_{.5}Si_{2.5}Al_{1.5}O_{10}(OH)_2$ (Eastonite-Siderophyllite)	1	0
$KAl_3Al_4O_{10}(OH)_2$	-3	-4
$\square\ Fm_3Si_4O_{10}(OH)_2$ (Talc)	4	3

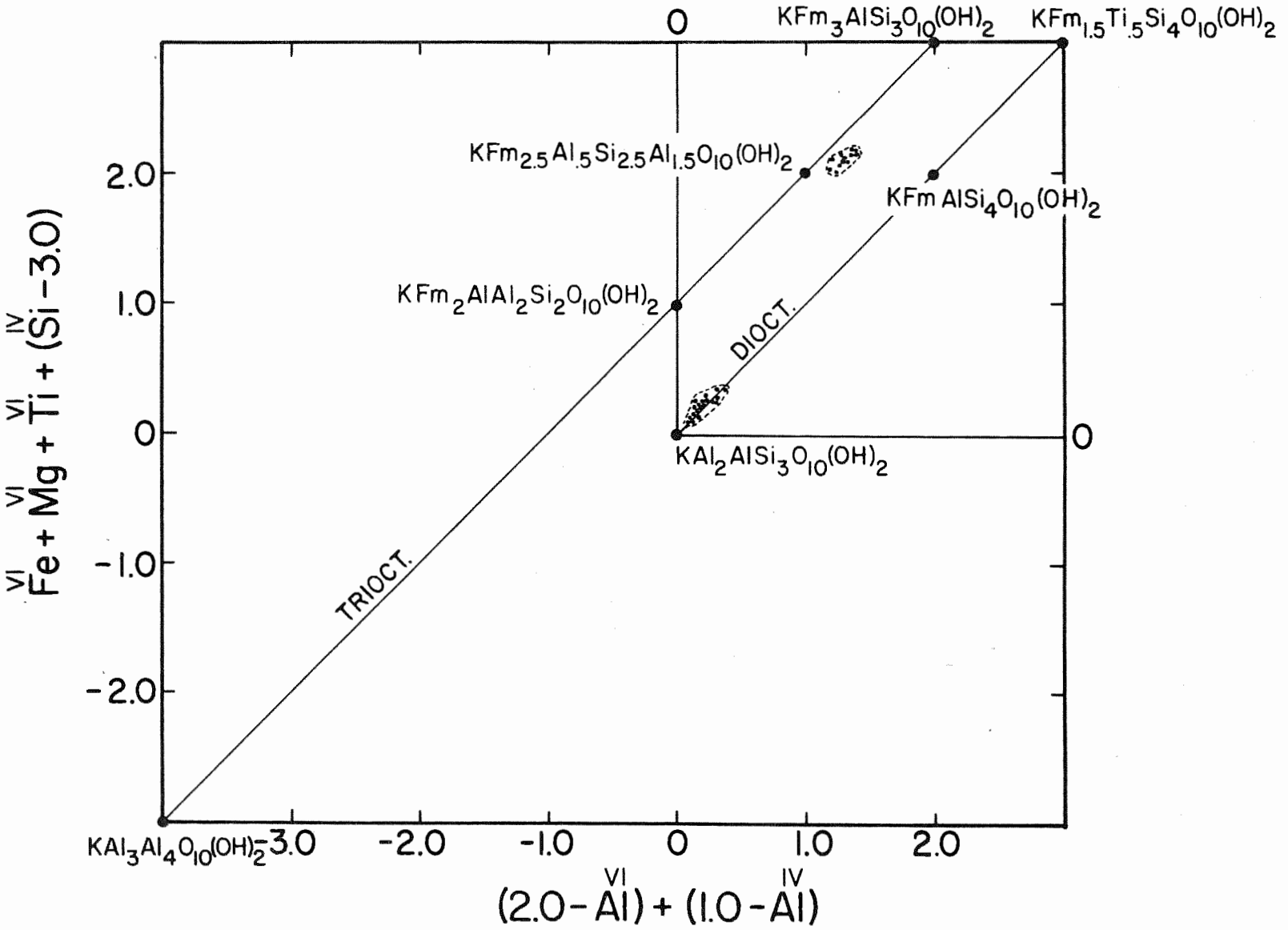

Fig. 6. Plot of substitution parameters in sheet silicates. Ideal dioctahedral and trioctahedral trends are indicated, as well as some mica compositions (see Table 7). Muscovites and biotites from this study are plotted; note the greater deviation of biotite from trioctahedral trend than deviation of muscovite from the dioctahedral trend.

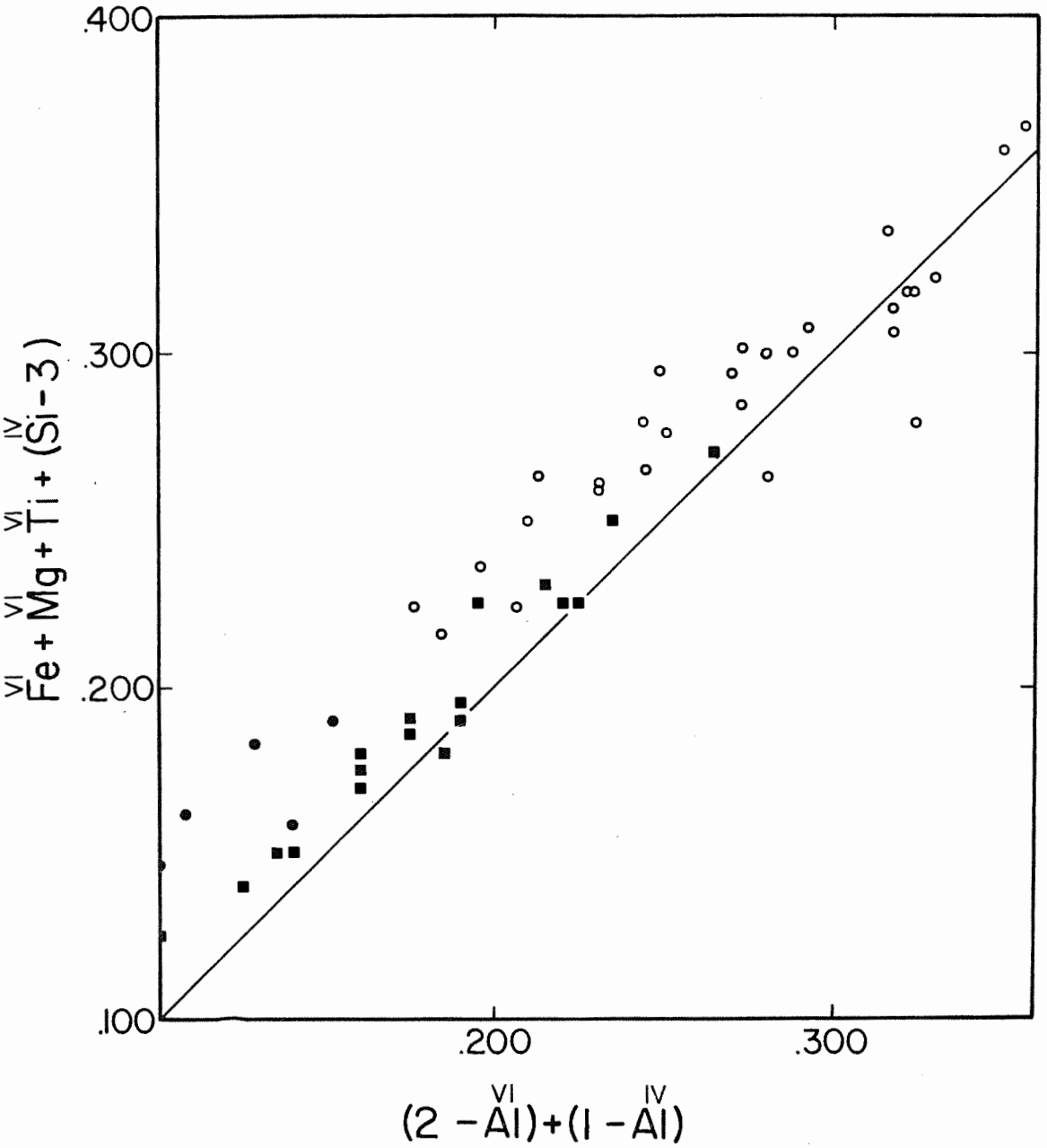

Fig. 7. Enlargement of part of the dioctahedral trend from Fig. 6, with compositions of muscovites plotted. Open circles are muscovites from this study; closed circles are unpublished data from Orange, Mass.; squares are data from Evans and Guidotti (1966). Most of the points fall above the ideal dioctahedral line, reflecting minor trioctahedral character.

An alternative way of illustrating muscovite compositions is to use the triangular projection A'KF (Eskola, 1915; Winkler, 1967), projected from SiO_2 and H_2O, as shown in Figure 8. It can be easily seen that the analyzed muscovites have a substantial ferromagnesian component, but their plotted positions on Figure 8 are somewhat misleading. The points fall off the muscovite-phengite trend because of alkali deficiency in the interlayer site which has the effect of moving the points away from the K corner.

Natural occurrences and experimental studies suggest that the margarite end member has the lowest thermal stability and K-muscovite the highest (A. B. Thompson, 1974; Chatterjee, 1971; Day, 1973). The maximum solid solution of paragonite end member in muscovite is approximately 30 mole percent, according to Thompson (1974). This limit is apparently nearly reached in upper kyanite-zone schists of the Orange area (Hall, 1970), though paragonite has not been shown to coexist with muscovite in that area. At higher grade, muscovite becomes more potassic as the thermal stability of paragonite is exceeded and the paragonite molecule in muscovite dehydrates to sodic feldspar plus Al-silicate. The data of Table 5, as well as the data of Evans and Guidotti (1966), suggest that the highest grade muscovite composition in the assemblage Qz-Plag-Mus-Sill-Ksp at moderate to high pressure is approximately 5 - 6 mole percent $NaAl_2Si_3AlO_{10}(OH)_2$. The implications of K-Na solid solution for phase relations will be thoroughly discussed below.

As noted earlier, Fe + Mg + Mn occupy about 6 to 8 percent of the octahedral sites in analyzed muscovite from Quabbin. Studies by Velde (1965) and Ernst (1963) have demonstrated that this phengite substitution

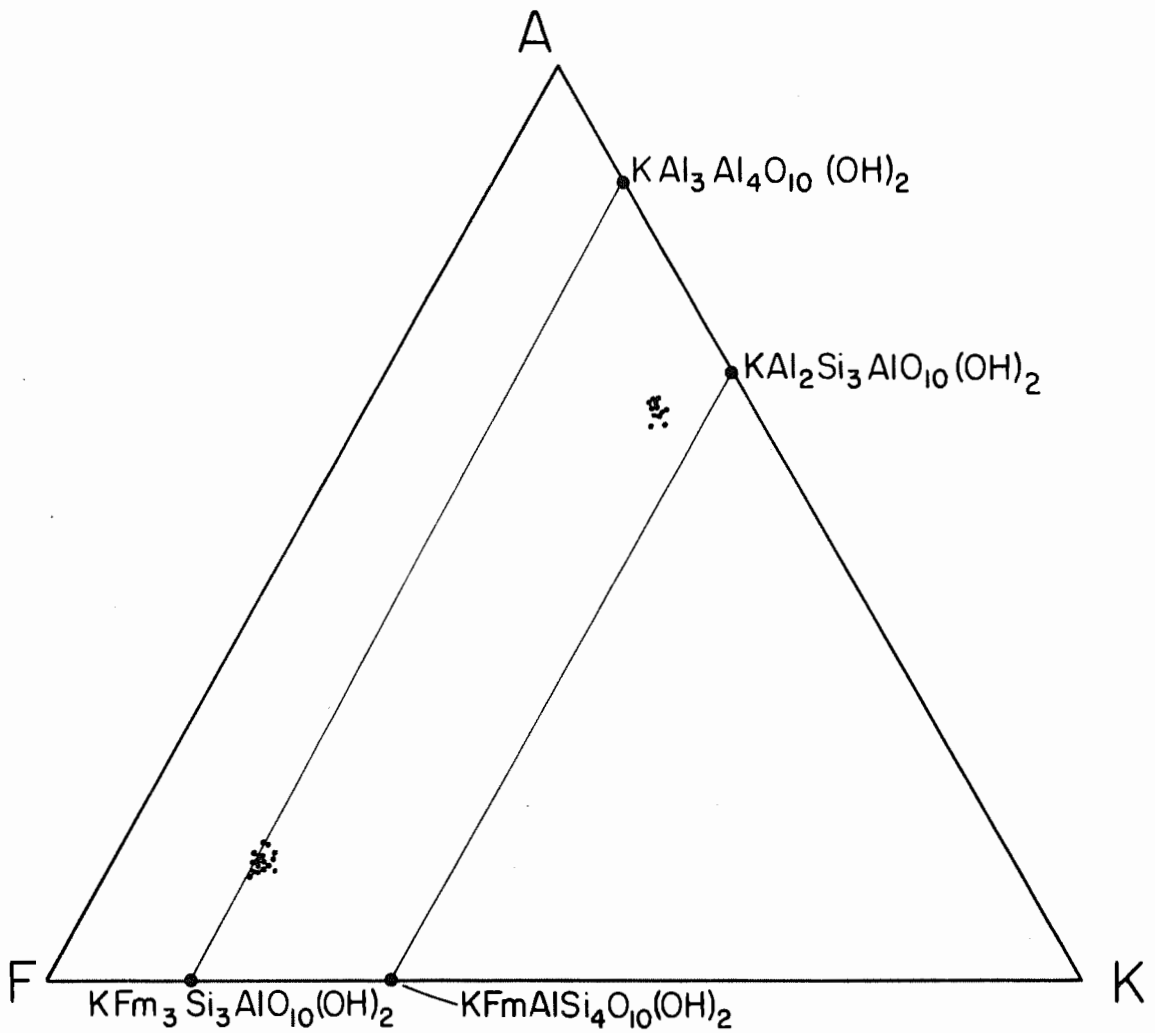

Fig. 8. A'FK diagram (Eskola, 1915) with muscovite and biotite end-members plotted. Also shown are analyzed muscovites and biotites from Quabbin. The substantial ferromagnesian component of muscovite is apparent, as well as the high Al content of biotite. It should be noted that the plotted positions are misleading since alkali deficiency in the interlayer sites has the effect of moving the points away from the K corner. As seen in Fig. 6, the muscovites are actually closer to the dioctahedral trend than biotites are to the trioctahedral trend.

is considerable at low metamorphic grade, decreasing as temperature increases. That data of the present study, as well as the data of Evans and Guidotti (1966) and Guidotti (1973), indicate that the phengite content of muscovite is nearly constant at 5 to 10 percent from kyanite to sillimanite-orthoclase grade. The Ti content of muscovite from Quabbin is greater than that of muscovite from similar metamorphic grade in western Maine (Evans and Guidotti, 1966) and of muscovite from lower grade rocks from the Orange area, from Ontario (Kwak, 1968; Hounslow and Moore, 1967) and from northwestern Maine (Guidotti, 1970, 1973). Kwak (1968) described the Ti increase in muscovite and biotite as a function of increasing metamorphic grade, possibly reflecting ilmenite breakdown with increasing grade.

Biotite

Biotite is a nearly universal constituent of aluminous schists of the upper amphibolite facies and is found in all the samples of this study, where it averages 25 - 35 modal percent. Characteristically red-brown in color, it occurs as coarse flakes and intergrown in masses with muscovite and sillimanite. Electron microprobe analyses of biotite from 18 samples are presented in Table 8.

Simple biotite may be considered as a solid solution between phlogopite, $KMg_3AlSi_3O_{10}(OH)_2$, and annite, $KFe_3AlSi_3O_{10}(OH)_2$. Natural biotites are commonly more aluminous, through the coupled substitution $^{VI}Al + {}^{IV}Al \rightarrow {}^{VI}(Fe,Mg) + {}^{IV}Si$, leading to two additional end-members, eastonite, $KMg_{2.5}Al_{.5}Si_{2.5}Al_{1.5}O_{10}(OH)_2$, and siderophyllite, $KFe_{2.5}Al_{.5}Si_{2.5}Al_{1.5}O_{10}(OH)_2$. This Al-Al substitution appears to be 10 to 15 percent complete in biotites of this study (60 to 90 percent eastonite-

siderophyllite), which is typical for biotites that coexist with such aluminous phases as aluminosilicates or staurolite (Thompson, 1957; Hall, 1970). The aluminous nature of biotites can be seen in Figures 6 and 8. The trend of biotite toward the hypothetical end-member $KAl_3Al_4O_{10}(OH)_2$ (100% Al-Al substitution) is notable.

The considerable titanium content of these biotites is typical for high-grade metamorphic rocks (Kwak, 1968). It appears that a systematic relation exists between octahedral Ti and octahedral Al. These parameters are plotted in Figure 9a; the slope of the plotted data provides a strong suggestion that titanium occurs as Ti^{+4} ions and that the substitution is similar to the one in muscovite:

$$^{VI}Ti^{+4} + {}^{VI}(Fe,Mg)^{+2} \rightarrow 2\ {}^{VI}Al^{+3}.$$

This is further supported by Figure 9b, which shows no correlation between Ti^{+4} and ^{IV}Al.

Further examination of Figure 6 and the structural formulas of Table 8 indicates that biotite deviates significantly from trioctahedral stoichiometry, with dioctahedral contribution ranging from 5.4 to 11.9%. This compares with content of non-divalent octahedral cations Al+Cr+Ti of 17.4 to 23.2% of total octahedral occupancy, which suggests that between 1/3 and 1/2 of the non-divalent cations are present as dioctahedral substitutions. This deviation from three octahedral cations can be explained by substitutions which maintain charge balance but not stoichiometry, such as:

$$Ti^{+4} + \square \rightarrow 2\ (Fe,Mg)^{+2}$$

$$2\ Al^{+3} + \square \rightarrow 3\ (Fe,Mg)^{+2}$$

$$2\ Cr^{+3} + \square \rightarrow 3\ (Fe,Mg)^{+2}$$

TABLE 8. MICROPROBE ANALYSES OF BIOTITES.

	C67	890	892U	853A	849A	869	C26	933A
SiO_2	35.82	35.64	35.47	36.58	37.47	35.46	35.71	36.65
TiO_2	3.02	3.25	2.99	3.39	2.71	3.23	2.59	3.37
Al_2O_3	18.83	19.65	19.76	18.74	18.22	19.08	19.91	18.03
Cr_2O_3	.08	.12	.14	.00	.10	.10	.14	.05
FeO	19.97	18.64	19.13	16.11	14.29	18.41	17.89	18.50
MnO	.31	.30	.16	.32	.41	.17	.25	.18
MgO	8.43	9.89	9.78	10.73	12.65	9.63	9.54	9.21
CaO	.00	.00	.00	.00	.00	.00	.00	.04
BaO	.37	.39	.34	.30	.29	.25	.25	.33
Na_2O	.00	.11	.43	.20	.25	.00	.00	.25
K_2O	8.82	9.30	9.01	9.39	9.50	9.27	9.66	9.25
Total	95.64	97.29	97.22	95.77	95.88	95.61	95.94	95.87
Formulas based on 11 oxygens								
Si	2.720	2.652	2.644	2.729	2.768	2.683	2.683	2.762
Al	1.280	1.348	1.356	1.271	1.232	1.317	1.317	1.238
	4.000	4.000	4.000	4.000	4.000	4.000	4.000	4.000
Al	.404	.376	.381	.377	.355	.384	.444	.364
Ti	.172	.182	.168	.190	.151	.182	.144	.191
Cr	.004	.007	.008	.000	.006	.004	.006	.003
Fe	1.268	1.160	1.193	1.005	.883	1.164	1.122	1.166
Mn	.018	.019	.010	.020	.026	.009	.015	.011
Mg	.953	1.097	1.087	1.193	1.393	1.083	1.067	1.034
	2.819	2.841	2.847	2.785	2.814	2.826	2.798	2.769
Ca	.000	.000	.000	.000	.000	.000	.000	.003
Ba	.008	.011	.010	.009	.008	.006	.006	.010
Na	.000	.016	.062	.029	.036	.000	.000	.037
K	.854	.883	.857	.894	.895	.893	.925	.889
	.862	.910	.929	.932	.939	.899	.931	.939
Fe/Fe+Mg	.574	.518	.525	.462	.395	.520	.516	.532

871	933B	L11Y	595C	B35	M09	M34	507B	T-10B	T-12A
34.97	35.24	35.36	35.24	36.62	36.79	34.85	36.70	36.37	35.87
3.48	3.46	3.09	3.50	3.46	4.05	4.02	3.77	3.10	4.07
19.49	18.76	19.73	19.54	19.54	18.08	19.58	18.08	19.80	18.83
.10	.04	.10	.09	.04	.02	.02	.00	.05	.06
19.35	19.30	16.89	16.82	17.20	18.31	18.61	18.79	17.16	17.96
.20	.06	.25	.27	.34	.05	.18	.04	.02	.00
8.82	8.37	10.53	10.77	9.13	7.74	8.22	8.99	9.64	8.55
.02	.00	.02	.03	.04	.02	.06	.02	.04	.06
.46	.30	n.a.	n.a.	.47	.45	.29	.32	.25	.32
.13	.19	.10	.01	.10	.12	.14	.20	.04	.08
9.63	9.51	9.45	10.00	8.81	9.64	9.46	9.27	8.71	9.28
96.63	95.23	95.52	96.27	95.75	95.26	95.44	96.19	95.18	95.09
2.639	2.691	2.652	2.633	2.735	2.791	2.649	2.756	2.723	2.718
1.361	1.309	1.348	1.367	1.265	1.209	1.351	1.244	1.277	1.282
4.000	4.000	4.000	4.000	4.000	4.000	4.000	4.000	4.000	4.000
.371	.378	.295	.351	.456	.408	.404	.356	.470	.400
.197	.197	.174	.194	.194	.231	.230	.211	.175	.232
.004	.002	.004	.004	.002	.001	.001	.000	.003	.004
1.221	1.232	1.059	1.049	1.074	1.162	1.183	1.179	1.074	1.138
.011	.002	.015	.015	.022	.003	.012	.002	.001	.000
.993	.952	1.177	1.199	1.016	.875	.931	1.005	1.075	.965
2.797	2.763	2.724	2.812	2.764	2.680	2.761	2.753	2.798	2.739
.000	.000	.000	.002	.003	.002	.005	.000	.003	.005
.012	.009	---	---	.014	.013	.009	.008	.007	.009
.018	.027	.013	.000	.014	.018	.021	.028	.006	.012
.925	.925	.902	.951	.840	.933	.917	.887	.832	.897
.943	.961	.915	.953	.871	.966	.952	.923	.848	.923
.550	.564	.470	.470	.519	.571	.562	.539	.500	.541

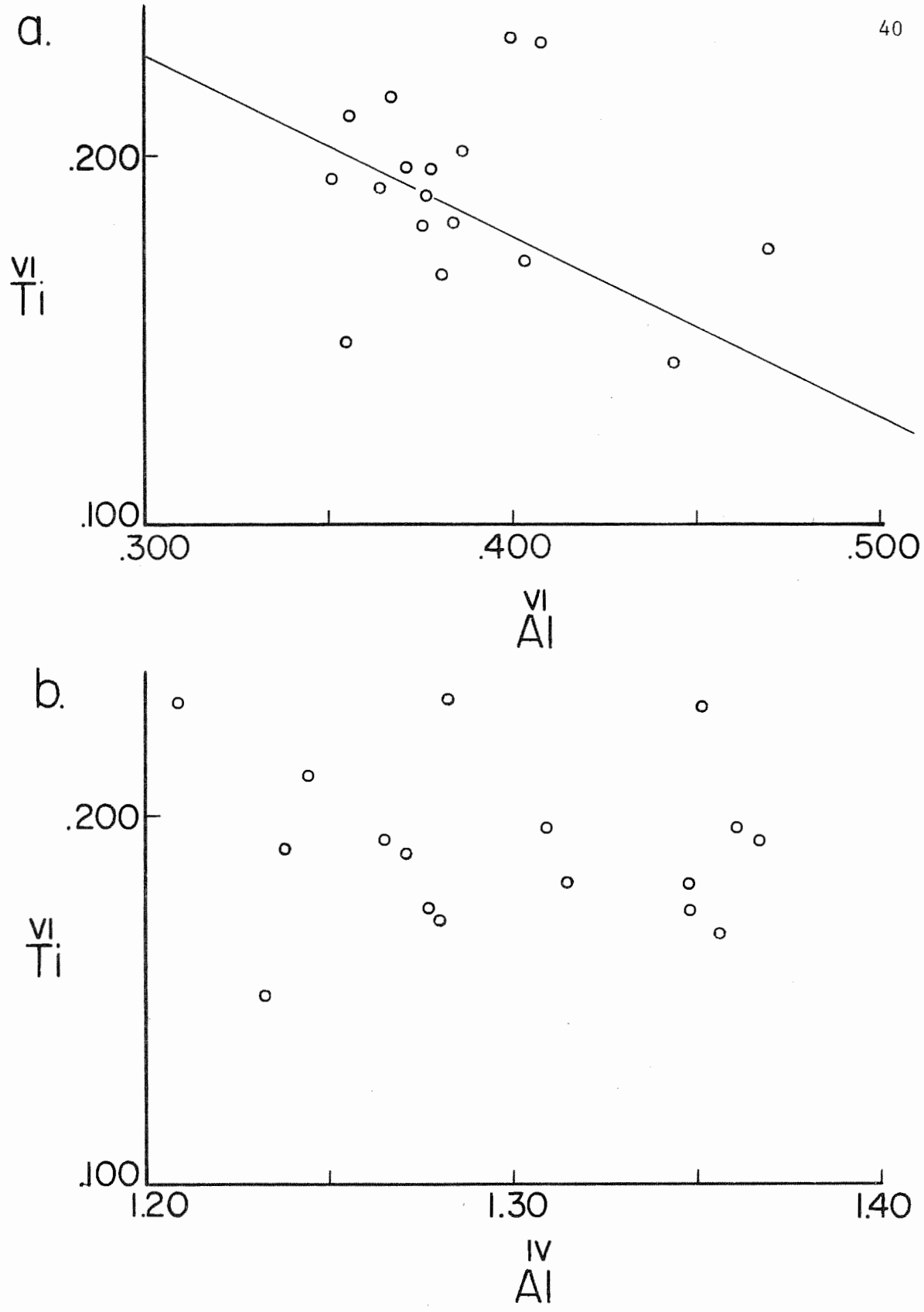

Fig. 9. a) Ti vs Al in biotite. b) Ti vs Al in biotite.
Note that the correlation is better in a) than in b), but it is not as good as in muscovite (see Fig. 5a).

This type of substitution is similar to that suggested to account for the slight trioctahedral character of muscovite, but it is in the reverse sense and of greater magnitude.

Fe/Fe+Mg is near .5 for most of the biotites analyzed. Two notable exceptions are from non-garnetiferous rocks, 853A and 849A, which have the most magnesian bulk compositions of any schists found in the Quabbin area. Biotites which coexist with garnet are slightly more magnesian than lower-grade biotites from the Orange area (Fe/Fe+Mg=.58) (Hall, 1970) and more iron-rich than biotites from central Massachusetts which coexist with garnet and cordierite (Fe/Fe+Mg=.40) (Barker, 1962; Hess, 1969; Field, 1975). This gradual compositional change probably represents progress of the continuous dehydration reaction

$$\text{Bio} + \text{Sill} = \text{Mg-richer Bio} + \text{Gar} + \text{Ksp} + \text{V}.$$

Garnet

Iron-rich garnet occurs in most of the schists examined in this study. It is rarely euhedral in habit, more commonly occurring as rounded anhedral grains. This is in contrast to the dominant euhedral habit of garnet from kyanite grade rocks (Robinson, 1963), but it is typical of sillimanite and sillimanite+orthoclase-grade garnets of the region. Individual garnet crystals range from about .1 mm to 1 cm, but the great majority are in the range of 1 to 5 mm. Almost all are slightly chemically zoned.

Because of inhomogeneity, garnets were analyzed both on cores and on edges (Table 9). Comparison with analyses of Evans and Guidotti (1966), Barker (1962) and Hess (1969) shows that the chemistry of these

TABLE 9. MICROPROBE ANALYSES OF GARNETS.

	892U	869		871		L11Y		595C
	rim	core	rim	core	rim	core	rim	rim
SiO_2	37.09	38.84	38.25	37.03	36.44	37.41	37.55	37.16
TiO_2	.09	.07	.03	.00	.00	.00	.00	.00
Al_2O_3	21.61	21.09	21.25	21.16	21.51	22.06	21.85	22.17
Cr_2O_3	.13	.10	.02	.00	.00	.08	.13	.11
FeO	29.32	30.42	29.93	32.04	31.37	28.53	28.18	26.75
MnO	7.00	5.97	6.80	5.19	5.86	5.62	6.82	7.98
MgO	3.05	3.71	2.64	3.64	2.63	4.36	3.27	4.54
CaO	1.24	1.00	1.02	1.36	1.51	1.90	1.88	1.79
Na_2O	.00	.03	.00	.00	.00	.00	.00	.02
K_2O	.05	.00	.00	.00	.00	.00	.00	.01
Total	99.58	101.23	99.95	100.41	99.32	99.96	99.73	100.52
Formulas based on 12 oxygens								
Si	2.985	3.060	3.058	2.971	2.961	2.969	2.996	2.943
Al	.015			.029	.039	.031	.004	.057
	3.000	3.060	3.058	3.000	3.000	3.000	3.000	3.000
Al	2.036	1.957	2.002	1.973	2.022	2.032	2.050	2.013
Ti	.005	.002	.000	.000	.000	.000	.000	.000
Cr	.008	.004	.000	.000	.000	.004	.007	.007
	2.049	1.963	2.002	1.973	2.022	2.036	2.057	2.020
Fe	1.974	2.003	2.002	2.150	2.132	1.894	1.881	1.772
Mn	.477	.397	.459	.353	.403	.377	.459	.535
Mg	.366	.434	.312	.435	.319	.515	.389	.536
Ca	.107	.083	.087	.117	.131	.161	.159	.152
Na	.000	.004	.000	.000	.000	.000	.000	.000
K	.005	.000	.000	.000	.000	.000	.000	.000
	2.933	2.921	2.860	3.055	2.985	2.947	2.888	2.999
Mol % Alm	67.5	68.7	70.0	70.4	71.4	64.3	65.1	59.2
Mol % Py	12.5	14.9	10.9	14.2	10.7	17.5	13.5	17.9
Mol % Gr	3.7	2.8	3.0	3.8	4.4	5.4	5.5	5.1
Mol % Sp	16.3	13.6	16.0	11.6	13.5	12.8	15.9	17.8

933A		933B		M09		507B		T10B	
core	rim	core	rim	core	rim	core	rim	core	rim
39.05	38.98	36.40	37.03	37.57	37.84	38.54	37.28	38.40	38.46
.11	.12	.02	.00	.01	.03	.02	.02	.00	.02
19.92	20.43	21.37	21.62	20.69	20.97	21.59	21.65	20.90	20.99
.08	.09	.02	.02	.04	.03	.04	.05	.03	.06
33.08	33.18	32.68	34.16	32.76	33.77	33.54	34.07	31.72	32.39
3.02	3.12	2.04	3.25	2.98	3.90	1.60	1.65	4.18	4.39
4.33	4.08	4.38	3.22	4.07	3.02	4.01	3.55	4.29	3.18
1.07	1.09	1.81	1.31	1.36	1.34	1.21	1.26	1.02	.98
.30	.27	.02	.00	.00	.00	.11	.22	.00	.00
.05	.04	.00	.00	.00	.00	.00	.00	.00	.00
100.99	101.39	98.71	100.61	99.50	100.92	100.65	99.76	100.54	100.48
3.087	3.068	2.949	3.005	3.019	3.024	3.038	2.987	3.045	3.061
		.051					.013		
3.087	3.068	3.000	3.005	3.019	3.024	3.038	3.000	3.045	3.061
1.857	1.894	1.989	2.013	1.960	1.972	2.006	2.031	1.954	1.970
.004	.006	.000	.000	.000	.000	.000	.000	.000	.001
.004	.004	.000	.000	.002	.000	.002	.002	.002	.004
1.865	1.904	1.989	2.013	1.962	1.972	2.008	2.033	1.956	1.975
2.187	2.184	2.214	2.256	2.201	2.253	2.209	2.284	2.103	2.156
.201	.207	.138	.215	.203	.262	.106	.110	.281	.296
.508	.478	.528	.378	.486	.358	.469	.423	.507	.377
.090	.090	.157	.109	.115	.112	.102	.108	.087	.084
.044	.039	.002	.000	.000	.000	.014	.033	.000	.000
.004	.002	.000	.000	.000	.000	.000	.000	.000	.000
3.034	3.000	3.039	2.958	3.005	2.985	2.900	2.958	2.978	2.913
73.2	73.6	72.9	76.3	73.2	75.5	76.5	78.1	70.6	74.0
17.1	16.3	17.4	12.8	16.2	12.0	16.2	14.5	17.1	12.9
3.0	3.0	5.2	3.7	3.8	3.8	3.6	3.7	2.9	2.9
6.7	7.1	4.5	7.3	6.8	8.8	3.7	3.8	9.4	10.2

garnets is typical for sillimanite-orthoclase zone schists. As with biotite, iron is considered solely as Fe^{+2} because the analyses do not suggest presence of Fe^{+3}, because of the typically minor ferric iron content of garnets in almandine-rich schists (Deer, Howie and Zussman, 1962), and because of the presence in the rocks of graphite and pyrrhotite. The analyses show a consistent pattern of zoning with Fe and Mn enrichment in garnet rims and Ca and Mg enrichment in cores. This zoning is different from that found in lower grade garnets by Sturt (1962), Albee (1965), Hietanen (1969), Hall (1970) and Guidotti (1970) and discussed by Hollister (1966), which typically have Mn-rich cores; but it agrees with zoning found in higher grade rocks (Hess, 1969). Garnets from two samples, 933B and T-12A, were analyzed in greater detail with analyses made at regular intervals across crystals. These profiles, shown in Figure 10 (see Appendix for details), demonstrate relatively smooth compositional trends from core to rim.

Normal garnet growth zoning (Hollister, 1966) may be disturbed by recrystallization or by participation of garnet in metamorphic reactions, both prograde and retrograde. Hess (1969) suggested for the garnets of Sturbridge, Massachusetts, that high Mn rims are indicative of re-equilibration during retrograde metamorphism. If retrograde metamorphism has occurred in the Quabbin Reservoir area, it has not disturbed other parts of the sillimanite-orthoclase grade mineralogy. Richardson (1974) has reported re-equilibration of garnet during cooling, at Phillipston, Massachusetts, but the effect appears to be limited to the outermost edge of his garnets. The smooth garnet zoning profiles for the Quabbin garnets suggest that if re-equilibration has taken place, it has been pervasive. This does not agree well, however, with the lack of textural or mineralogic evidence of retrogression.

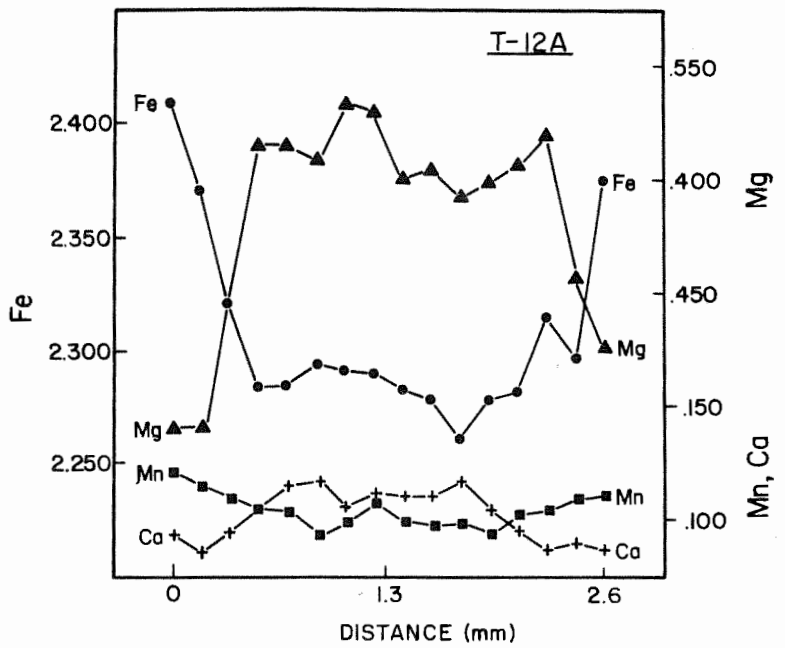

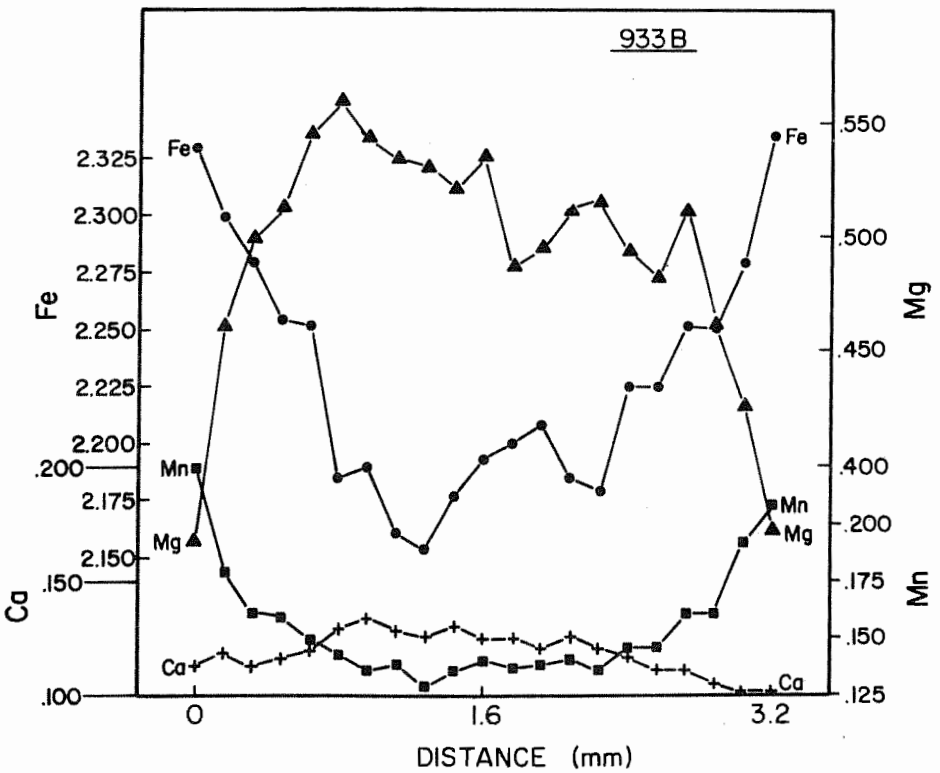

Fig. 10. Fe, Mg, Mn and Ca profiles across zoned garnets from samples 507B and T12A. Note the rise in Fe and Mn and drop in Mg near the edges. Maps of the analyzed garnets and tables of analyses are given in the Appendix.

Plagioclase

Plagioclase occurs both in schists and in migmatites, but plagioclases in schist account for the majority of the plagioclase analyses done in this study (Table 10). The compositions range from An 17 to An 40 and most crystals examined were compositionally homogeneous. The wide range of plagioclase compositions indicates a considerable variation in bulk composition of schists, especially variation of Ca/(Ca+Na). Optical and X-ray examination yield no evidence of unmixing, even in the low-An specimens which are theoretically within the peristerite range (Smith, 1972). X-ray diffractometer scans have been made on a number of plagioclases to determine the structural state, using the method of Bambauer *et al.* (1965), that is, plotting $[2\theta(131)-2\theta(\bar{1}31)]$ versus analyzed composition. All plagioclases examined displayed low structural state.

At Quabbin, most plagioclases show no discernable zoning, either optically or in probe analyses. This result was not expected, since plagioclase participates in muscovite dehydration reactions and might be expected to have rims enriched in either Na or Ca, as noted by Evans and Guidotti (1966). They report normal zoning (an average of 6 mol. percent An) and ascribe it to the albite-producing reaction which occurs in the sillimanite-muscovite zone:

$$(K,Na)Musc + Qz = K\text{-richer } Musc + Ab + Sill + V.$$

On the other hand, albite is consumed in the orthoclase-producing reaction:

$$Musc + Qz + (Na,Ca)Plag + Ksp \quad + Sill + Ca\text{-richer } Plag + V.$$

Evans and Guidotti suggest that more albite is produced in the first reaction than is consumed in the second, resulting in the normal zoning which they report. Other investigators in high-grade terranes have found reverse zoning in plagioclase (e.g., Barker, 1962). The lack of zoning at Quabbin is puzzling but can be interpreted as evidence that the conditions were such that homogeneous equilibrium could be established in the plagioclase.

Potassic Feldspar

The first appearance of potassic feldspar as a groundmass phase in pelitic schists marks the beginning of the sillimanite-orthoclase zone of regional metamorphism. This key phase is found in the groundmass and as porphyroblasts in schist and gneiss, and as larger crystals in pegmatites and migmatite neosome layers. Structural state analysis (see b-c plot below) has shown that most of it occurs as the orthoclase polymorph, so it will be referred to as orthoclase hereafter, except when known specifically to be microcline. Orthoclase occurs in minor amounts in schists, as small interstitial grains, in apparent textural equilibrium with all other phases. It is absent from schists at the lower-grade end of the belt, coexists with muscovite and sillimanite over a considerable area in the middle, and finally completely replaces muscovite at the high-grade end of the belt. It is found in coarser feldspathic layers and in gneisses (without sillimanite) at all grades.

Microprobe analyses of orthoclase are tabulated in Table 11, which is divided into schist feldspars, migmatite feldspars, and gneiss feldspars. Compositions range from Or 83 to Or 91. Most orthoclases contain substantial Ba but no Ca. Compositions are quite similar to those

TABLE 10. MICROPROBE ANALYSES OF PLAGIOCLASE FELDSPAR.

	C67	890	892U	853A	849A	869	C26	933A core	933A	933A rim	933B* A	933B* B	871
SiO_2	64.17	62.30	61.77	60.72	60.55	63.20	61.67	61.08	61.42	60.91	61.23	60.52	60.05
Al_2O_3	22.38	24.38	24.13	24.49	25.02	23.37	23.94	23.23	24.17	24.01	24.80	24.61	25.10
FeO	.00	.00	.09	.04	.00	.00	.02	.07	.16	.23	.00	.00	.00
MgO	.07	.00	.00	.10	.00	.00	.00	.05	.05	.02	.00	.00	.00
CaO	3.66	5.80	5.56	6.58	6.10	4.48	5.28	5.02	4.91	5.04	6.07	6.01	6.89
Na_2O	9.68	7.85	8.12	8.29	7.95	9.34	9.37	9.04	9.08	8.94	8.87	8.06	7.75
K_2O	.16	.18	.21	.21	.14	.10	.21	.21	.16	.21	.14	.15	.14
Total	100.13	100.50	99.89	100.43	99.80	100.48	100.49	98.69	99.94	99.36	101.11	99.37	99.93
Formulas based on 8 oxygens													
Si	2.829	2.743	2.741	2.696	2.694	2.783	2.730	2.749	2.730	2.728	2.697	2.705	2.677
Al	1.163	1.256	1.259	1.282	1.306	1.213	1.249	1.232	1.265	1.267	1.288	1.295	1.319
	3.992	3.999	4.000	3.978	4.000	3.996	3.979	3.981	3.995	3.995	3.985	4.000	3.996
Al			.003		.006							.002	
Fe	.000	.000	.003	.001	.000	.000	.001	.002	.005	.008	.000	.000	.000
Mg	.005	.000	.000	.007	.000	.000	.000	.002	.002	.000	.000	.000	.000
Ca	.173	.274	.264	.313	.291	.211	.250	.242	.233	.240	.285	.288	.329
Na	.827	.670	.699	.714	.686	.798	.804	.788	.781	.775	.758	.699	.670
K	.009	.010	.012	.012	.008	.006	.012	.012	.008	.012	.007	.009	.008
	1.014	.954	.981	1.047	.991	1.015	1.067	1.046	1.029	1.035	1.050	.998	1.007
Mol % An	17.1	28.7	27.1	30.1	29.5	20.8	23.4	23.2	22.8	23.4	27.1	28.9	32.7
Mol % Ab	82.0	70.2	71.7	68.7	69.6	78.6	75.4	75.6	76.4	75.5	72.2	70.2	66.5
Mol % Or	0.9	1.1	1.2	1.2	0.9	0.6	1.2	1.2	0.8	1.1	0.7	0.9	0.8

*933B - A: Plagioclase from schist.
B: Plagioclase from leucocratic layer in migmatite.

	L11Y	592	592A	594Y	595C	B33	B35	M09	M34	507B	T-10B	T-12A
SiO_2	57.06	63.42	65.09	61.84	60.50	61.21	60.17	60.79	59.83	64.10	62.86	61.96
Al_2O_3	26.93	22.89	21.52	24.13	25.05	24.37	24.75	24.95	25.25	22.87	22.89	24.13
FeO	.03	.00	.00	.00	.00	.00	.06	.00	.15	.09	.00	.00
MgO	.03	.00	.00	.00	.00	.00	.00	.00	.00	.16	.00	.00
CaO	8.54	4.31	3.23	6.04	6.57	4.96	6.91	6.50	6.29	3.32	4.50	5.71
Na_2O	6.96	9.17	10.33	8.62	7.76	9.41	7.57	7.90	8.36	9.45	9.56	8.14
K_2O	.15	.20	.11	.20	.15	.16	.21	.13	.18	.20	.10	.13
Total	99.69	99.99	99.89	100.82	100.02	100.11	99.67	100.27	100.05	100.22	99.91	100.06
Formulas based on 8 oxygens												
Si	2.567	2.804	2.842	2.729	2.690	2.720	2.688	2.695	2.667	2.820	2.788	2.743
Al	1.427	1.193	1.147	1.255	1.310	1.275	1.303	1.303	1.326	1.180	1.197	1.257
	3.994	3.997	3.989	3.984	4.000	3.995	3.991	3.998	3.993	4.000	3.985	4.000
Al					.003					.006		.003
Fe	.000	.000	.000	.000	.000	.000	.002	.000	.005	.003	.000	.000
Mg	.001	.000	.000	.000	.000	.000	.000	.000	.000	.010	.000	.000
Ca	.411	.204	.152	.286	.313	.236	.331	.308	.299	.157	.214	.271
Na	.607	.786	.881	.737	.669	.811	.656	.679	.722	.806	.822	.699
K	.008	.011	.006	.011	.009	.008	.012	.006	.009	.011	.006	.007
	1.032	1.001	1.039	1.034	.994	1.055	1.001	.993	1.035	.993	1.042	.980
Mol % An	40.1	20.4	14.6	27.7	31.6	22.4	33.1	31.0	29.0	16.1	20.5	27.7
Mol % Ab	59.2	78.5	84.8	71.3	67.5	76.9	65.7	68.4	70.1	82.8	78.9	71.5
Mol % Or	0.7	1.1	0.6	1.0	0.9	0.7	1.2	0.6	0.9	1.1	0.6	0.8

TABLE 11. MICROPROBE ANALYSES OF POTASSIC FELDSPARS.

	853A	847C	869	849A	C26	872	933A	592
SiO_2	64.54	65.94	65.32	64.36	64.77	64.12	64.21	64.45
TiO_2	.07	.04	.00	.00	.04	.04	.10	.06
Al_2O_3	17.93	18.41	18.19	18.82	18.94	19.14	18.03	18.61
Cr_2O_3	.02	.00	.00	.00	.00	.00	.05	.04
FeO	.04	.03	.11	.00	.09	.09	.09	.05
MnO	.00	.01	.00	.00	.06	.00	.00	.03
MgO	.13	.10	.10	.00	.02	.07	.05	.04
CaO	.00	.00	.00	.00	.07	.00	.00	.00
BaO	1.14	.51	.78	.80	.43	.45	.96	1.08
Na_2O	1.40	1.54	1.49	1.53	1.54	1.61	1.36	1.64
K_2O	14.30	14.23	14.07	13.28	14.27	14.41	15.00	14.34
Total	99.58	100.81	100.05	98.79	100.23	99.94	99.84	100.34
Formulas based on 8 oxygens								
Si	3.000	3.007	3.006	2.989	2.976	2.959	2.989	2.975
Al	.982	.989	.985	1.011	1.024	1.040	.989	1.012
	3.982	3.996	3.991	4.000	4.000	3.999	3.978	3.987
Al				.020	.002			
Ti	.001	.000	.000	.000	.001	.001	.002	.001
Cr	.000	.000	.000	.000	.000	.000	.001	.001
Fe	.001	.000	.004	.000	.003	.002	.002	.001
Mn	.000	.000	.000	.000	.002	.000	.000	.000
Mg	.008	.006	.006	.000	.001	.004	.002	.002
Ca	.000	.000	.000	.000	.003	.000	.000	.000
Ba	.020	.008	.014	.015	.008	.008	.016	.019
Na	.125	.135	.132	.137	.137	.144	.122	.146
K	.847	.827	.825	.787	.837	.848	.891	.844
	1.002	.976	.981	.979	.994	1.007	1.036	1.014
Mol % Or	85.4	85.3	85.0	83.8	85.0	84.8	86.6	83.6
Mol % Ab	12.6	13.9	13.6	14.6	13.9	14.4	11.9	14.5
Mol % An	0	0	0	0	0.3	0	0	0
Mol % Cn	2.0	0.8	1.4	1.6	0.8	0.8	1.5	1.9

592A	594Y	B35	M34	507B	T-10B	T-11F	T-12A	871
64.20	65.60	64.54	65.18	65.32	64.32	65.08	63.96	64.00
.00	.02	.11	.00	.05	.09	.04	.01	.00
18.47	17.74	18.25	18.28	18.92	18.95	18.98	19.54	19.07
.00	.05	.04	.03	.00	.04	.00	.00	.00
.01	.00	.14	.06	.03	.00	.00	.00	.04
.00	.00	.04	.05	.00	.00	.01	.00	.00
.00	.06	.00	.05	.04	.00	.05	.01	.00
.00	.00	.04	.03	.00	.00	.00	.00	.00
n.a.	.57	.72	.85	.43	.42	.45	.84	.79
1.07	1.51	1.50	1.26	1.47	1.74	1.45	1.25	1.20
15.44	14.20	14.26	14.77	14.18	14.11	14.32	14.71	15.10
99.20	99.75	99.64	100.56	100.45	99.68	100.36	100.32	100.19
2.987	3.023	2.989	2.999	2.988	2.971	2.984	2.951	2.962
1.013	.963	.996	.991	1.012	1.029	1.016	1.049	1.038
4.000	3.986	3.985	3.990	4.000	4.000	4.000	4.000	4.000
				.008	.003	.009	.012	.002
.000	.000	.002	.000	.002	.003	.000	.000	.000
.000	.001	.001	.001	.000	.001	.000	.000	.000
.000	.000	.005	.002	.001	.000	.000	.000	.002
.000	.000	.001	.002	.000	.000	.000	.000	.000
.000	.004	.000	.003	.003	.000	.002	.000	.000
.000	.000	.001	.001	.000	.000	.000	.000	.000
---	.009	.012	.015	.008	.008	.006	.015	.014
.097	.134	.133	.112	.130	.156	.127	.111	.108
.916	.834	.843	.867	.827	.832	.836	.865	.892
1.013	.982	.998	1.023	.979	1.003	.980	1.003	1.018
90.4	85.4	85.3	87.1	85.7	83.5	86.3	87.3	87.9
9.6	13.7	13.4	11.3	13.5	15.7	13.1	11.2	10.7
0	0	0.1	0.1	0	0	0	0	0
--	0.9	1.2	1.5	0.8	0.8	0.6	1.5	1.4

TABLE 11. MICROPROBE ANALYSES OF POTASSIC FELDSPARS (Continued).

	L11T	933B	594Y	T-10	851Z	L11Y	507
SiO_2	64.31	63.46	64.25	64.86	64.75	63.36	64.32
TiO_2	.05	.00	.00	.04	.06	.06	.10
Al_2O_3	18.70	18.31	18.87	18.50	18.73	18.61	18.97
Cr_2O_3	.00	.00	.02	.03	.01	.04	.00
FeO	.00	.00	.03	.00	.06	.06	.01
MnO	.00	.00	.00	.05	.00	.00	.00
MgO	.01	.02	.02	.00	.06	.02	.00
CaO	.00	.05	.03	.00	.00	.00	.00
BaO	.14	1.06	n.a.	.40	.52	.39	.77
Na_2O	1.45	1.48	1.16	1.18	1.13	1.14	.72
K_2O	15.01	14.39	14.71	14.98	14.76	14.82	14.62
Total	99.67	98.79	99.11	100.05	100.07	98.50	99.50
Formulas based on 8 oxygens							
Si	2.976	2.977	2.980	2.992	2.984	2.969	2.980
Al	1.020	1.011	1.020	.006	1.016	1.027	1.020
	3.996	3.988	4.000	3.998	4.000	3.996	4.000
Al			.012		.002		.016
Ti	.001	.000	.000	.001	.002	.001	.002
Cr	.000	.000	.001	.001	.000	.001	.000
Fe	.000	.000	.001	.000	.002	.001	.000
Mn	.000	.000	.000	.002	.000	.000	.000
Mg	.000	.002	.001	.000	.004	.000	.000
Ca	.000	.002	.001	.000	.000	.000	.000
Ba	.001	.019	---	.007	.009	.007	.013
Na	.129	.135	.104	.106	.101	.103	.063
K	.885	.860	.870	.882	.868	.885	.863
	1.016	1.018	1.002	.999	.988	.998	.957
Mol % Or	87.2	84.6	89.2	88.6	88.8	88.9	91.9
Mol % Ab	12.7	13.3	10.7	10.6	10.3	10.4	6.7
Mol % An	0	0.2	0.1	0	0	0	0
Mol % Cn	0.1	1.9	--	0.8	0.9	0.7	1.4

reported by Evans and Guidotti (1966). An attempt was made to use compositional differences (including Ba) as an indicator of rock type, but it was unsuccessful because differences are small and considerable overlap occurs.

It has been suggested that the structural state of alkali feldspar in high-grade metamorphic rocks might be an important clue to physical conditions during metamorphism (Evans and Guidotti, 1966). Alkali feldspar exhibits a continuum of crystal structure variations which reflect Al/Si ordering in tetrahedral sites; ordering is most likely a function of composition and thermal history. The method of Wright and Stewart (1968) was used to study the alkali feldspars from Quabbin Reservoir rocks. Smear mounts of feldspar separates were scanned using Cu radiation on a G. E. XRD-5 diffractometer. Each sample was scanned from 55° 2θ to 15° 2θ at a speed of .4° 2θ per minute. Measured peaks were used to obtain lattice parameters through use of a lattice parameter refinement computer program. The results are presented in Table 12 and shown graphically on a b-c plot in Figure 11. A convenient index of ordering is the value Δbc (Stewart and Ribbe, 1969), which is graphically derived, ranging from .500 for high sanidine to 1.000 for maximum microcline, and is independent of K/Na ratio.

Guidotti, Herd and Tuttle (1973) studied the structural state of alkali feldspars from high-grade metamorphic rocks of western Maine. They report an average Δbc for schist feldspars (Guidotti's Type IV assemblage) of .75 - .78. This compares with an average Δbc of .774 for the feldspars of this study, which also agrees with Guidotti et al. in finding that gneiss feldspars are more ordered than schist feldspars and that migmatite feldspars show complete overlap, structurally and

TABLE 12. ALKALI FELDSPAR STRUCTURAL STATE DATA.

SAMPLE	X-RAY COMP. (Ab %)	PROBE COMP. (Ab %)	3 PEAK STRUCT	REFINED STRUCT	Δbc	a (Å)	b (Å)	c (Å)	α	β	γ	VOL. (A^3)	QUAL. (131)
						SCHIST FELDSPARS							
853A	12.5	13.1	$Ben^{+1/3}$	$Ben^{-1/4}$	.736	8.564 ±.006	12.989 ±.006	7.198 ±.003	90°	115° 57.5' ±2.5'	90°	719.92 ±.56	Sharp
T-10B	11.0	13.0	$SH^{-1/4}$	$SH^{-1/2}$	.802	8.571 ±.007	12.972 ±.008	7.200 ±.003	90°	115° 59.6' ±2.9'	90°	719.51 ±.65	V. Sharp
507B	13.0	14.0	$Ben^{-1/3}$	$SH^{-1/4}$	.780	8.569 ±.005	12.977 ±.005	7.199 ±.002	90°	116° 1.6' ±1.6'	90°	719.28 ±.42	V. Slt. Brdn.
T-11F	6.0	14.5	$SH^{-1/4}$	$SH^{-1/2}$	.816	8.581 ±.006	12.985 ±.007	7.207 ±.004	90°	115° 59.2' ±3.3'	90°	721.84 ±.61	Sharp
T-12A	14.5		$SH^{+1/2}$	$Or^{-1/4}$	.701	8.555 ±.006	12.986 ±.006	7.192 ±.005	90°	115° 58.8' ±3.2'	90°	718.24 ±.50	Sharp
B35	12.5	13.4	$SH^{-1/2}$	$SH^{-1/2}$	.804	8.562 ±.003	12.979 ±.004	7.203 ±.002	90°	116° 1.9' ±1.7'	90°	719.25 ±.32	Slt. Brdn.
594Y	12.5	13.5	SH	$SH^{-1/3}$	.784	8.558 ±.004	12.978 ±.003	7.200 ±.001	90°	116° 2.3' ±1.1'	90°	718.44 ±.30	V. Sharp

TABLE 12. ALKALI FELDSPAR STRUCTURAL STATE DATA (Continued)

SAMPLE	X-RAY COMP. (Ab %)	PROBE COMP. (Ab %)	3 PEAK STRUCT	REFINED STRUCT	Δbc	a (Å)	b (Å)	c (Å)	α	β	γ	VOL. (Å^3)	QUAL. (131)
592	15.0	13.1	$SH^{+1/2}$	$SH^{-1/4}$	.769	8.552 ±.005	12.973 ±.007	7.196 ±.003	90°	115° 58.8' ±2.1'	90°	717.70 ±.53	Sharp
507B*	13.0	14.8	$Ben^{-1/4}$	SH^{-}	.771	8.552 ±.010	12.982 ±.008	7.200 ±.004	90°	116° 0.9' ±3.9'	90°	718.33 ±.83	Sharp
						MIGMATITE FELDSPARS							
L11T	12.5	12.5	$SH^{-1/4}$	$SH^{-1/2}$	.805	8.556 ±.006	12.969 ±.006	7.199 ±.002	90°	115° 56.6' ±2.2'	90°	718.11 ±.56	V. Sharp
L11W	12.5	7.0	SH	$SH^{-1/4}$	.780	8.552 ±.005	12.975 ±.005	7.198 ±.002	90°	115° 57.9' ±1.8'	90°	718.13 ±.41	Slt. Brdn.
847C	14.0	13.5	$SH^{-1/4}$	$SH^{-1/3}$	.800	8.548 ±.006	12.978 ±.005	7.202 ±.003	90°	115° 56.6' ±2.3'	90°	718.45 ±.49	Sharp
889	11.5	7.0	Mic	Mic	1.000	8.558 ±.007	12.965 ±.006	7.222 ±.003	90° 35.8' ±4.2'	115° 59.1' ±3.1'	87° 44.5' ±3.3'	719.84 ±.54	Split
872	12.0	14.0	$SH^{-1/3}$	$SH^{-1/3}$	.800	8.558 ±.004	12.978 ±.003	7.202 ±.001	90°	116° 0.4' ±1.3'	90°	718.92 ±.31	Sharp

TABLE 12. ALAKALI FELDSPAR STRUCTURAL STATE DATA (Continued)

SAMPLE	X-RAY COMP. (Ab %)	PROBE COMP. (Ab %)	3 PEAK STRUCT	REFINED STRUCT	Δbc	a (Å)	b (Å)	c (Å)	α	β	γ	VOL. (Å^3)	QUAL. (131)
933B	9.5	12.5	$\beta^{+1/2}$	$\beta^{+1/3}$	.820	8.560 ±.006	12.971 ±.005	7.202 ±.002	90°	115° 58.3' ±1.8'	90°	718.92 ±.49	Sharp
892W			Mic	Mic	1.000	8.552 ±.012	12.951 ±.007	7.217 ±.003	90° 41.8' ±4.6'	115° 59.8' ±4.2'	87° 42.9' ±5.2'	717.84 ±.88	Split
						GNEISS FELDSPARS							
L11Y	12.0	10.4	$SH^{+1/4}$	SH	.767	8.553 ±.005	12.984 ±.004	7.200 ±.002	90°	115° 59.5' ±1.9'	90°	718.73 ±.44	Sharp
660A	12.0		β^{+}	$\beta^{-1/2}$	.871	8.561 ±.005	12.962 ±.004	7.205 ±.002	90°	115° 58.4' ±1.5'	90°	718.73 ±.37	Sharp
C21B	10.0		β	$\beta^{+1/4}$	.841	8.566 ±.010	12.969 ±.007	7.204 ±.003	90°	115° 57.0' ±2.8'	90°	719.70 ±.81	V. Slt. Brdn.
507	11.5	8.5	$SH^{-1/4}$	$\beta^{-1/4}$	.864	8.554 ±.007	12.962 ±.010	7.204 ±.002	90°	115° 58.1' ±2.4'	90°	718.10 ±.62	Mod. Brdn.
N37	14.0		Ben^{-}	SH	.764	8.552 ±.003	12.985 ±.003	7.200 ±.001	90°	115° 57.3' ±1.1'	90°	718.91 ±.24	V. Sharp

TABLE 12. ALKALI FELDSPAR STRUCTURAL STATE DATA (Continued)

SAMPLE	X-RAY COMP. (Ab %)	PROBE COMP. (Ab %)	3 PEAK STRUCT	REFINED STRUCT	Δbc	a (Å)	b (Å)	c (Å)	α	β	γ	VOL. (Å^3)	QUAL. (131)
Q00	12.0		$\beta^{+1/3}$	$SH^{-1/3}$	.801	8.575 ±.007	12.975 ±.006	7.201 ±.002	90°	115° 57.1' ±2.2'	90°	720.45 ±.57	Slt. Brdn.
851Z	10.5	10.0	$SH^{-1/3}$	$SH^{-1/3}$	.784	8.558 ±.004	12.973 ±.002	7.198 ±.001	90°	115° 58.8' ±1.1'	90°	718.42 ±.29	Slt. Brdn.
T-12B	12.0	16.5	$\beta^{+1/2}$	$SH^{-1/3}$	.789	8.554 ±.005	12.974 ±.004	7.199 ±.002	90°	116° 0.3' ±1.6'	90°	718.02 ±.39	V. Slt. Brdn.

* Large porphyroblast

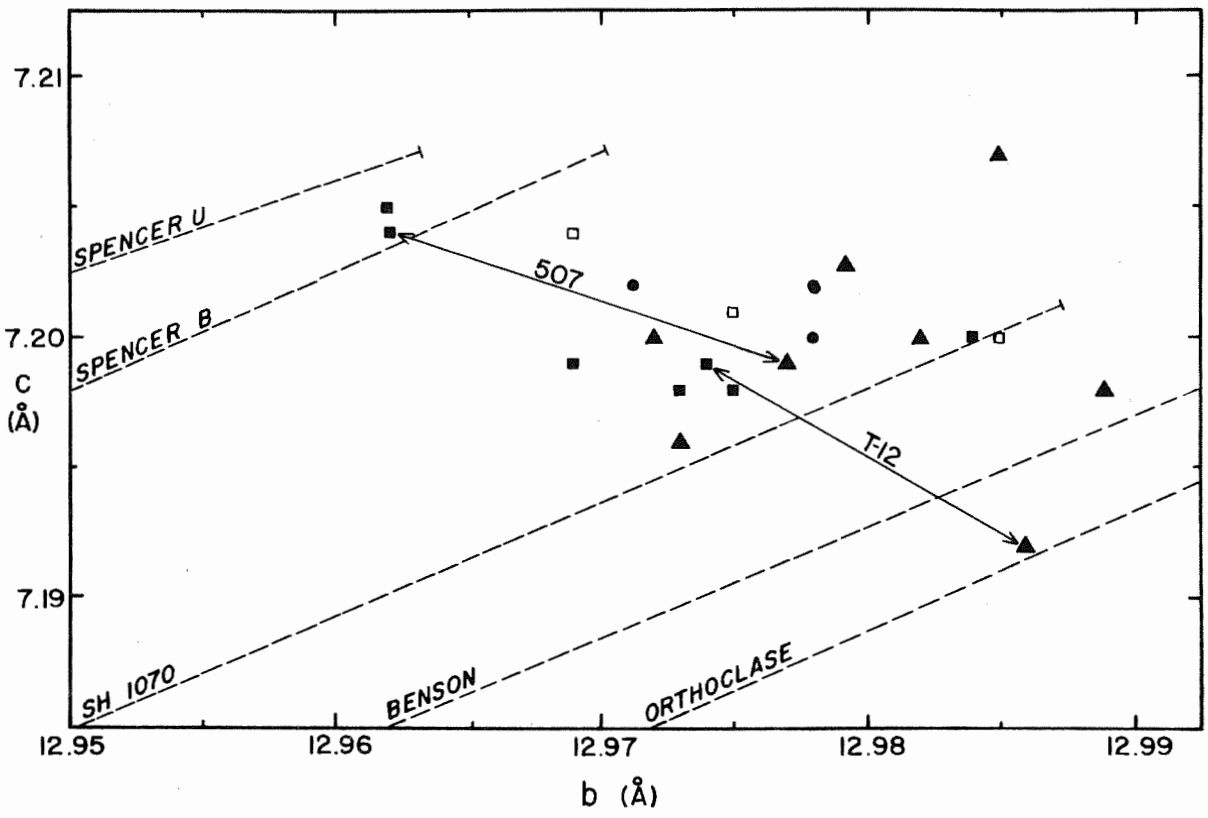

Fig. 11. b - c plot (Wright and Stewart, 1968) showing the structural state of a number of potassic feldspars from the Quabbin area. Solid triangles are pelitic schist samples; solid circles are migmatite leucocratic layers; solid squares are gneisses in the Partridge Formation; open squares are Monson Gneiss samples. 507 and T-12 are outcrops in which adjacent pelitic schist and felsic gneiss layers have potassic feldspar of different structural state (see discussion in text). In this diagram ordered feldspars plot toward the upper left corner, more disordered feldspars toward the lower right.

compositionally, with schist feldspars. Figure 12 is a summary diagram of structural state data obtained in this study.

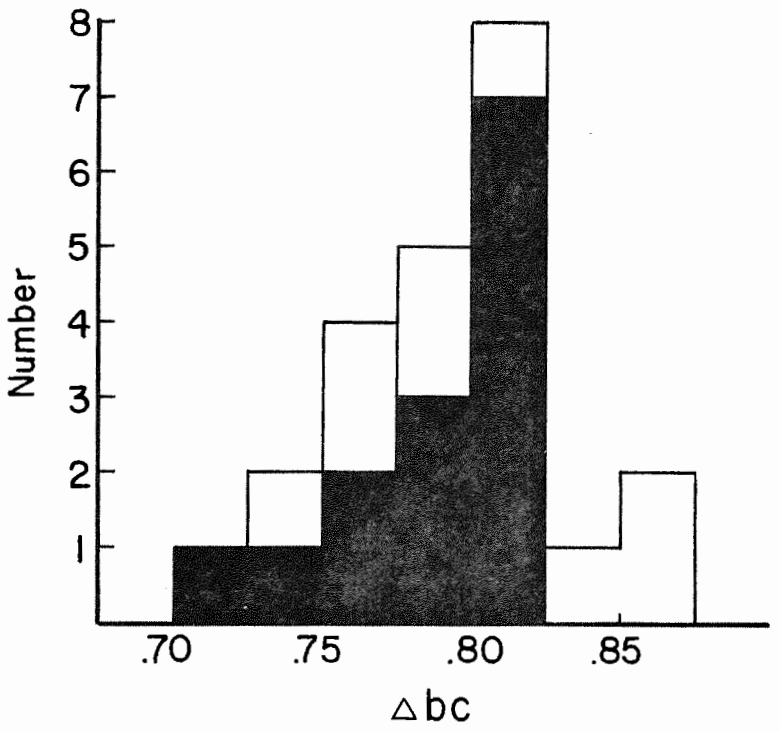

Fig. 12. Summary diagram of alkali feldspar structural state data from schists and gneisses. The darkened area of the histogram indicates the frequency of Δbc values for schist feldspars; the remainder are feldspars from gneisses.

An interesting problem is illustrated in Figure 11. The arrows indicate samples in which adjacent schist and gneiss units in the same outcrop have feldspars of different structural state. Among the possible explanations for this anomalous behavior are:

1) Structural state may reflect the conditions at the time of crystallization of the feldspar and may not be likely to change much as temperature is raised or lowered. Potassic feldspar in low-alumina rocks crystallized (or recrystallized) at lower grade than

alkali feldspar in schists which formed as a result of muscovite dehydration. Therefore, the schist feldspar has a higher structural state.

2) All the alkali feldspars attained the same high structural state at the peak of metamorphism but only gneiss feldspars readjusted their structural state after the temperature began to decline. This explanation implies some chemical or kinetic control of the ordering process. The chemical control could be similar to one reported by Newton and Goldsmith (1973) in their experiments. They noted the powerful catalytic effect of H_2O in speeding up exsolution, but observed that even miniscule amounts of alumina in excess of feldspar stoichiometry retarded exsolution. They ascribed this effect to a decreased catalytic action of H_2O as it combined chemically with the excess alumina to form hydrous aluminosilicate. It has been established that ordering processes are similarly sensitive to the catalytic effect of H_2O. If the alumina in aluminum silicates is as accessible to combination as the alumina in Newton's experiments, the structure state difference between aluminous schists and low-aluminum gneisses can be explained by this mechanism.

Kinetic control of ordering may be due to differing responses of schists and gneisses to applied stress. Stress can be accommodated in mica-rich schists by slippage along the micaceous folia. In gneiss, however, stress causes crushing, granulation, and -- most important -- accumulation of intracrystalline strain in larger grains. The kinetics of ordering may be greatly accelerated in the gneiss feldspars, therefore, if ordering helps to alleviate the accumulated strain.

Opaque Minerals

Ilmenite has a limited occurrence in the rocks studied. It is quite fine-grained where it does occur, so fine-grained as to be nearly impossible to analyze quantitatively with the microprobe. The only important compositional variable in ilmenite from high-grade metamorphosed pelitic rocks is substitution of Mn for Fe, which has been reported up to about 20 mole percent (Guidotti, 1970). Semiquantitative probe analyses of Quabbin Reservoir ilmenites show MnO and MgO contents of less than 1 weight percent in all cases, indicating that the ilmenite is nearly pure $FeTiO_3$. The relative scarcity of ilmenite in these schists is problematic, since ilmenite is common in similar rocks at lower and higher grades in west-central Massachusetts (Hall, 1970; Field, 1975). The apparent explanation is that ilmenite is consumed in a reaction which occurs in the upper sillimanite zone, such as

Gar + Mus + Ilm = Sill + Ti-Bio + Qz (Guidotti, 1970),

and produced in a similar reaction which occurs after the breakdown of muscovite:

Sill + Ti-Bio + Qz = Gar + Ksp + Ilm + V.

The notable increase of Ti in biotite in the sillimanite zone supports the idea that it is receiving the Ti from ilmenite breakdown.

Pyrrhotite was found in all the rocks studied. Uncorrected probe analyses suggest that it has typical non-magmatic pyrrhotite chemistry (Fe/S $\simeq$ 7/8) with less than one percent of other elements. In some specimens, pyrrhotite has begun to alter to marcasite, FeS_2, which is readily identifiable in reflected light by its colloform texture.

Several specimens were recognized in which pyrrhotite and pyrite appear to coexist. The pyrite was closely examined to insure that it was not marcasite alteration after pyrrhotite. The coexistence of pyrite and pyrrhotite is significant because it indicates rather high values of f_{S_2} and also indicates that the f_{S_2} was buffered by the assemblage. For a further discussion of this, see Guidotti (1970).

Graphite, like sulfide, is a universal consitiuent of the schists examined. Its presence with sulfide indicates a rather reduced character of the rocks. It also suggests that the gas composition and f_{O_2} during metamorphism were controlled by the graphite-gas buffer (French, 1966).

ELEMENT FRACTIONATION

Muscovite-Biotite

The substantial ferromagnesian component of muscovite makes it possible to calculate the fractionation of Fe and Mg between muscovite and coexisting biotite. An exchange reaction for Fe-Mg distribution can be written as follows:

$$\text{Mg-Mus} + \text{Fe-Bio} = \text{Fe-Mus} + \text{Mg-Bio}.$$

The expression for the equilibrium distribution of iron and magnesium between the two phases is

$$K_{D\ \text{Fe-Mg}}^{\text{Mus-Bio}} = \frac{a_{Mg}^{Mus^2} \cdot a_{Fe}^{Bio^3}}{a_{Fe}^{Mus^2} \cdot a_{Mg}^{Bio^3}}.$$

The exponents are required because the stoichiometry of the exchange site is different in muscovite and biotite. In this treatment, the minor trioctahedral character of muscovite and dioctahedral character of biotite are ignored. All the Fe and Mg in muscovite are assumed to occur as dioctahedral phengite-type substitutions. Assuming ideal solution behavior of Fe and Mg, the distribution equation can be rewritten:

$$K_{D\ \text{Fe-Mg}}^{\text{Mus-Bio}} = \frac{X_{Mg}^{Mus^2} \cdot X_{Fe}^{Bio^3}}{X_{Fe}^{Mus^2} \cdot X_{Mg}^{Bio^3}}.$$

The mole fractions are calculated ignoring octahedral cations other than Fe and Mg. Calculated K_D values are presented in Table 13, in which K_D has been calculated using both ideal and actual mica stoichiometry for comparison. These data are plotted in Figure 13. The reason

TABLE 13. MUSCOVITE-BIOTITE Fe-Mg FRACTIONATION.

Sample		X_{Fe}	X_{Mg}	X_{Fe}/X_{Mg}	K_D Mus-Bio[1] Mg-Fe	K_D Mus-Bio[2] Mg-Fe
C67	Mus	.535	.465	1.151	.544	.573
	Bio	.571	.429	1.331		
890	Mus	.447	.553	.808	.550	.550
	Bio	.514	.486	1.057		
892U	Mus	.493	.507	.972	.711	.728
	Bio	.523	.477	1.096		
853A	Mus	.397	.603	.658	.739	.708
	Bio	.457	.543	.842		
849A	Mus	.354	.646	.548	1.175	1.070
	Bio	.388	.612	.634		
869	Mus	.504	.496	1.016	.858	.866
	Bio	.518	.482	1.075		
871	Mus	.500	.500	1.000	.505	.528
	Bio	.551	.449	1.227		
C26	Mus	.511	.489	1.045	.913	.922
	Bio	.513	.487	1.053		
595C	Mus	.420	.580	.724	.813	.780
	Bio	.467	.533	.876		
B35	Mus	.396	.604	.656	.469	.464
	Bio	.491	.509	.965		
M34	Mus	.483	.517	.934	.426	.448
	Bio	.560	.440	1.273		

[1]Calculated using ideal mica stoichiometry.

[2]Calculated using actual octahedral site occupancy.

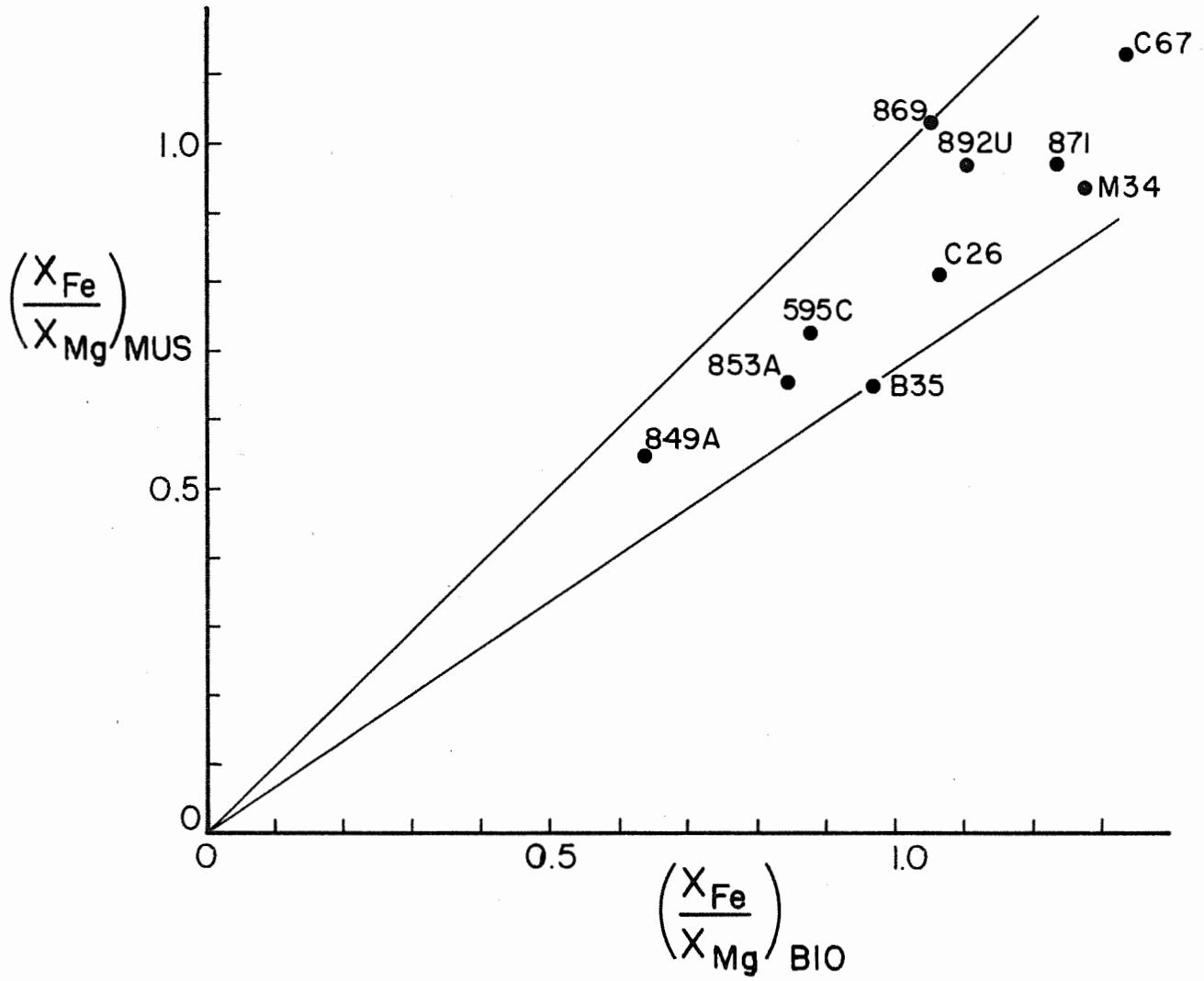

Fig. 13. Plot of Fe/Mg in Mus vs Fe/Mg in coexisting Bio. The lines which envelop the data have slopes of .95 and .75. The diagram illustrates that muscovite is systematically enriched in Mg relative to biotite, and that Fe/Mg fractionation between muscovite and biotite is apparently independent of Fe/Mg ratio in the rock.

for the scatter is not clear; fractionation does not appear to be a systematic function of temperature. It is possible that the scatter may indicate minor disequilibrium, but the more likely explanation is that it is caused by inaccuracies in muscovite analyses. The Fe and Mg contents of muscovite are rather low, and minor errors will be magnified in calculation of iron-magnesium ratios. In any case, the data can be interpreted as indicating roughly equal distribution of Fe and Mg between coexisting micas, with slight fractionation of Mg into muscovite. This is consistent with muscovite crystal chemistry since Mg is the smaller cation and can more readily be accommodated in the dioctahedral layers of muscovite.

It has been pointed out by a number of authors that the Ti content of biotite and muscovite increases with increasing metamorphic grade in ilmenite-bearing rocks (Evans and Guidotti, 1966; Hounslow and Moore, 1967; Kwak, 1968; Hietanen, 1969). The high Ti content of micas from Quabbin agrees with this trend, although the muscovite and biotite in most of the rocks of this study are not saturated with Ti since ilmenite and rutile are absent. The Ti content of coexisting micas is a function of metamorphic grade only in rocks containing rutile or ilmenite. In the absence of a titanian oxide phase, the Ti content is solely a function of bulk composition. The Ti contents of coexisting micas display a regular pattern (Fig. 14) despite the lack of titanium saturation in most of the Quabbin samples. This suggests that titanium fractionation is independent of titanium saturation. The graph in Figure 14 shows a strong fractionation of Ti into biotite. Further, this fractionation appears to be independent of temperature. This fractionation is most likely a function of crystal chemistry of micas; the highly-

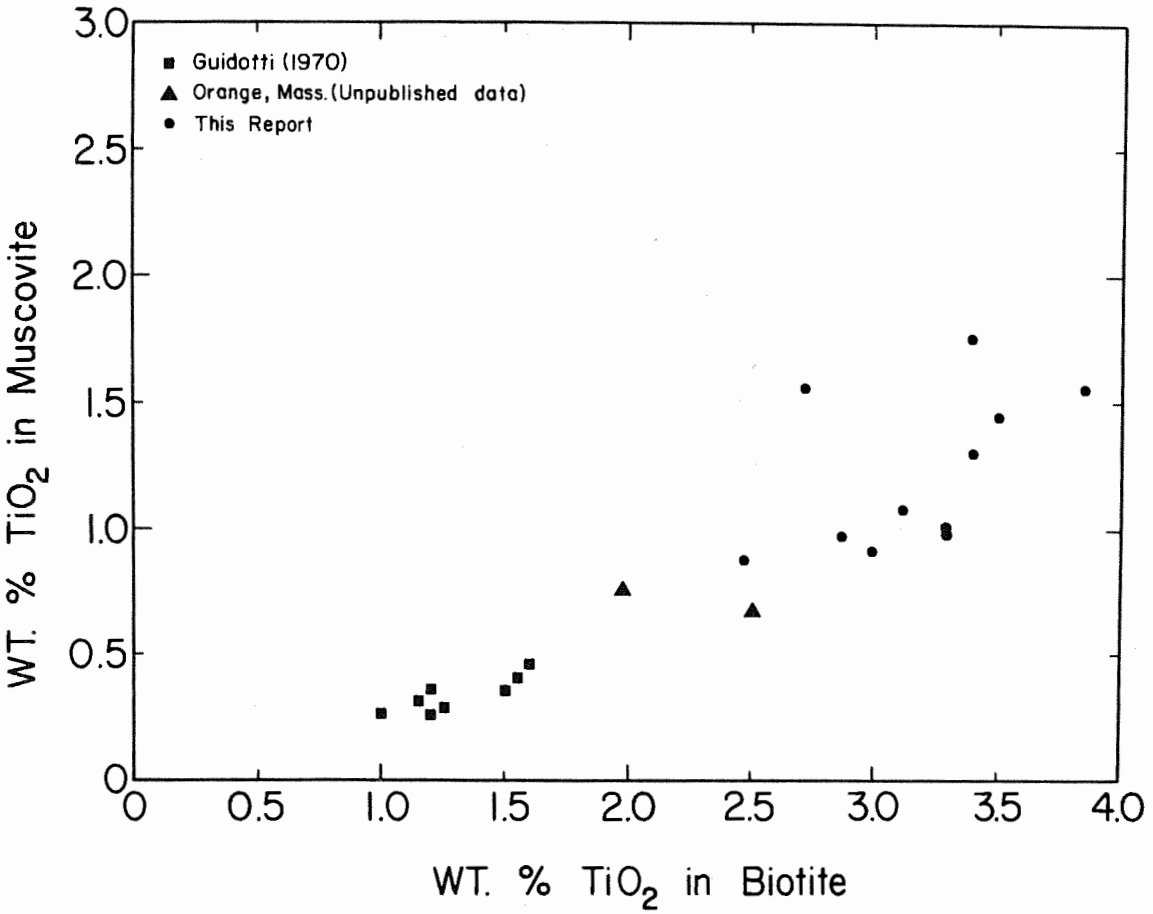

Fig. 14. Comparison of wt.% TiO_2 in coexisting micas from high-grade metamorphic rocks. Data from Guidotti (1970) and Orange, Mass., are from sillimanite-staurolite and sillimanite-muscovite zones and all coexist with ilmenite. Most of the points from the present study are from ilmenite-free rocks.

charged Ti cation is more readily accommodated in the Fe-Mg octahedral layers of biotite than in the Al-rich octahedral layers of muscovite. This preference is apparently not a function of temperature.

Garnet-Biotite

In similar fashion, the fractionation of iron and magnesium between coexisting garnet and biotite can be calculated. This exchange reaction is written:

$$\text{Mg-Gar} + \text{Fe-Bio} = \text{Fe-Gar} + \text{Mg-Bio}$$

and the equilibrium distribution is given by:

$$K_{D\ \text{Mg-Fe}}^{\text{Gar-Bio}} = \frac{a_{Mg}^{Gar} \cdot a_{Fe}^{Bio}}{a_{Fe}^{Gar} \cdot a_{Mg}^{Bio}} .$$

Again the assumption of ideal solution behavior is made, as discussed by Saxena and Hollander (1969), and the above expression becomes:

$$K_{D\ \text{Mg-Fe}}^{\text{Gar-Bio}} = \frac{X_{Mg}^{Gar} \cdot X_{Fe}^{Bio}}{X_{Fe}^{Gar} \cdot X_{Mg}^{Bio}} .$$

These calculations are given in Table 14 and plotted in Figure 15. Garnet edge and core compositions were used in the calculations.

The K_D values given in Table 13 are largely in agreement with those found in other studies. Hietanen (1969) gives K_D values of .224 for sillimanite-muscovite zone rocks and .137 for kyanite zone rocks in Idaho; Lyons and Morse (1970) report .17 - .23 for sillimanite-orthoclase zone and .13 - .19 for sillimanite-muscovite zone in west-central New Hampshire. Lyons and Morse point out that their data support the theoretical prediction that K_D is a function of temperature.

The rocks from Quabbin almost certainly represent a rather limited range of temperature, so a small range of K_D should be expected. The scatter actually found is similar to that found in other studies, such as Lyons and Morse (1970). Ideally, fractionation can be used as a geothermometer, based on this thermodynamic relationship:

$$\Delta G = \Delta G^{\circ} + RT \ln K_D .$$

For equilibrium fractionation, assuming ideal solution behavior:

TABLE 14. GARNET-BIOTITE Fe-Mg FRACTIONATION.

Sample		X_{Fe}	X_{Mg}	X_{Fe}/X_{Mg}	K_D Gar-Bio Mg-Fe	ln K_D	T (^oC)
892U	Gar rim	.844	.156	5.400	.202	-1.602	600 (±50)
	Biotite	.523	.477	1.100			
869	Gar core	.822	.178	4.611	.232	-1.461	630
	Gar rim	.865	.135	6.422	.168	-1.784	545
	Biotite	.518	.482	1.076			
871	Gar core	.832	.168	4.958	.248	-1.394	645
	Gar rim	.870	.130	6.673	.186	-1.683	570
	Biotite	.551	.449	1.228			
933A	Gar core	.812	.188	4.281	.264	-1.332	660
	Gar rim	.820	.180	4.515	.252	-1.379	650
	Biotite	.530	.470	1.129			
933B	Gar core	.807	.193	4.190	.311	-1.168	700
	Gar rim	.856	.144	5.961	.218	-1.525	600
	Biotite	.564	.436	1.296			
595C	Gar rim	.768	.232	3.307	.266	-1.325	665
	Biotite	.467	.533	.876			
M09	Gar core	.819	.181	4.518	.293	-1.228	685
	Gar rim	.863	.137	6.292	.211	-1.554	600
	Biotite	.570	.430	1.331			
507B	Gar core	.825	.175	4.722	.247	-1.398	640
	Gar rim	.844	.156	5.386	.218	-1.526	605
	Biotite	.540	.460	1.173			
T10B	Gar core	.806	.194	4.128	.244	-1.411	640
	Gar rim	.851	.149	5.736	.176	-1.737	560
	Biotite	.500	.500	1.000			
T12A	Gar core	.814	.186	4.295	.274	-1.297	670
	Gar rim	.864	.136	6.347	.185	-1.686	570
	Biotite	.541	.459	1.179			

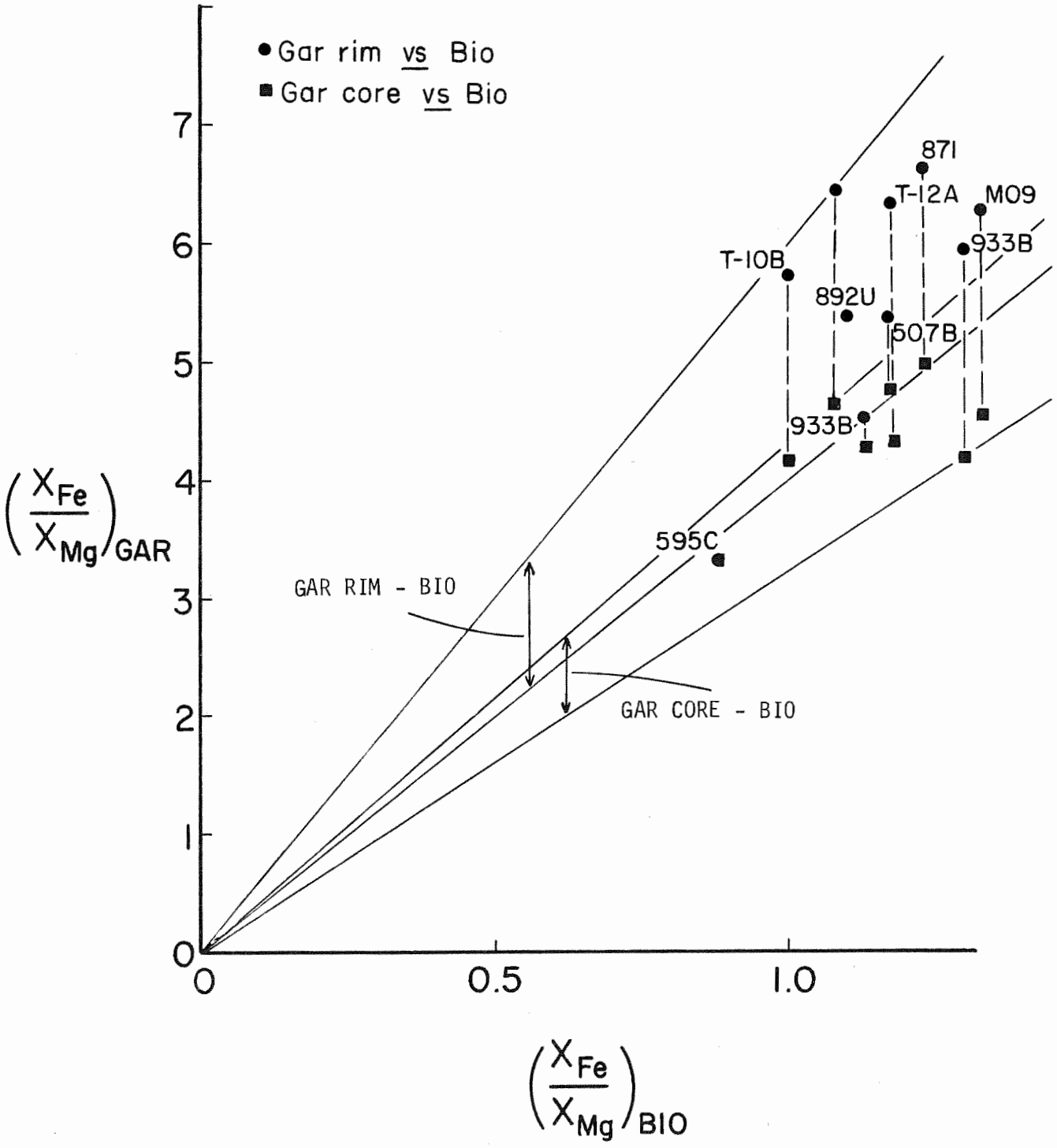

Fig. 15. Plot of Fe/Mg in garnet cores and rims vs Fe/Mg in biotite. The two envelopes in the diagram show almost total lack of overlap of the two sets of data. Garnet 595C is very small and unzoned.

$$\ln K_D = - \frac{\Delta G^\circ}{RT} .$$

Therefore, it should be possible to calculate temperature from the above equation if G° is known. Either G° can be evaluated from hydrothermal experiments, as was done by Currie (1971) for garnet-cordierite exchange, or thermal dependence of K_D can be calibrated from independent geothermometers. Alan Thompson (personal communication, 1974) has calibrated the temperature dependence of garnet-biotite fractionation from garnet-cordierite data and has kindly provided the temperature values given in Table 13. These temperatures obtained for garnet rim - biotite pairs appear to be 50 - 100°C lower than would be expected, while the garnet core - biotite pairs yield more reasonable temperatures. The discrepancy may be due to failure of rim - biotite K_D to reflect peak metamorphic temperatures (disequilibrium or effects of minor elements) or, more likely, to some retrograde compositional adjustment. The minor amount of garnet relative to biotite suggests that such composition changes would have much greater effects on garnet than on biotite.

Muscovite-Alkali Feldspar-Plagioclase

It is useful to consider the distribution of K and Na among these three phases. With only minor simplification, plagioclase (Table 10) can be described with one compositional variable, the Ca/Na ratio, and muscovite and orthoclase are variable only in terms of K/Na ratio. These parameters are plotted in Figure 16, which shows eight muscovite-orthoclase-plagioclase assemblages from Quabbin. The expected compositional relations, depicted in the inset of Figure 16, are that the more potassic muscovite and orthoclase should coexist with more calcic

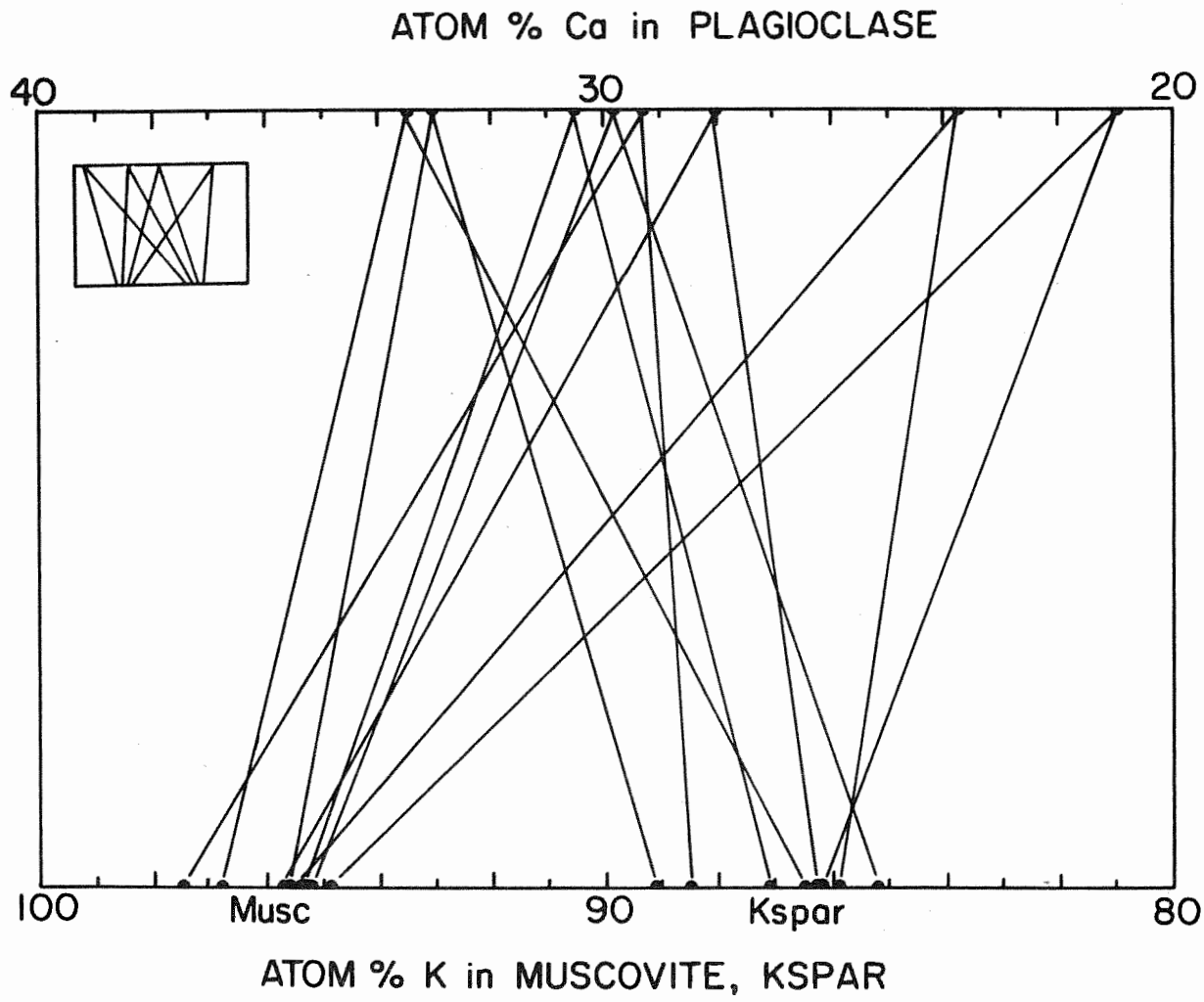

Fig. 16. Plot illustrating compositions of plagioclase, muscovite and orthoclase which coexist. The inset shows the expected distribution of three-phase triangles. The actual compositions show somewhat less regularity than ideal.

plagioclase, and that the more sodic orthoclase and muscovite should coexist with more sodic plagioclase. It is also expected that the variation in Ca/Na of plagioclase should be much greater than the variation in K/Na of muscovite and orthoclase. An alternative way of showing the data is to plot the compositional ratios of muscovite-orthoclase, muscovite-plagioclase and orthoclase-plagioclase pairs (Fig. 17). The data points in the plots of Figure 17 should show linear trends with positive slope, which they do in a general way. The scatter in Figure 17 is representative of crossing of muscovite-plagioclase or orthoclase-plagioclase tielines in Figure 16. Disequilibrium could disrupt any smooth composition trends that are predicted by assuming equilibrium. It seems, however, that a more likely explanation involves the analytical error inherent in microprobe analyses. The precision of Na determinations is a recognized problem, especially where concentrations are low (see Evans and Guidotti, 1966, p. 29). The composition differences being examined here are so small that it may be requiring too much of the data to expect that the trends in Figure 17 should be any better than they are. The solution to the problem may lie in the acquisition of considerable numbers of replicate analyses for better statistics.

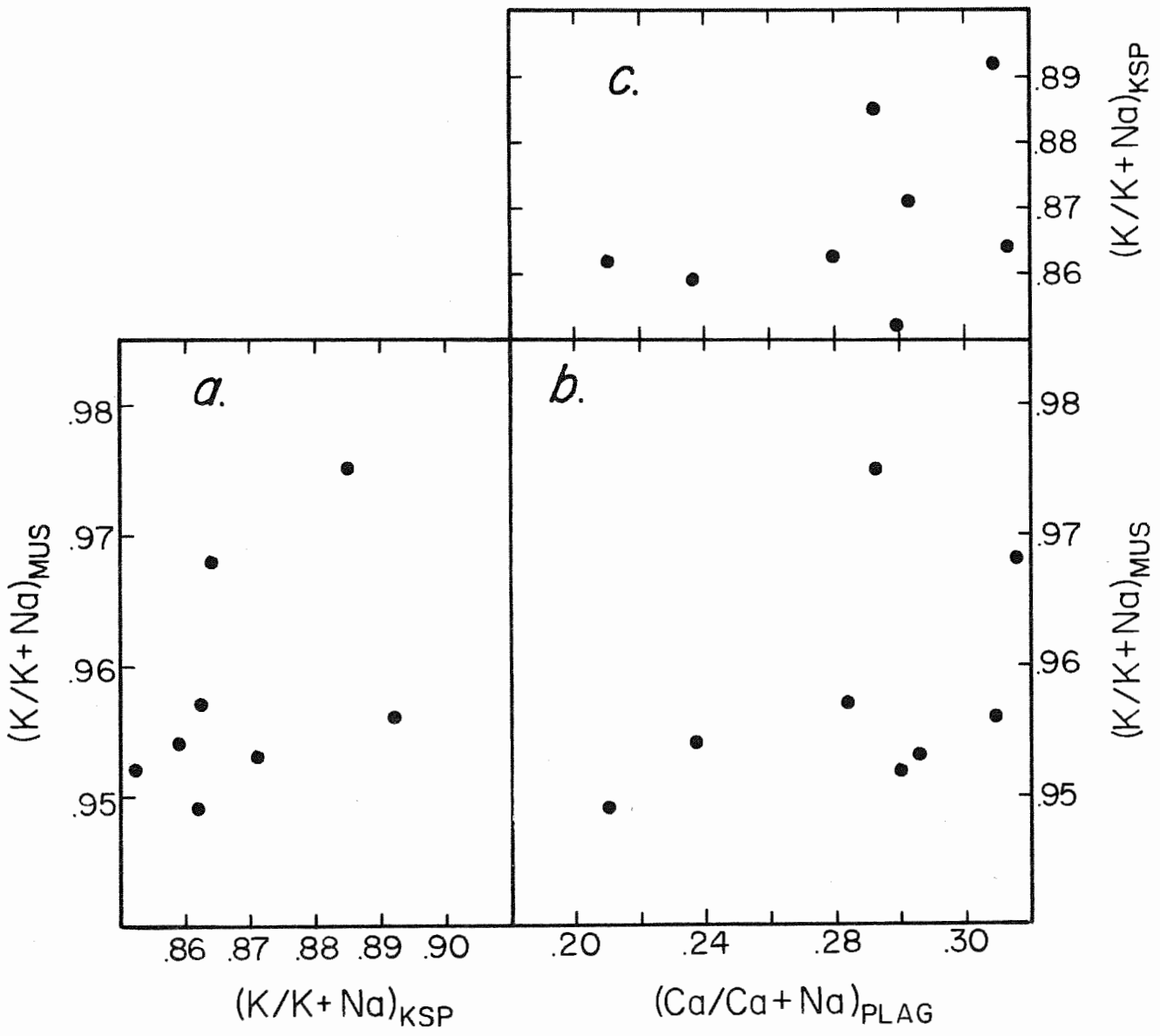

Fig. 17. a) Plot of compositions of coexisting muscovite and orthoclase in aluminous schists. b) Plot of compositions of coexisting muscovite and plagioclase in schists. c) Plot of compositions of coexisting orthoclase and plagioclase in schists. All data are for minerals in mus-sill-or-plag-qz assemblages. All three diagrams should demonstrate linear trends for the data points, with positive slope. The trends are discernible; reasons for scatter are discussed in the text.

PHASE RELATIONS

Phase equilibria in pelitic schists can be described to a first approximation in an eight component system: K_2O-Na_2O-CaO-FeO-MgO-Al_2O_3-SiO_2-H_2O (J. B. Thompson, 1957). Additional components which may be important include MnO, TiO_2, ZnO, BaO, and CO_2 (Albee, 1972; A. B. Thompson, 1974). In such a complex system, the best approach appears to be to start with simple subsystems and gradually add extra components. A fuller understanding of the petrology of the Quabbin Reservoir schists can be obtained by comparing observed phase relations with phase relations developed on theoretical and experimental bases.

System K_2O-Na_2O-Al_2O_3-SiO_2-H_2O

There are a number of compositions and joins in this system which are represented by phases occurring in high-grade metamorphosed pelitic rocks. These include Al_2SiO_5(andalusite, kyanite, sillimanite), SiO_2 (quartz), $KAlSi_3O_8$-$NaAlSi_3O_8$ (orthoclase-albite), and $KAl_2Si_3AlO_{10}(OH)_2$-$NaAl_2Si_3AlO_{10}(OH)_2$ (muscovite-paragonite). Only equilibria which are SiO_2- and vapor-saturated are of interest to the present study. The chemography of the relevant part of the system is illustrated in Figure 18, a silica- and vapor-saturated ternary projection onto the plane $KAlO_2$-$NaAlO_2$-Al_2O_3. The compositions of the solid phases are indicated on the diagram, as is the lowest-temperature silicate liquid (Luth, Jahns and Tuttle, 1964). Phase relations in this plane have been discussed by J. B. Thompson (1961), Evans and Guidotti (1966), Guidotti (1970) and A. B. Thompson (1974). Aluminum silicate phase relations have been studied experimentally by a number of investigators. The most

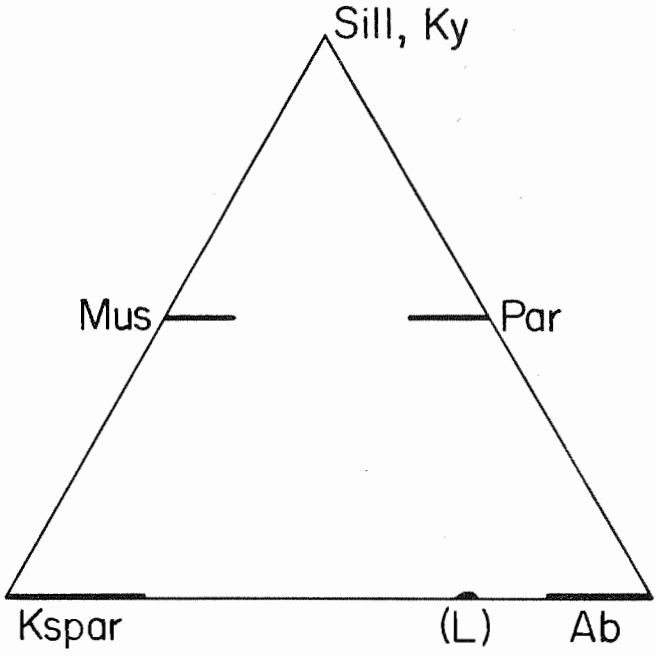

Fig. 18. SiO_2- and H_2O-saturated ternary projection $KAlO_2$-$NaAlO_2$-Al_2O_3 illustrating the compositions of phases found in high-grade metamorphic rocks. Mica and feldspar solid solutions are approximately correct.

widely accepted interpretations of the Al_2SiO_5 triple point are those of Richardson, Gilbert and Bell (1969) and Holdaway (1971). Likewise, the quartz and vapor-saturated dehydration of muscovite has been examined experimentally by several writers, including Evans (1965), Althaus et al. (1970), Kerrick (1972), Day (1973) and Chatterjee and Johannes (1975). Experimental determinations of the melting reaction Or + Qz + V = Liq have been summarized by Lambert, Robertson and Wyllie (1969), while the melting of Or + Ab + Qz + V was reported by Luth, Jahns and Tuttle (1964). The experimentally determined locations of these equilibria in P - T projection are shown in Figure 19.

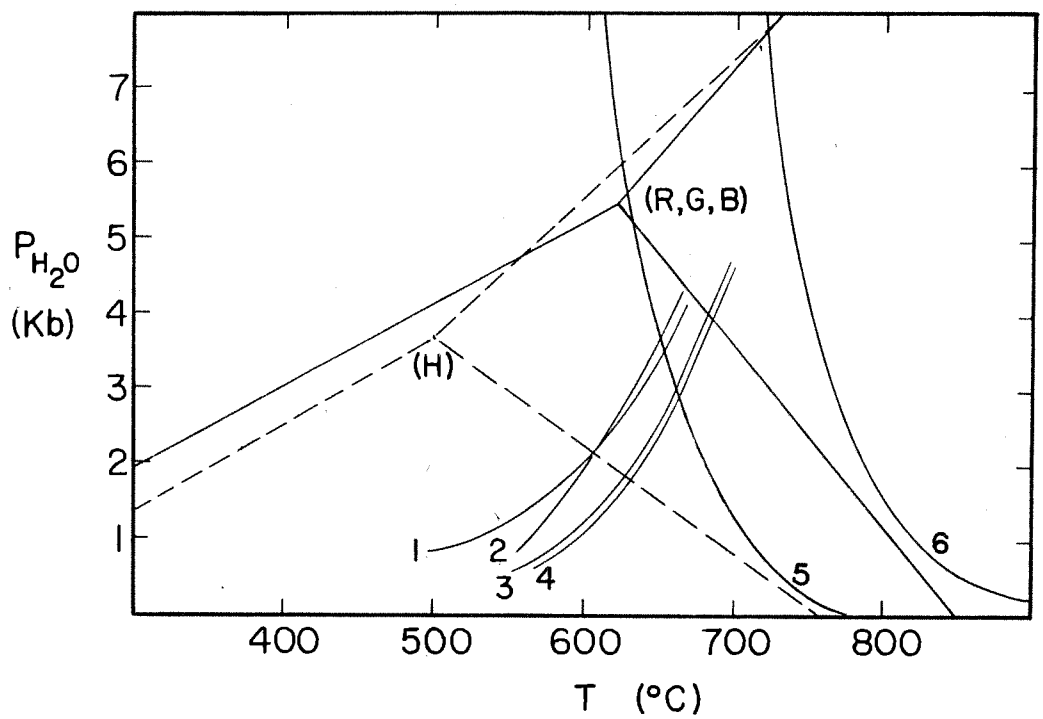

Fig. 19. $\underline{P}_{H_2O}$- $\underline{T}$ projection showing some experimentally determined equilibria in the system K_2O-Na_2O-Al_2O_3-SiO_2-H_2O. The aluminum silicate triple points of Richardson, Gilbert and Bell (1969) and Holdaway (1971) are given. Numbered curves are: 1) Muscovite dehydration according to Evans (1965); 2) Muscovite dehydration (Kerrick, 1972); 3) Muscovite dehydration (Althaus et al, 1970); 4) Muscovite dehydration (Day, 1973); 5) Melting of qz-or-ab-H_2O (Luth, Jahns and Tuttle, 1964); 6) Melting of qz-or-H_2O (Lambert, Robertson and Wyllie, 1969).

Topological facies types (J. B. Thompson, 1961) involving muscovite are illustrated in Figure 20. Each of these facies types is separated from the next by a specific discontinuous reaction, as indicated on the diagram. In addition, there are continuous reactions that distinguish individual facies within the same facies type. Two of these continuous reactions are shown in detail in Figure 21. The change in muscovite and albite compositions with increasing temperature in facies type II reflects the reaction

Musc + Ab + Qz = K-richer Musc + K-richer Ab + Sill + V (Fig. 21a).

The change in muscovite and orthoclase compositions with increasing temperature in facies type III reflects the continuous reaction

Musc + Or + Qz = K-richer Musc + K-richer Or + Sill + V (Fig. 21b).

It should be noted that the composition changes shown in Figure 21b would be observed only in rocks with extremely high K/Na ratios, such as calc-silicates. The most potassic muscovite which occurs in normal pelitic rocks is the muscovite composition in equilibrium with Ab + Sill when the Musc-Ab tieline switches to an Or-Sill tieline.

As mentioned above, the system contains a silicate melt at high temperatures. Under conditions of $\underline{P}_f = \underline{P}_t$, the melting curve of aluminous granite

Or + Ab + Qz + Sill(or Mullite) + V = Liquid

must intersect the univariant curve for muscovite dehydration, generating the invariant point shown schematically in Figure 22. The diagram was constructed according to Schreinemaker's rules for the SiO_2-saturated

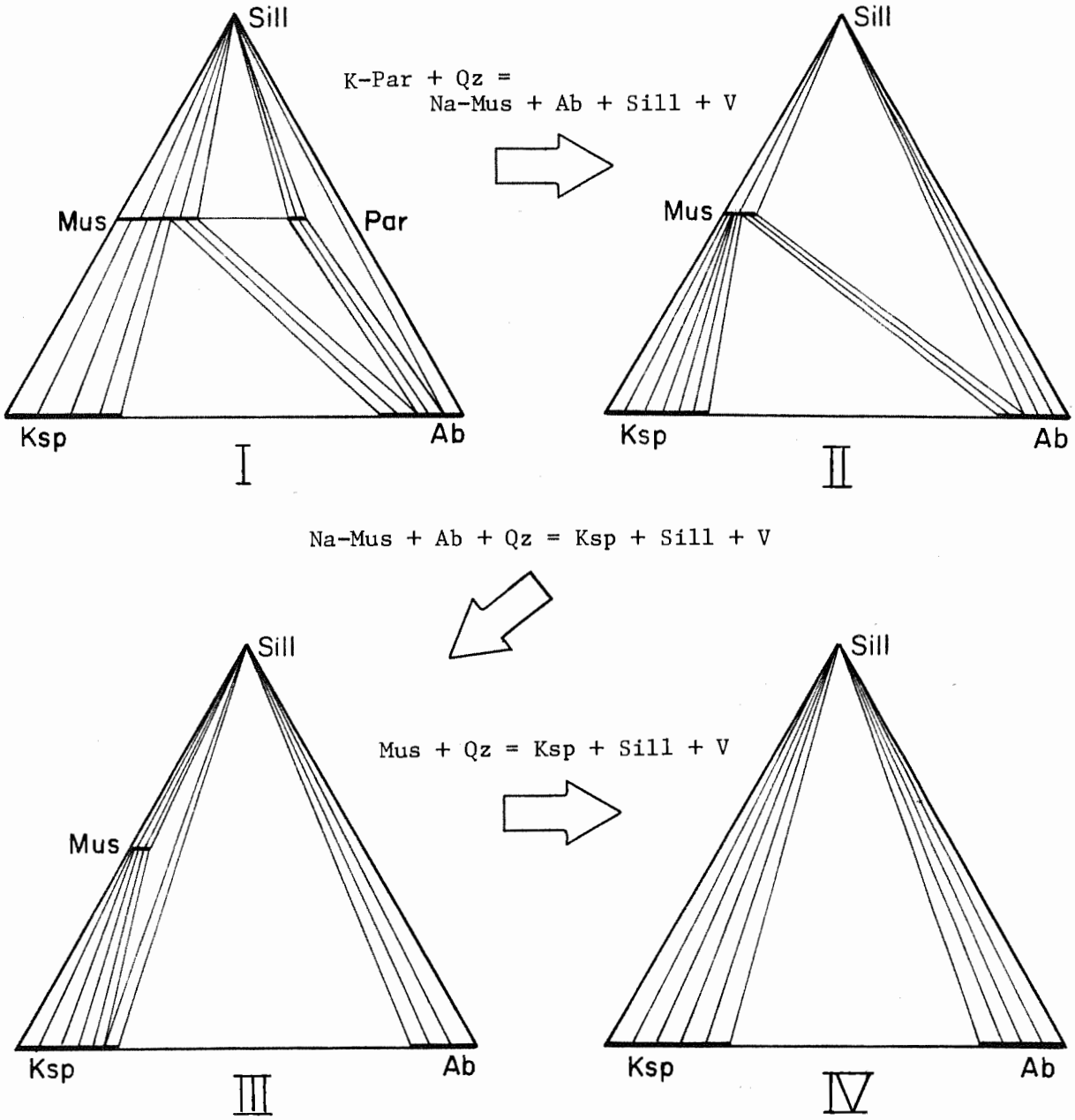

Fig. 20. Topologic facies types (Thompson, 1961), separated by discontinuous reactions, for high-grade pelitic rocks. All diagrams are projected from quartz and H_2O. Continuous reactions within each facies type are discussed in the text.

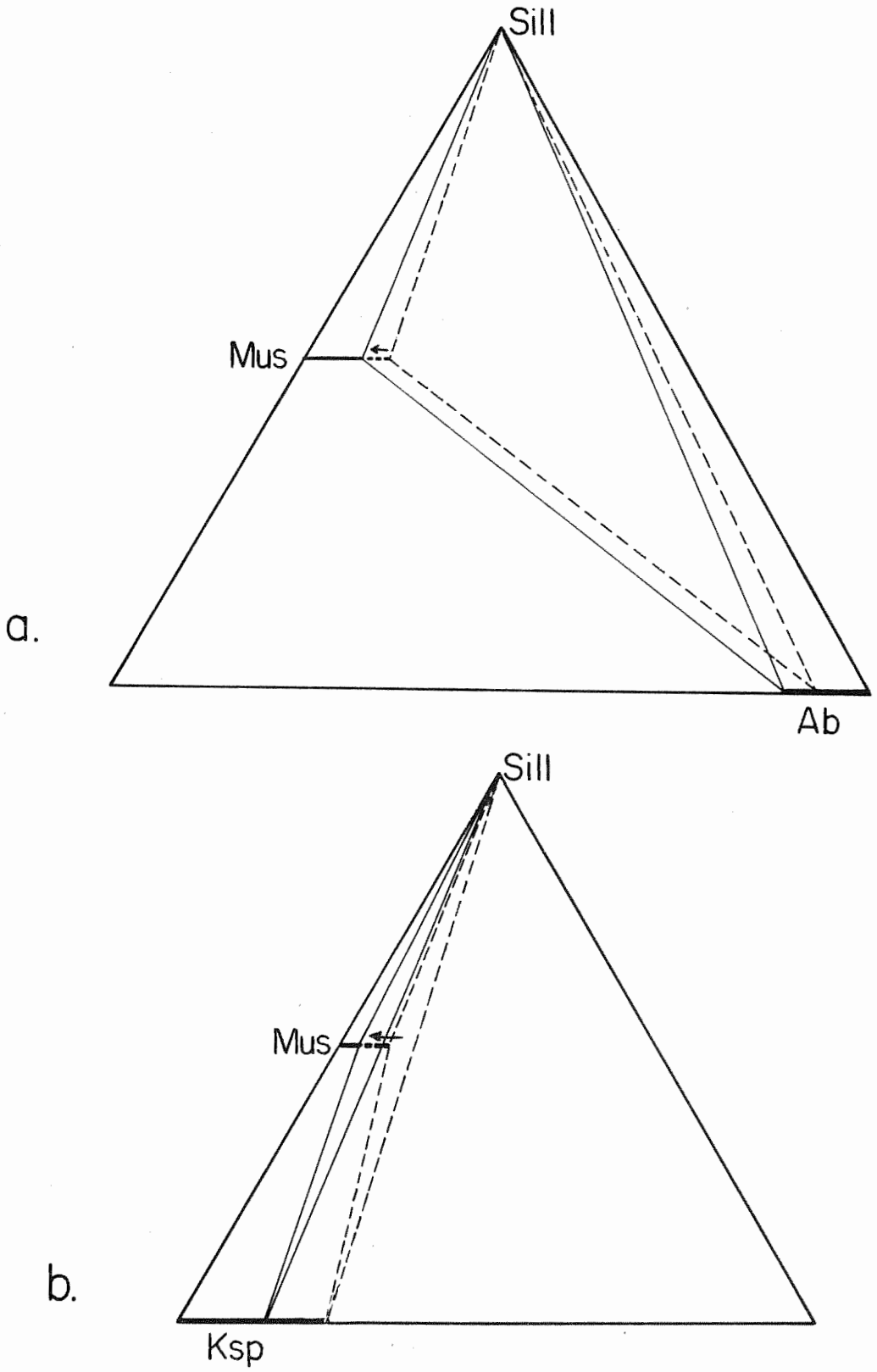

Fig. 21. a) Continuous reaction in the sill-mus zone with K-enrichment in muscovite and albite. b) Continuous reaction in the sill-or zone with K-enrichment of muscovite and orthoclase (only observed in rocks with very high K/Na ratio).

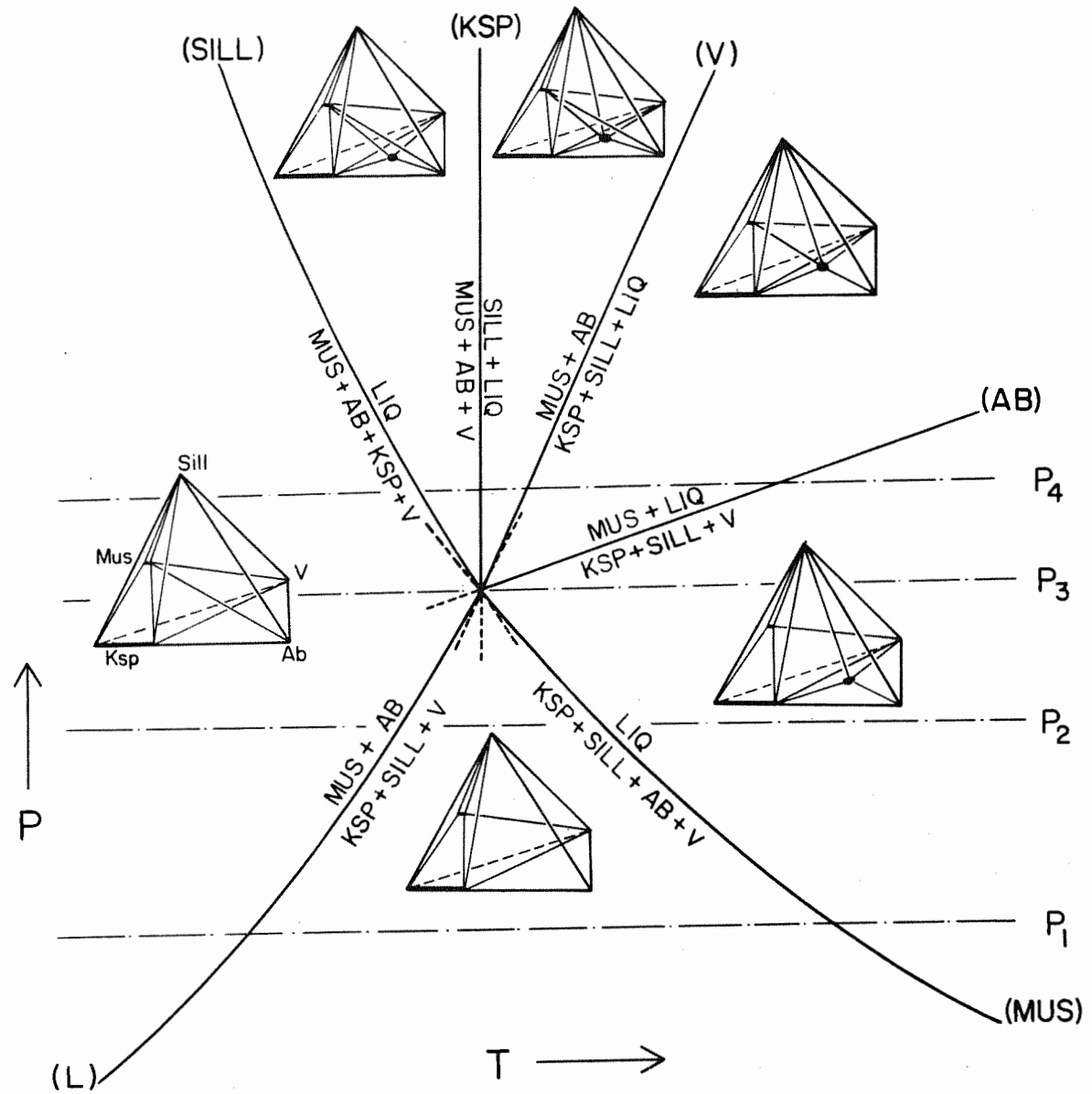

Fig. 22. Schematic invariant point for the SiO_2-saturated quaternary system $KAlSi_3O_8$-$NaAlSi_3O_8$-Al_2SiO_5-H_2O. The topology of the invariant point has been derived according to Schreinemakers' rules and its orientation established from known reaction curves (L) and (Mus). Slopes are not calculated but are qualitatively correct. In the chemographic representations, muscovite is not plotted at the proper location but is shifted in order to show more clearly the topologic relations of phases within each divariant field.
P_1 through P_4 refer to the positions of the isobaric $\underline{T}$ - $\underline{X}$ diagrams of Figure 23.

quaternary system Al_2SiO_5-$KAlSi_3O_8$-$NaAlSi_3O_8$-H_2O. The orientation of the diagram is based upon the known orientation of these two reactions:

$$Mus + Ab + Qz = Or + Sill + V. \quad (L)$$

$$Or + Ab + Qz + V = Liquid. \quad (Mus)$$

The slopes of the other curves have not been calculated but are estimated. It is apparent from Figure 22 that a thermal gradient at pressures above the invariant point, under vapor-saturated conditions, will produce the following sequence:

1) Melting of muscovite granite (Sill);
2) Melting in sill-bearing compositions (Ksp);
3) Dry melting of muscovite granite (V);
4) Dehydration of muscovite in presence of liquid (Ab).

This sequence of reactions is particularly important in its implications to the observed sequence of metamorphic and structural events in the Quabbin area, and will be discussed below.

Melting relations and solid-solid reactions in compositions saturated with quartz, vapor and aluminum silicate can also be portrayed in isobaric $\underline{T}$ - $\underline{X}$ sections for pressures above, below and at the invariant point. The sections in Figure 23 were constructed using the data of Eugster *et al.* (1972), Chatterjee (1972), Day (1973), Thompson and Waldbaum (1969) and Morse (1970). The pressures given in Figure 23 were based on the pressure of the invariant point which was estimated from the data given in Figure 19. In Figure 23, at pressures $\underline{P}_1$ and $\underline{P}_2$ below the invariant point, the solidus has not yet impinged upon any muscovite stability field. The $\underline{T}$ - $\underline{X}$ section at the invariant point

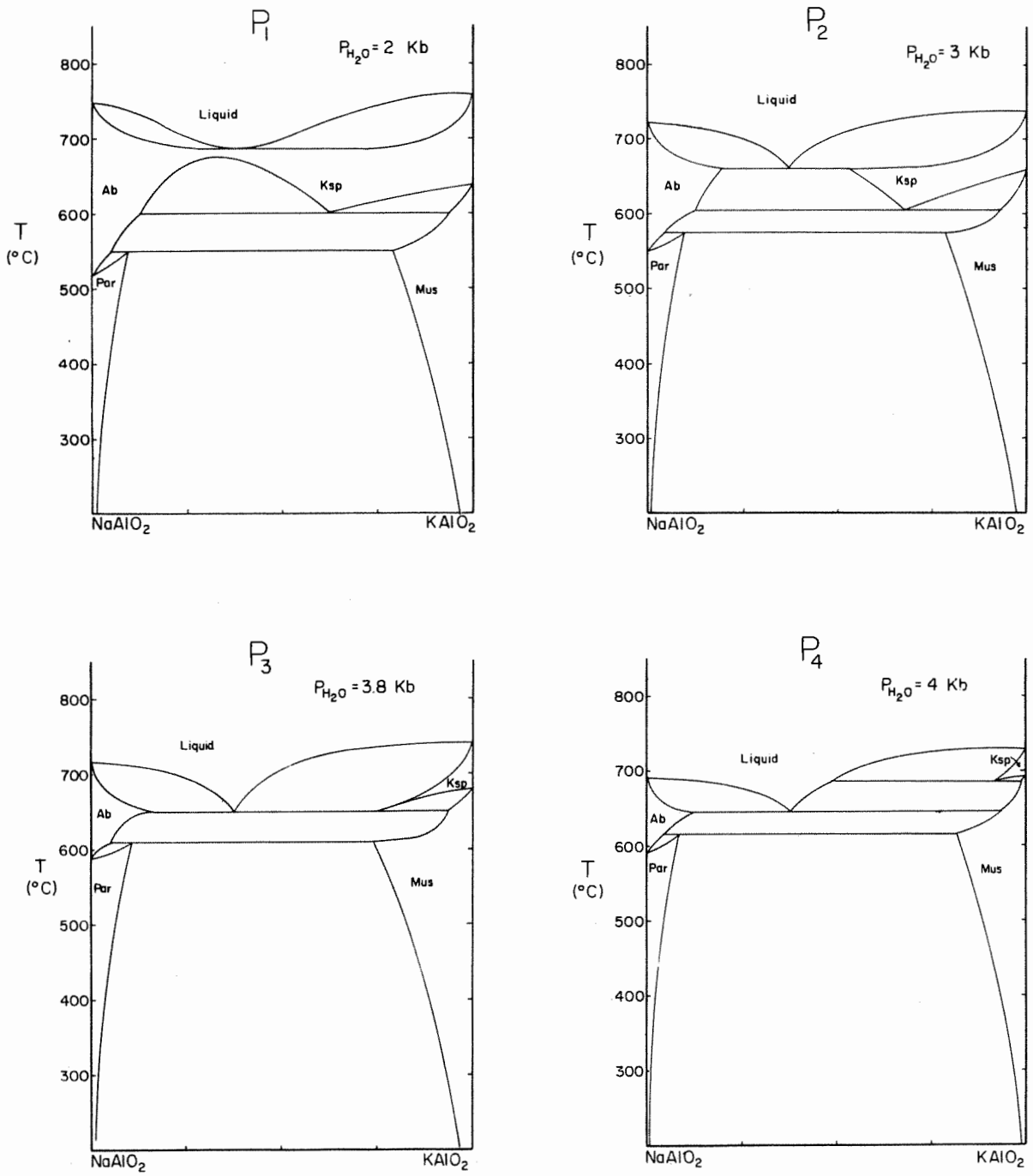

Fig. 23. Isobaric T - X plots for the SiO_2-, Al_2SiO_5- and vapor-saturated binary join $NaAlO_2$-$KAlO_2$ at four different values of P_{H_2O} above, below and at the invariant point of Figure 22.

Data for melting is from Morse (1970), for paragonite end-member relations from Chatterjee (1972), for muscovite end-member dehydration from Day (1973), for the feldspar two-phase field from Thompson and Waldbaum (1969) and for the mica two-phase field from Eugster et al (1972).

($\underline{P}_3$) shows the first coexistence of muscovite + liquid. At pressure $\underline{P}_4$ above the invariant point, the incongruent melting of muscovite clearly occurs at temperatures below the dehydration of muscovite.

An interpretation of the metamorphic and structural sequence in outcrops at Quabbin suggests that a melting event occurred early in the sequence, earlier than or contemporaneous with dehydration of muscovite to Ksp plus sillimanite. This is strong evidence that the reaction sequence at pressures above the invariant point of Figure 22 is not unlike the actual sequence observed in the Quabbin area.

System $\underline{CaO-Na_2O-K_2O-Al_2O_3-SiO_2-H_2O}$

The addition of calcium to the preceding system has one principal effect at high metamorphic grade -- it introduces the anorthite component into plagioclase and thus permits a closer approximation of natural assemblages. In order to portray the phase relations involving plagioclase rather than albite, it is useful to construct a tetrahedron by adding Ca to the AKNa triangle of Figure 18. This tetrahedron, discussed by Guidotti (1963), Robinson (1963) and Evans and Guidotti (1966), is shown in Figure 24a. Lighter tie lines show compositions of coexisting phases while the darker lines indicate the extent of the univariant four-phase volume mus-plag-or-sill. This volume is quite thin, as shown in Figure 24b, which is a projection from sillimanite onto the base of the tetrahedron. As noted by Robinson (1963) and Evans and Guidotti (1966), the position of this four-phase volume is a function of metamorphic grade. Precisely at the first coexistence of sillimanite and orthoclase (breaking the mus-ab tieline), the four-phase "volume" has zero thickness and the plagioclase apex lies exactly

at the albite corner. With increasing temperature the volume attains greater thickness as the composition of plagioclase in stable coexistence with mus + or + sill becomes more calcic, and the volume sweeps through the tetrahedron as indicated by the direction of the arrow in Figure 24b. It is apparent from the figure that orthoclase appears as a result of muscovite breakdown first in Ca-poor pelitic rocks and progressively later in Ca-richer bulk compositions. In addition, it is evident that in any individual rock the plagioclase must become more calcic between the first appearance of orthoclase and the final disappearance of muscovite. Figure 25 shows a typical bulk composition and the assemblages mus + Na-richer plag (before the reaction) and Ksp + Ca-richer plag (after the reaction). The sillimanite projection is used in Figure 26 to show actual compositions of muscovite, plagioclase and orthoclase in four-phase assemblages from the Quabbin area.

An important conclusion to be drawn from the above discussion, as noted by earlier workers, is that plagioclase composition in the four-phase assemblage may be used as an indicator of metamorphic grade. The phase relations indicate that for any bulk composition containing the assemblage mus + or + plag + sill (+ qz), the compositions of the four phases are fixed for any set of fixed physical conditions. Thus the plagioclase composition in the four-phase assemblage can be regarded as a function of the physical conditions. Considered from a different angle, this means that for <u>systematically</u> variable conditions the four-phase assemblage will have less calcic plagioclase at lower grade, and more calcic plagioclase at higher grade. This of course presumes no <u>local</u> variation in intensive variables, of which <u>a</u> H_2O is the only one likely to vary independently over small areas. Local variation in

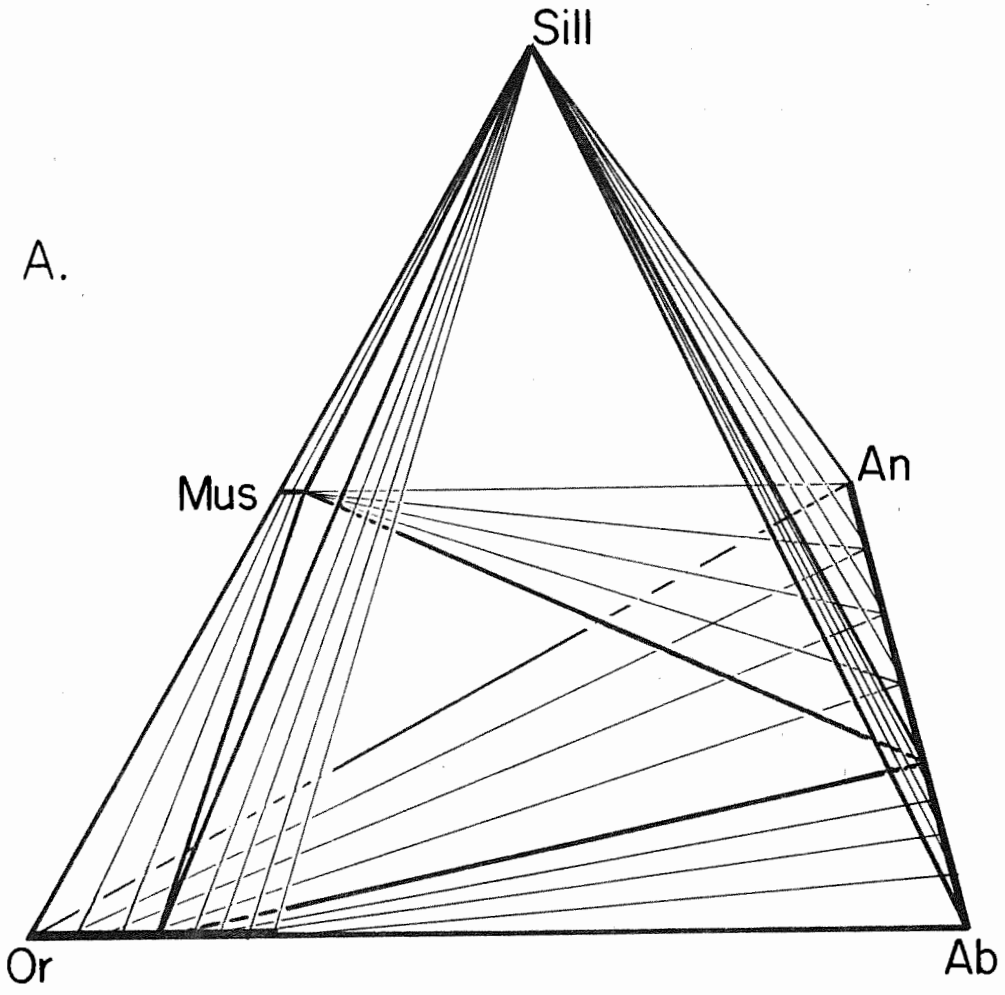

Fig. 24. a) AKNaCa tetrahedron after Evans and Guidotti (1966). Heavy lines within the tetrahedron delineate the four-phase volume mus-sill-or-plag.
b) Sillimanite projection in the AKNaCa tetrahedron onto the KNaCa base. The thinness of the four-phase volume is emphasized in this projection. The arrow shows the movement of the four-phase volume with increasing temperature. Note that plagioclase composition is a more sensitive indicator of movement than either muscovite or potassic feldspar.

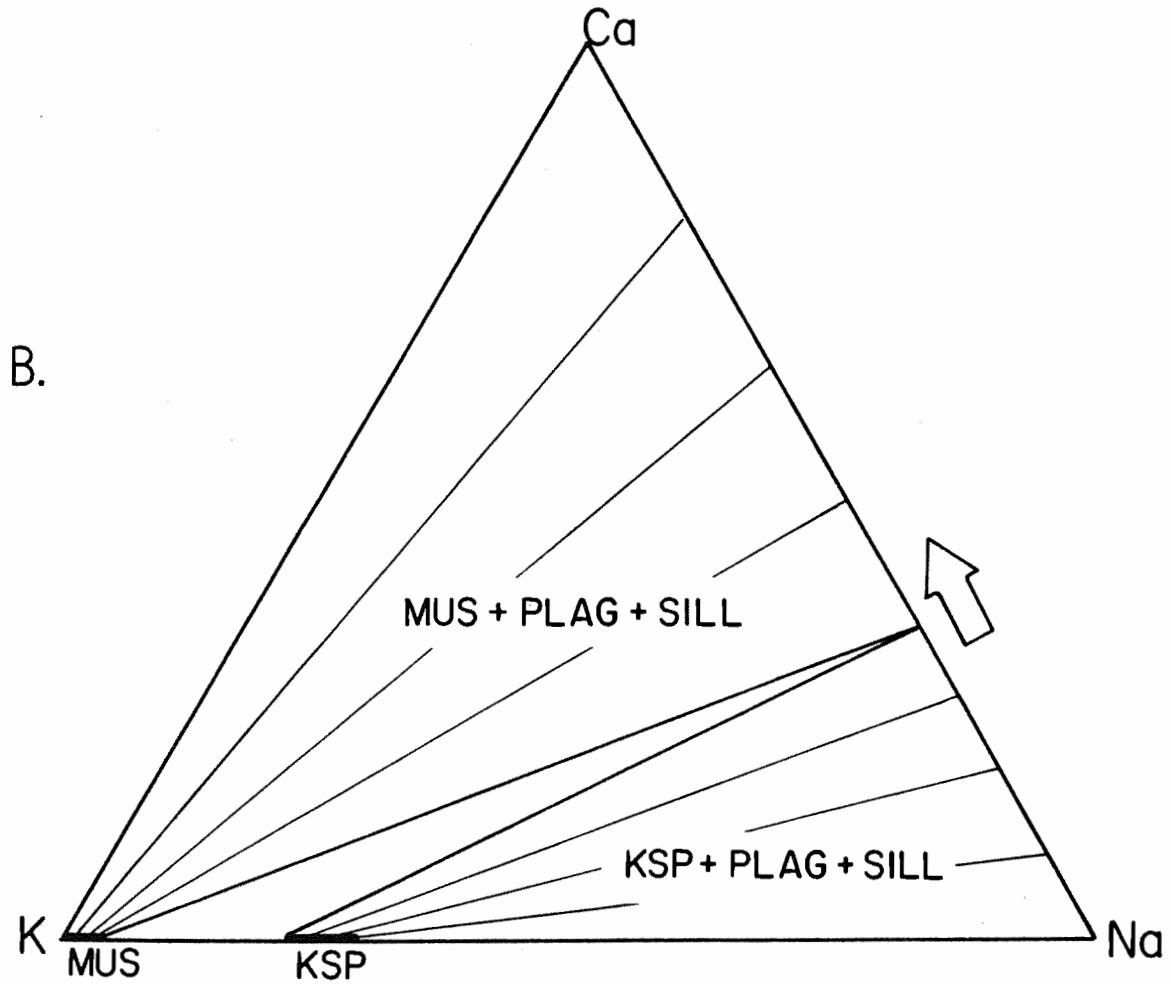
B.
Ca
MUS + PLAG + SILL
KSP + PLAG + SILL
K
Na
MUS
KSP

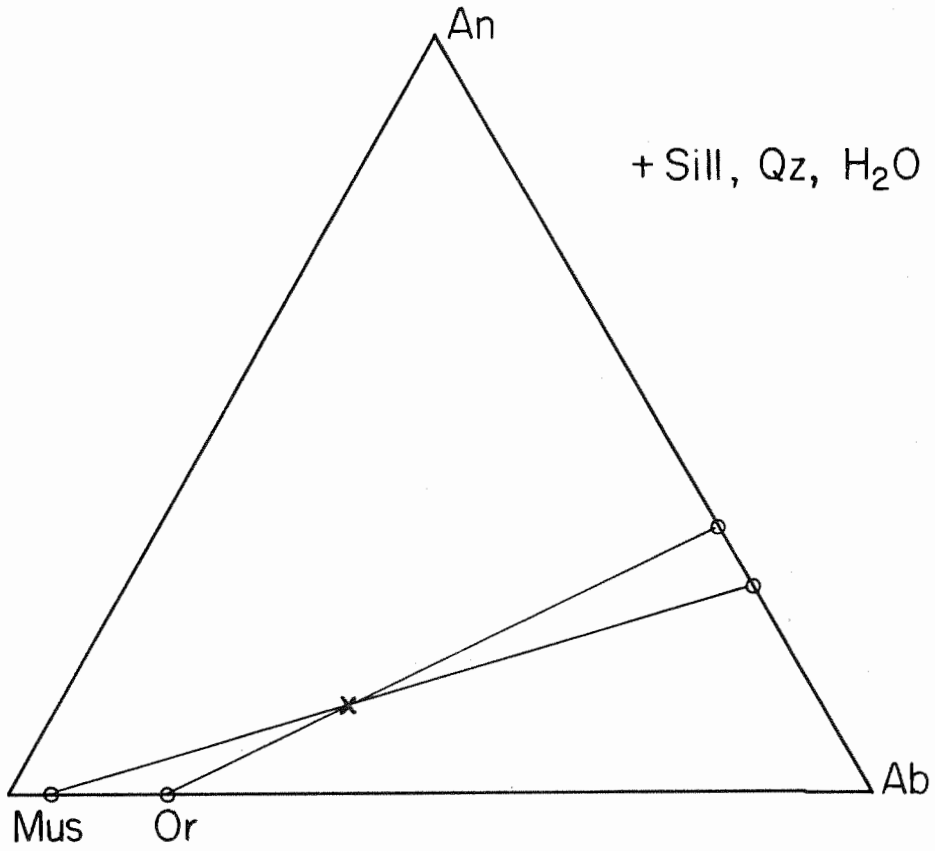

Fig. 25. Sillimanite projection in the AKNaCa tetrahedron, showing a typical bulk composition, X. The diagram illustrates the necessary change in plagioclase composition for a rock of this composition in the change from mus-sill-plag to or-sill-plag. The magnitude of change in this case is about 6 mol. % An.

intensive variables would probably be reflected by random rather than systematic compositional variation of plagioclase in the four-phase assemblage.

It is important to know the temperature interval over which muscovite breaks down in rocks of varying bulk composition. This question can be answered by applying results of experimental investigations. As shown above (Fig. 22), the minimum temperature of muscovite breakdown in the presence of a granitic liquid is given by the invariant point resulting from intersection of muscovite dehydration and granite melting curves in the Ca-free system. It has already been pointed out that

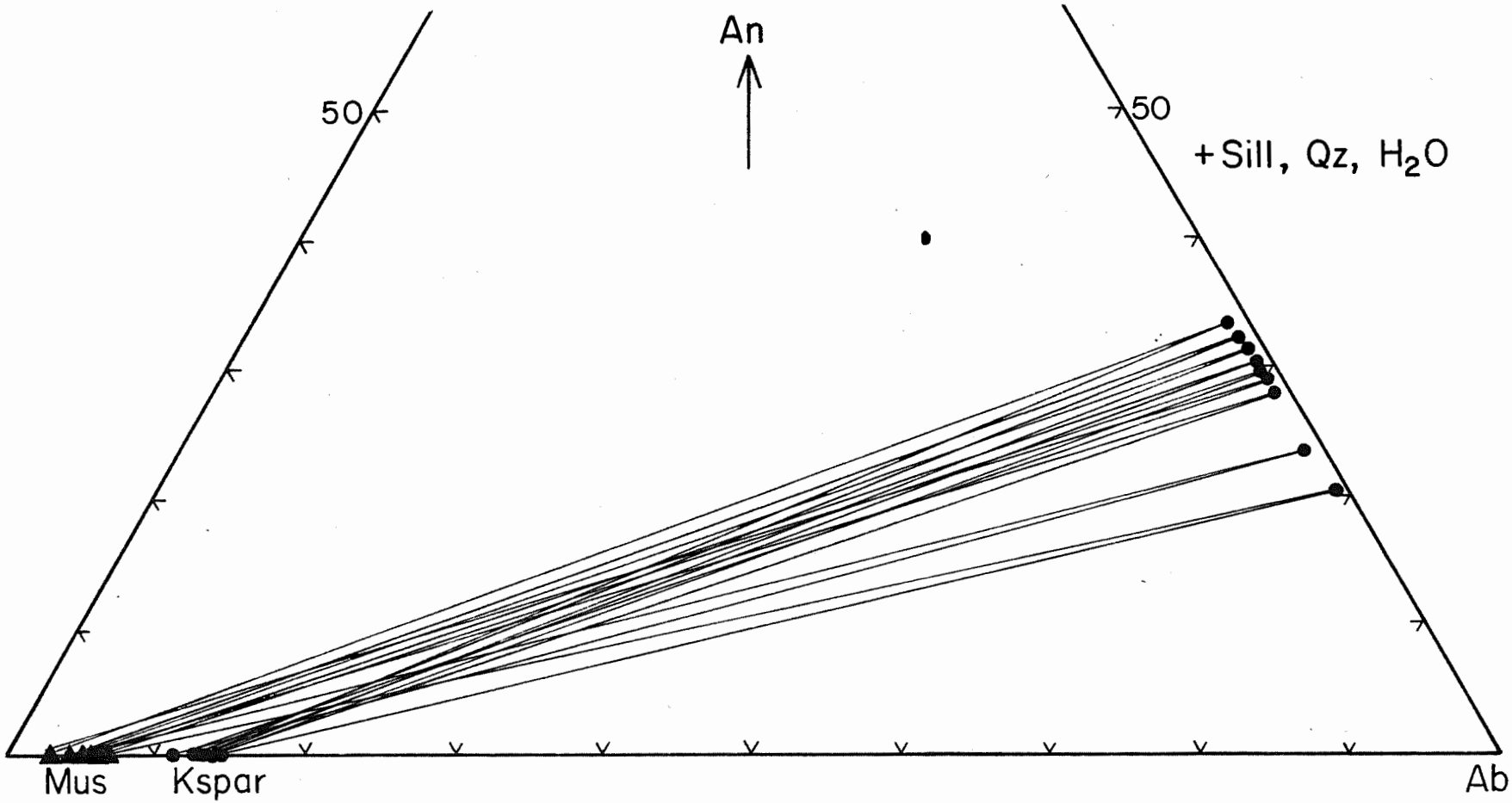

Fig. 26. Sillimanite projection onto the base of the AKNaCa tetrahedron showing the compositions of muscovite, orthoclase and plagioclase in mus-sill-or-plag-qz assemblages. This diagram emphasizes the narrow composition ranges of orthoclase and muscovite, and the relatively restricted range of plagioclase.

pure K-muscovite can only exist in a sodium-free environment (K/Na = ∞), that is, with pure Ca-plagioclase. Therefore, an invariant point (Ab) analogous to the one above (An) can be generated by the intersection of the dehydration curve of pure K-muscovite and the melting curve for Ksp + An + Qz + Sill + V. These two invariant points represent sections taken at the two different end compositions through a bundle of reaction surfaces in P - T - Composition space. The actual location of the Ca-free invariant point can be estimated by plotting the data of Kerrick (1972) on K,Na-muscovite dehydration and that of Luth, Jahns and Tuttle (1964) on granite melting. The Na-free point can be obtained by using the data of Day (1973) on the dehydration of pure K-muscovite and the melting curve for Ksp + An + Qz + V, extrapolated from the data of James and Hamilton (1969). These curves are plotted on Figure 27, which shows that the invariant points are only about 50°C apart, implying that the four-phase volume must sweep quite rapidly through the AKNaCa tetrahedron with increasing temperature. This means that changes in plagioclase composition might serve as a very sensitive indicator of increasing temperature in an area where four-phase assemblages occur. An attempt to apply this to the Quabbin rocks is reported in the next section.

It has been pointed out that muscovite breakdown in the Quabbin Reservoir area rocks was accompanied or preceded by production of a granitic partial melt. The melt composition can be closely approximated in the system CaO-Na_2O-K_2O-Al_2O_3-SiO_2-H_2O, specifically within the tetrahedron AKNaCa which has been discussed. The melt must interact with the four-phase volume mus-sill-Ksp-plag (see Fig. 24) over a certain range of T and P_f. The experimental curves plotted in Figure 27

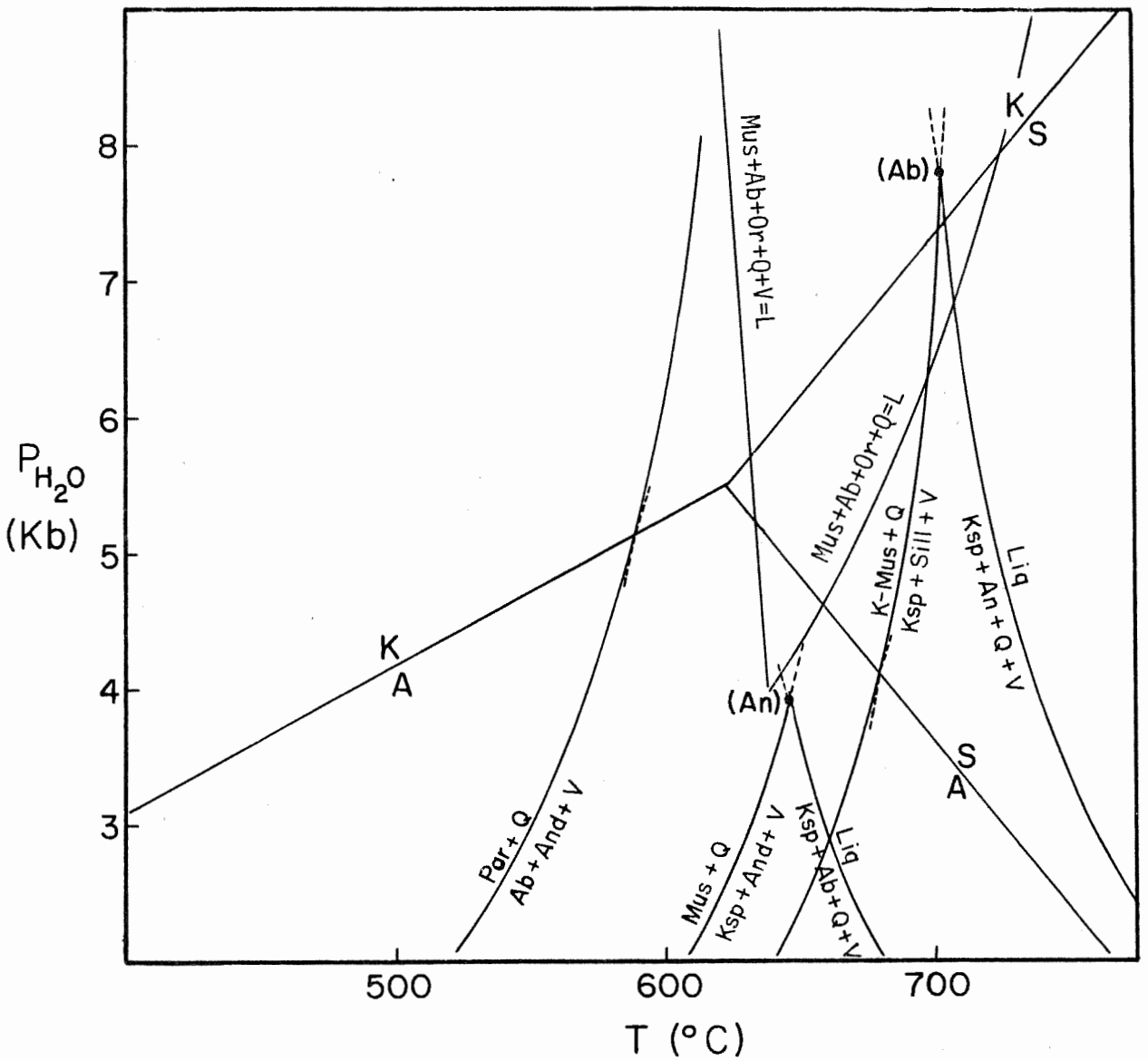

Fig. 27. P_{H_2O}-T projection showing invariant points generated by intersection of dehydration and melting reactions in Ca-free (An) and Na-free (Ab) systems. The muscovite dehydration curves are from Kerrick (1972) and Day (1973). Melting of or-ab-qz-v is from Luth, Jahns and Tuttle (1964) and melting of or-an-qz-v is extrapolated from data of James and Hamilton (1969). Also given are paragonite stability (Chatterjee, 1972) and the Al-silicate triple point (Richardson et al, 1969). The location of (An) is corroborated by the data on wet and dry melting of muscovite granite (Peto and Thompson, 1974) which must intersect at (An) (see Fig. 22). Note that the two invariant points, as plotted, are only about 50 °C apart.

can be used as a basis for interpreting the extent and nature of this interaction. At pressures below invariant point (An), there can be no interaction of melting and solid reaction. At all pressures between (An) and (Ab) a single topology is generated, changing only its shape at different pressures. This topology is illustrated in Figure 28 for a particular pressure, $\underline{P}_{H_2O}$ = 5 Kb. Under this condition, melt appears in the AKNaCa tetrahedron before sillimanite becomes stable with K-feldspar. But the four-phase volume mus-Ksp-sill-plag must sweep more rapidly through the tetrahedron than the volume mus (or Ksp)-sill-plag-liq because the slope of the solid reaction surface in $\underline{T}$ - Composition projection has a shallower slope than the melting surface, that is, it is more sensitive to temperature. This leads to the reaction at $\underline{T}_4$:

Mus + Liq = Ksp + Plag + Sill.

The sequence of ternary projections in Figure 28 ($\underline{T}_1$ through $\underline{T}_6$) represent increasing temperatures. These ternary diagrams can be used to construct pseudobinary $\underline{T}$ - $\underline{X}$ diagrams for plagioclase- and muscovite (or K-feldspar)-saturated portions of the sillimanite projections (labeled A and B in Fig. 28). These pseudobinary sections are useful for showing the sequence of events to be expected for different Ca/Na ratios. In the 5 Kb case illustrated in Figure 28, if the plagioclase is more sodic than An 43, melting will occur before muscovite dehydration; if it is more calcic, dehydration occurs first. Construction of these diagrams from experimental data (Fig. 27) for different $\underline{P}_{H_2O}=\underline{P}_t$ values gives this "changeover" composition as An 8 at 4 Kb, An 43 at 5 Kb and An 68 at 6 Kb. Since the most calcic plagioclase found in schist at Quabbin was about An 35, and since the pressure for the area

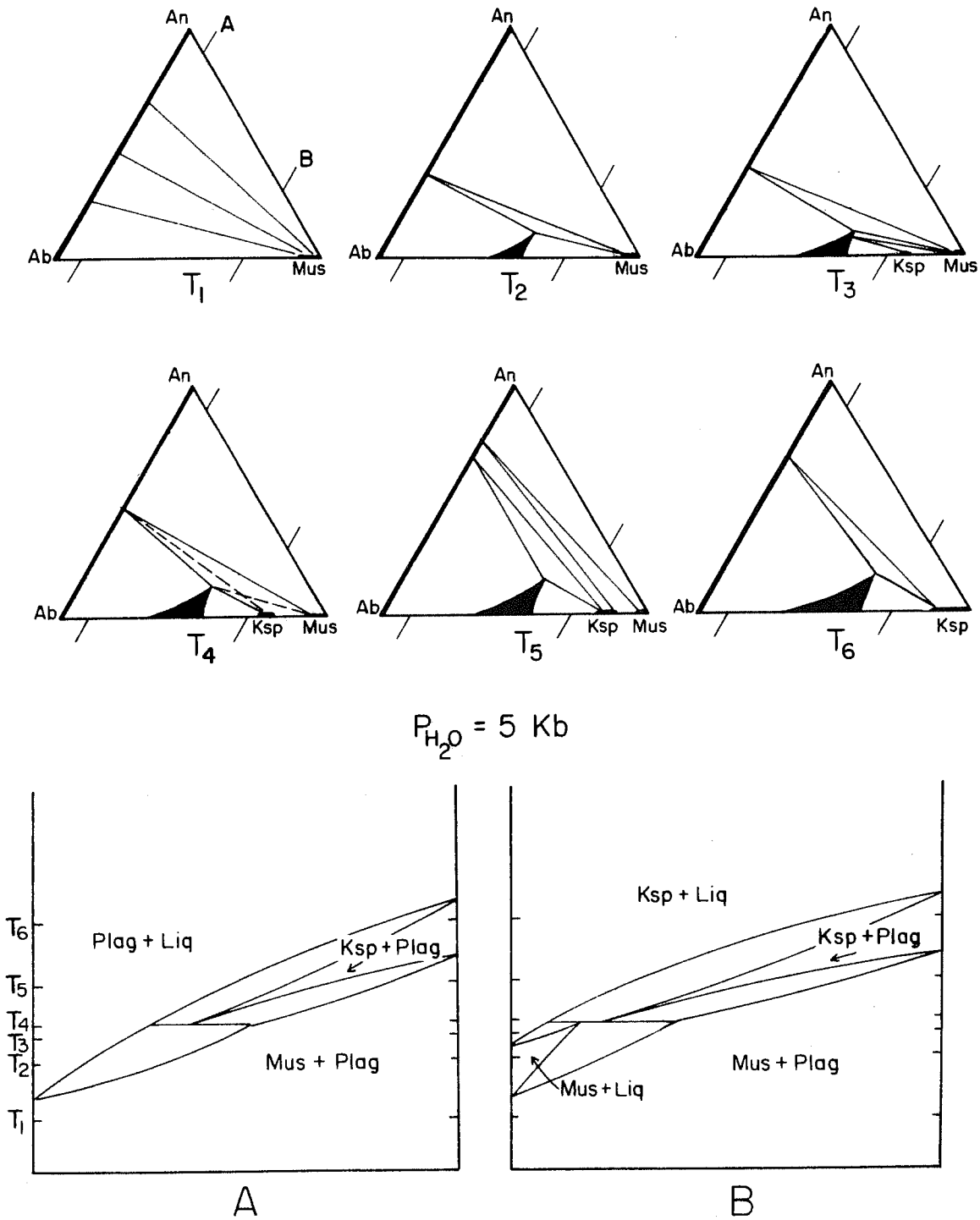

Fig. 28. Six isobaric and isothermal projections onto the KNaCa plane projected from qz, sill and H_2O, showing the interaction of solid and melting reactions in the AKNaCa tetrahedron. The isothermal diagrams are summarized on pseudobinary sections A and B for plagioclase-saturated or muscovite(or Ksp)-saturated compositions, respectively.

has been estimated at about 6 Kb, it would seem apparent that the Quabbin schists were on the melting side of the "changeover," in agreement with field relations.

The preceding discussion has assumed that $\underline{P}_{H_2O} = \underline{P}_t$, which is an unlikely condition for a natural system. In relating the foregoing theoretical discussion to the Quabbin field area, it is necessary to consider two things: 1) that the fluid phase was not pure H_2O, and 2) that $\underline{P}_f$ may not have been equal to $\underline{P}_t$, especially after the beginning of melting. As Kerrick (1972) notes, the data of French (1966) suggest that the maximum mole fraction of H_2O in a fluid phase which coexists with graphite is about 0.8, the remainder of the fluid consisting of CO_2 and other C-O-H gas species. This dilution will have the effect of lowering muscovite dehydration temperature and raising melting temperature, moving the invariant point (see Fig. 22) to higher $\underline{P}$ and $\underline{T}$. But considering that the gradient at Quabbin was still above the intersection of dehydration and melting curves for plagioclase compositions between An 15 and An 35, the physical conditions or fluid composition may have changed significantly upon the appearance of a melt fraction. If the regions of melt constituted a passageway for fluids to higher levels in the crust, then an equilibrium of the "fissure" type (Thompson, 1955) might have been established, with $\underline{P}_f < \underline{P}_t$. A likely concurrent effect would be strong fractionation of H_2O from fluid into melt, since the solubility of CO_2 (and probably other non-H_2O species) in granitic melt is practically nil (Eggler, Mysen and Seitz, 1974).

To model the possible effects on reaction and melting equilibria by a shift to fissure-type equilibrium, Figure 29 has been constructed from the data of Kerrick (1972). This pseudobinary diagram (similar to

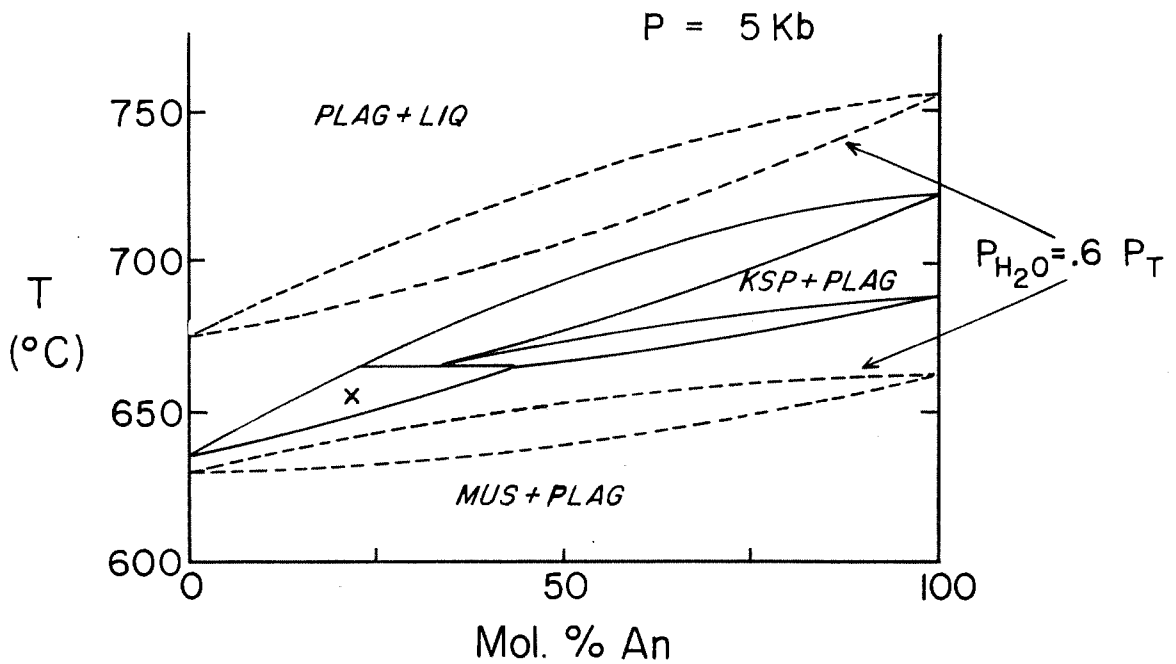

Fig. 29. Isobaric pseudobinary $\underline{T}$ - $\underline{X}$ section for the plagioclase saturated portion of the KNaCa projection, as in Fig. 28. Quartz, sillimanite and vapor are present in all fields. The solid-line section is for the condition $\underline{P}_{H_2O} = \underline{P}_t$ and the dotted-line section is for $\underline{P}_{H_2O} = .6\ \underline{P}_t$ (constructed from the data of Kerrick (1972). The diagram illustrates how a change in water vapor pressure can cause the isothermal transition (at point x in the diagram) from muscovite schist with coexisting melt to Ksp-sill schist with solidified migmatite.

those in Fig. 28) shows the position of melting and dehydration curves at 5 Kb for $\underline{P}_{H_2O} = \underline{P}_t$ and $\underline{P}_{H_2O} = .6\ \underline{P}_t$. It is apparent that, to a first approximation, this mechanism allows transition isothermally and isobarically from a muscovite schist with coexisting partial melt to sillimanite-Ksp schist with interlayered solid leucocratic granitic layers. The structural and metamorphic features observed at Quabbin suggest that muscovite dehydration and solidification of migmatites were nearly simultaneous, just prior to the second folding (see Table 1). The fissure-type equilibrium hypothesis provides a reasonable approximation of the observed geologic relations.

System K_2O-FeO-MgO-MnO-Al_2O_3-SiO_2-H_2O

This is the simplest system in which to model phase relations of ferromagnesian silicates in pelitic rocks (Thompson, 1957). For pelitic rocks of the Quabbin area, only biotite, garnet and cordierite need be considered in addition to muscovite (or Ksp) and quartz. The two alternative ways to portray the phase relations graphically are the A'KF projection (Eskola, 1915; Winkler, 1967) and projections within the AKFM tetrahedron (Thompson, 1957).

The A'KF projection (see Fig. 8) with the phases muscovite, orthoclase, biotite, garnet, cordierite and sillimanite plotted can be treated as a ternary phase diagram. Figure 30 shows this ternary system and part of the petrogenetic grid in $\underline{P}_{H_2O}$ - $\underline{T}$ space which can be constructed for it. The diagram is deceptively simple because it combines Fe, Mg and Mn and does not illustrate reactions and assemblages with varying Fe/Mg ratio. Most of the reactions are not simple univariant lines, as shown, but are at least divariant because of solid

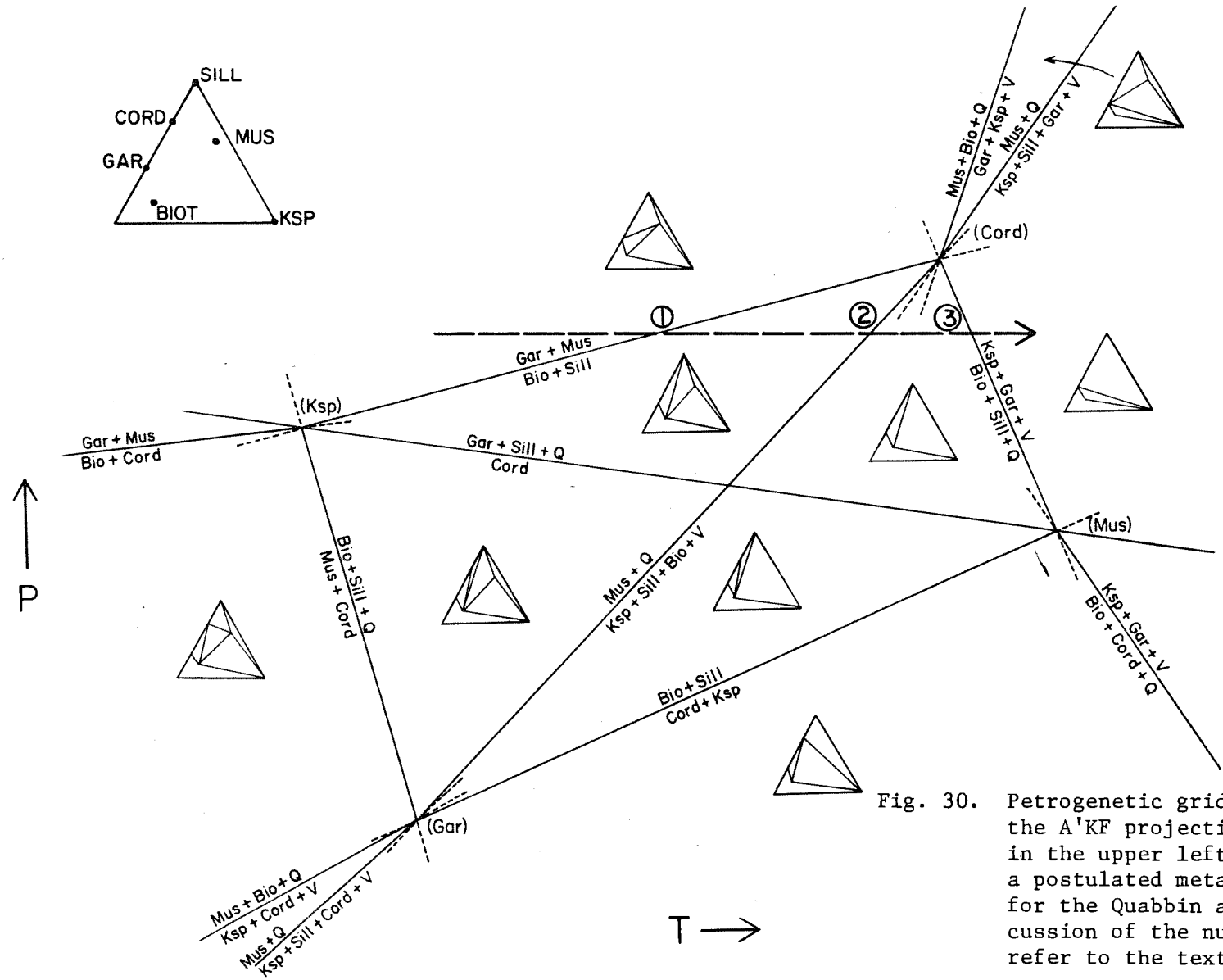

Fig. 30. Petrogenetic grid constructed for the A'KF projection illustrated in the upper left. The arrow shows a postulated metamorphic gradient for the Quabbin area. For discussion of the numbered reactions, refer to the text.

solution effects. But the grid is useful to show the general framework of metamorphic reactions which characterize the upper part of the sillimanite-muscovite zone and the sillimanite-orthoclase zone.

Three reactions on the grid are of particular relevance to the Quabbin Reservoir area. The first reaction, which has been discussed by Guidotti (1970), is:

$$\text{Garnet} + \text{Muscovite} = \text{Biotite} + \text{Sillimanite} + \text{Quartz}. \quad (1)$$

The significance of this reaction lies in the effect on Fe/Mg ratio of garnet and biotite, discussed in more detail below. The second reaction is muscovite dehydration:

$$\text{Muscovite} + \text{Quartz} = \text{Orthoclase} + \text{Sillimanite} + \text{Biotite} + \text{V}. \quad (2)$$

The phengite content of muscovite necessitates inclusion of a ferromagnesian phase as a product in this reaction. The final reaction is a garnet-producing one:

$$\text{Biotite} + \text{Sillimanite} + \text{Quartz} = \text{Garnet} + \text{Orthoclase} + \text{V}. \quad (3)$$

This reaction, like the first one above, has important effects on the compositions of garnet and biotite. There is evidence, discussed elsewhere in the paper, to suggest that these reactions have occurred in the Quabbin area. Cordierite has been included in the grid for completeness even though it has not been recognized in pelitic rocks in the area. It does occur in pelitic rocks in the next quadrangle to the east (Field, 1975).

The obvious weakness of the A'KF diagram is its lack of treatment of Fe/Mg ratios of minerals as variables of the system. This problem

is solved by use of the AFM projection (Thompson, 1957) in the AKFM tetrahedron (Fig. 31). It is legitimate to project within the tetrahedron from any phase which is a universal constituent of assemblages to be compared and which is of fairly constant composition. Since most of the Quabbin area schists contain alkali feldspar, the orthoclase corner has been used as a projection point, with phase compositions projected onto the front AFM face of the tetrahedron. It should be noted in Figure 31 that phengitic muscovite which coexists with orthoclase will plot near the Al-rich corner of the AFM diagram.

The general topology of the AFM projection for the lower-grade part of the sillimanite-orthoclase zone is shown in Figure 32a. For plotting purposes, Mn is considered to be minor and has been combined with Fe and the F corner. The majority of schists examined for this study have the three-phase assemblage sill-gar-bio, as noted by the X in Figure 32a. Two-phase assemblages sill-bio, as noted by X', should occur in more magnesian bulk compositions and should contain more magnesian biotite. Actual compositions obtained by electron microprobe are plotted in Figure 32b. Excluding muscovite, it is interesting that all the assemblages plotted are gar-sill-bio except three -- 853A, 849A and B35 -- which are sill-bio. Two of these rocks have the most magnesian biotites, which is expected. Not expected, however, is the spread of Fe/Mg ratios of garnets and biotites from different schists, all of which come from a very limited range of metamorphic grade. The explanation appears to lie in the behavior of the minor component MnO. A minor element may significantly affect phase relations if it does not occur in all phases of the assemblage; in this case, Mn is only present in significant quantity in garnet. The effect of Mn can be represented

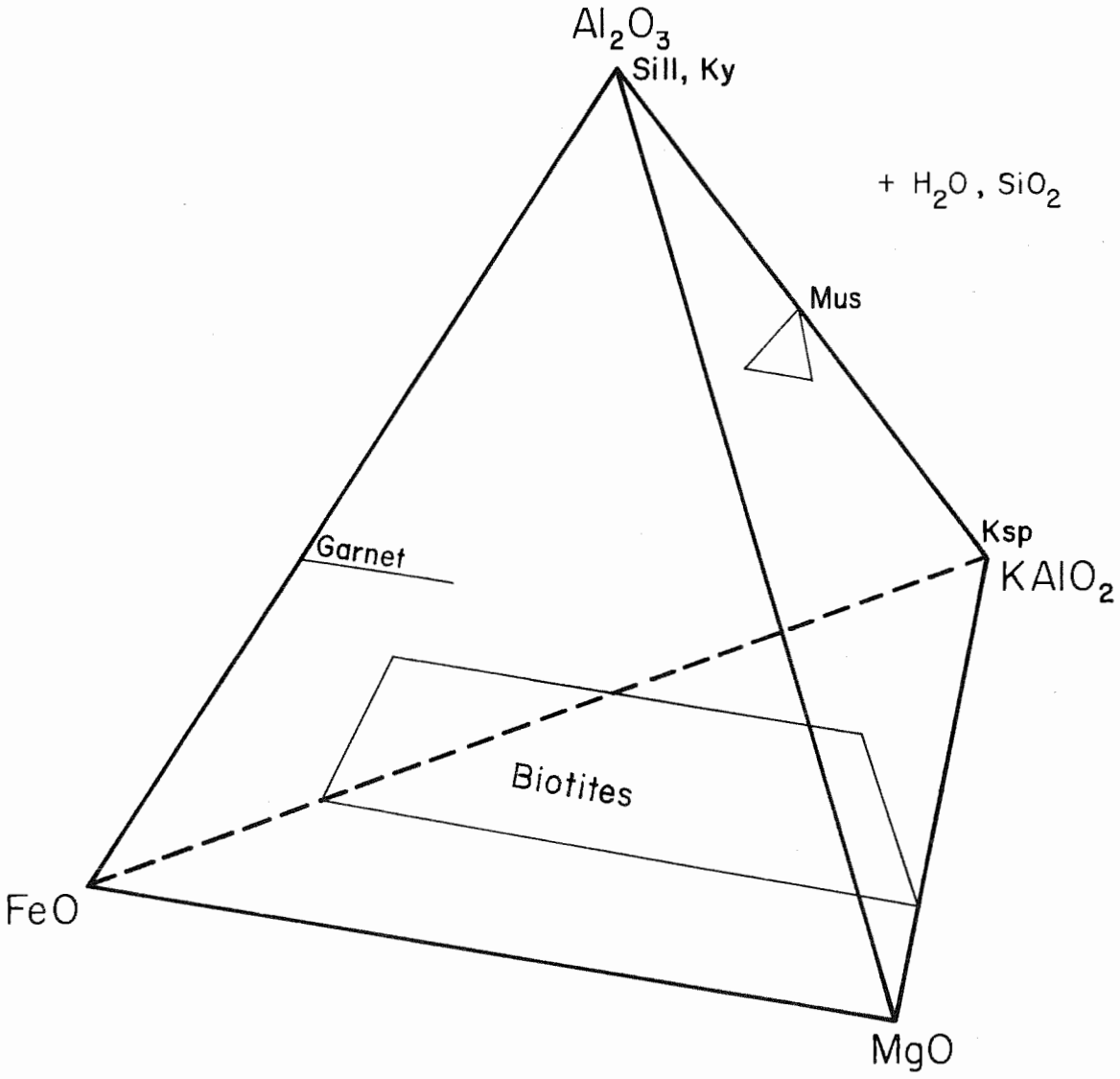

Fig. 31. AKFM tetrahedron, after Thompson (1957) showing approximate compositions for minerals found in schists at Quabbin. Note that the ferromagnesian component of muscovite requires that its composition field extend into the interior of the tetrahedron. If muscovite is present in Ksp-bearing rocks, it will be projected from Ksp to an area near the A apex of the front face in a standard Ksp projection (Barker, 1962).

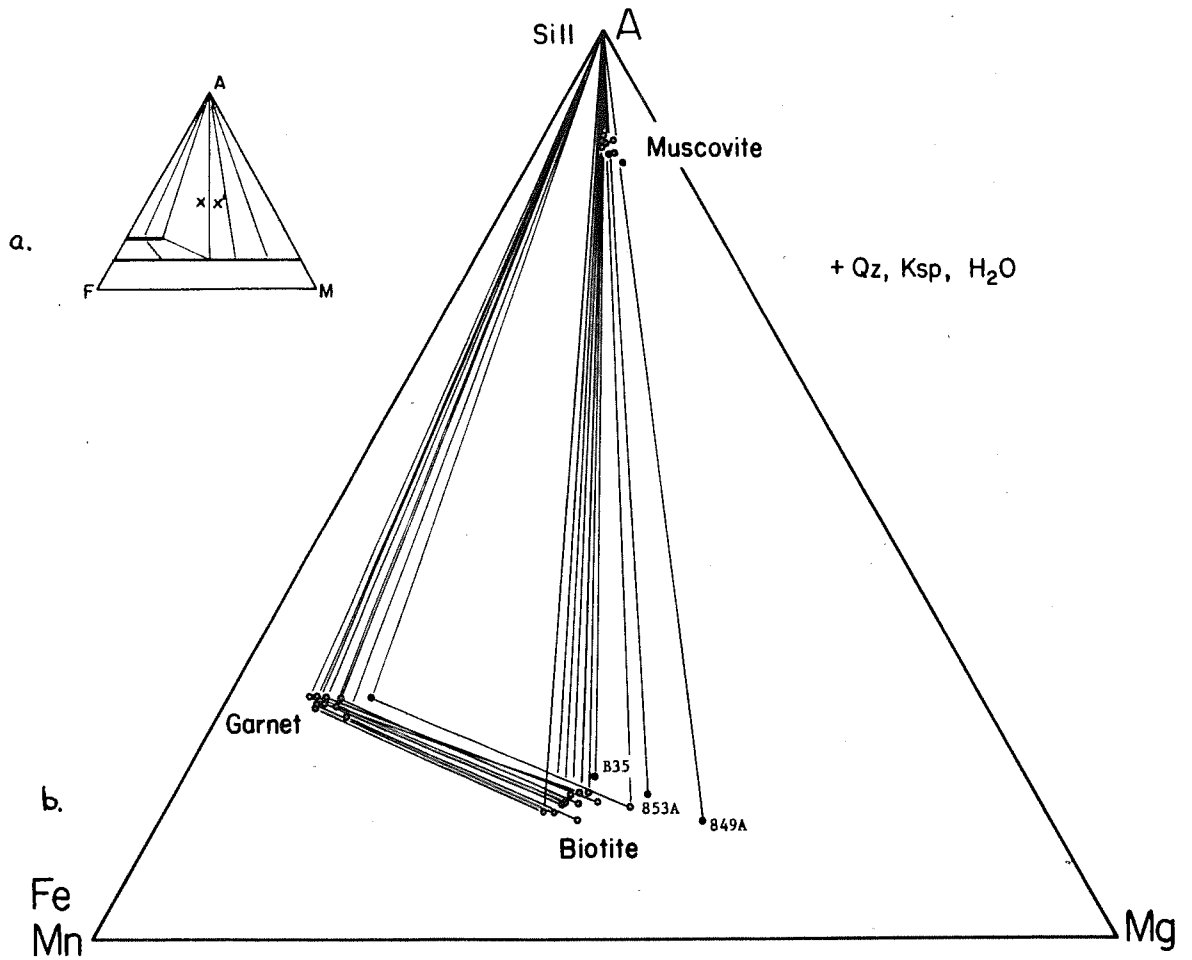

Fig. 32. a) Schematic AFM (Ksp) projection showing the two types of assemblages found at Quabbin - gar-bio-sill for bulk composition x and bio-sill for bulk composition x'.
b) Analyzed garnets, biotites and muscovites from Quabbin plotted on the Ksp projection. Note the three garnet-free rocks, B35, 853A and 849A; the explanation for the anomalous position of biotite B35 is discussed in the text. Also note the plotted position for muscovites in the assemblage mus-Ksp-sill-qz-biotite±gar.

graphically by expanding the AFM triangle of Figure 32 into an AFeMgMn tetrahedron. By projection from the A apex (sillimanite) onto the Fe-Mg-Mn base, the gar-sill-bio three-phase triangles are effectively expanded into the third dimension (Fig. 33). It is apparent that Mn behavior is systematic -- more manganese-rich garnet coexists with more magnesian biotite. The implication of this is that a rock with very low Mn content might have a bio-sill assemblage with biotite richer in iron than in a gar-sill-bio assemblage, apparently violating the topology of the AFM projection. This is an excellent example of the effects which minor elements may have on major element phase chemistry.

The compositional effects of reactions mentioned earlier may now be evaluated with AFM diagrams. For the reaction which may occur in the upper sillimanite zone,

$$\text{Gar} + \text{Mus} = \text{Bio} + \text{Sill} + \text{Qz},$$

it is apparent that decrease in garnet, while maintaining roughly constant garnet-biotite Fe/Mg fractionation, necessitates increasing the Fe/Mg ratio of coexisting garnet and biotite. In effect, this says that the sill-gar-bio three-phase triangle moves in the direction of Fe on the AFM diagram, as shown in Figure 34a, a continuous reaction destroying garnet. On the other hand, the sillimanite-orthoclase zone reaction

$$\text{Bio} + \text{Sill} = \text{Gar} + \text{Ksp} + \text{V}$$

must involve opposite movement of the three-phase triangle, a continuous reaction producing garnet (Fig. 34b). Petrologic evidence is ambiguous but does not preclude the first reaction in the Quabbin rocks. Evidence strongly suggests the occurrence of the second reaction. The

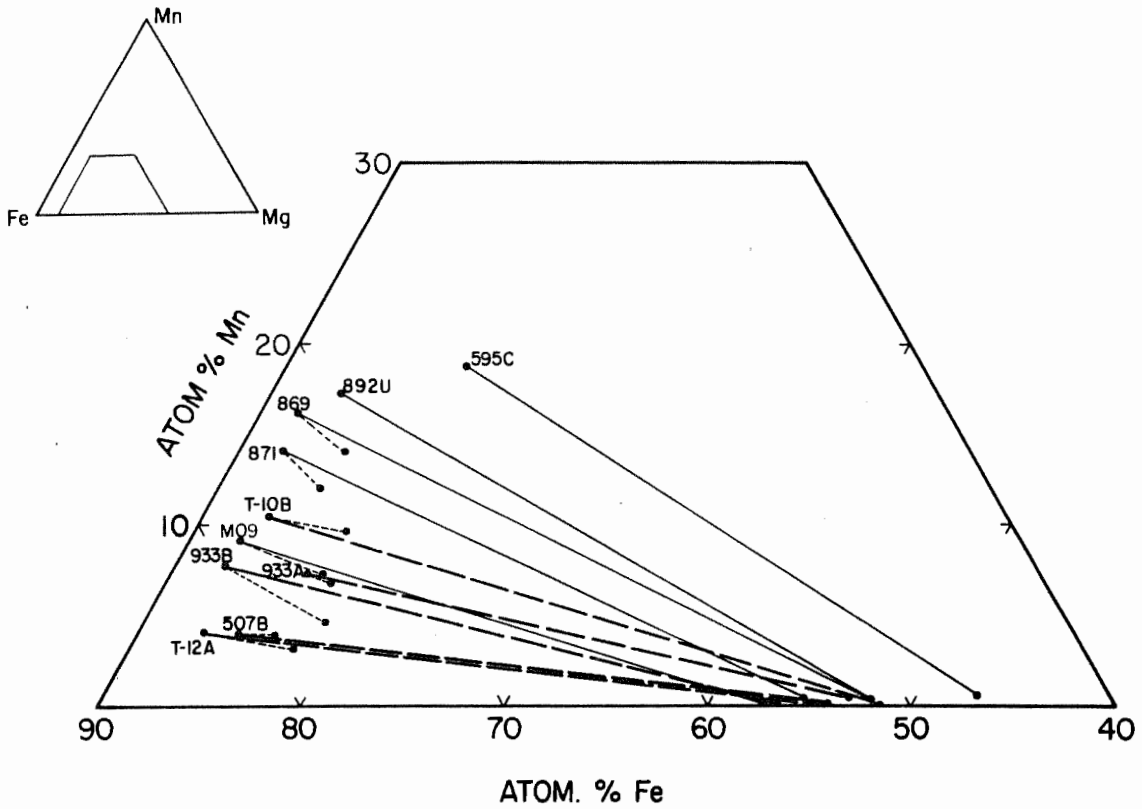

Fig. 33. Projection of sill-bio-gar three-phase triangles from sill onto the base of an AFeMgMn tetrahedron expanded from the AFM diagram. This figure illustrates the range of Mn content in garnet and how the Fe/Mg ratio of garnet and coexisting biotite are controlled by the Mn content of the garnet. The fine lines delineate gar-bio pairs from mus-bearing rocks; thick dashed lines indicate rocks which have Ksp and sill rather than muscovite. Tie lines connect garnet rims and biotites, but garnet cores are also plotted, connected by dashed lines with garnet rims.

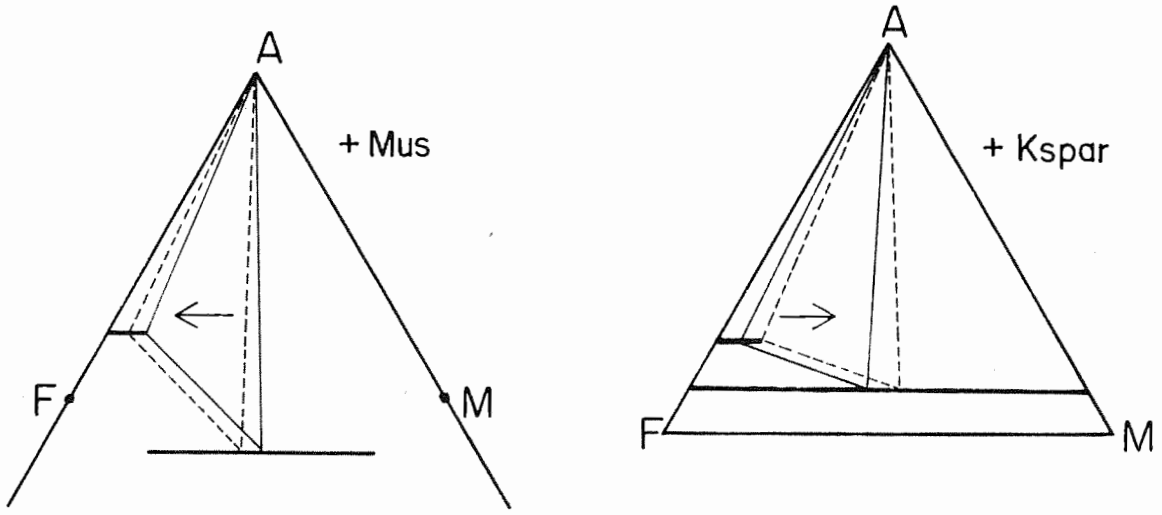

Fig. 34. a) AFM muscovite projection showing the shift in the sill-gar-bio three-phase field due to the continuous reaction Gar + Mus = Sill + Bio + Qz.
b) AFM Ksp projection with opposite shift in the three-phase field because of the continuous reaction Sill + Bio + Qz = Gar + Ksp + V.

importance of these reactions is that their effects might be recorded as zoning in the outer edges of garnets, making it hazardous to interpret reverse zoning as simple prograde or retrograde effects.

CONDITIONS OF METAMORPHISM

Plagioclase Isopleths

As noted in the previous section, the topology of the system CaO-Na_2O-K_2O-Al_2O_3-SiO_2-H_2O under conditions of heterogeneous equilibrium requires that plagioclase composition in the assemblage qz-plag-mus-or-sill be a function of metamorphic grade (see Figs. 24a and 24b). Figure 28 suggests the same systematic behavior of plagioclase composition in the assemblage qz-plag-mus-sill-melt. The implication of this systematic behavior is that the An content of plagioclase can provide an indicator of metamorphic gradient. An-richer plagioclase in the qz-plag-mus-sill-or(or melt) assemblage indicates higher temperature than more sodic plagioclase in the same assemblage. The presence of a qz-plag-mus-sill assemblage indicates that, for a particular plagioclase composition, temperature was too low to have initiated reaction. The assemblage qz-plag-sill-or(or melt) indicates that the reaction has gone to completion. Therefore these assemblages allow prediction of maximum and minimum temperatures, respectively.

Figure 35 shows an outline map of the northern part of the Greenwich syncline at Quabbin Reservoir and outcrop locations of samples with important assemblages. The triangular points are qz-plag-mus-sill-or assemblages and the round points are qz-plag-mus-sill or qz-plag-or-sill assemblages. Next to each point is the An content of plagioclase in that sample. Contours are based on triangular points, but the circular points provide some control, as noted above. The contours have

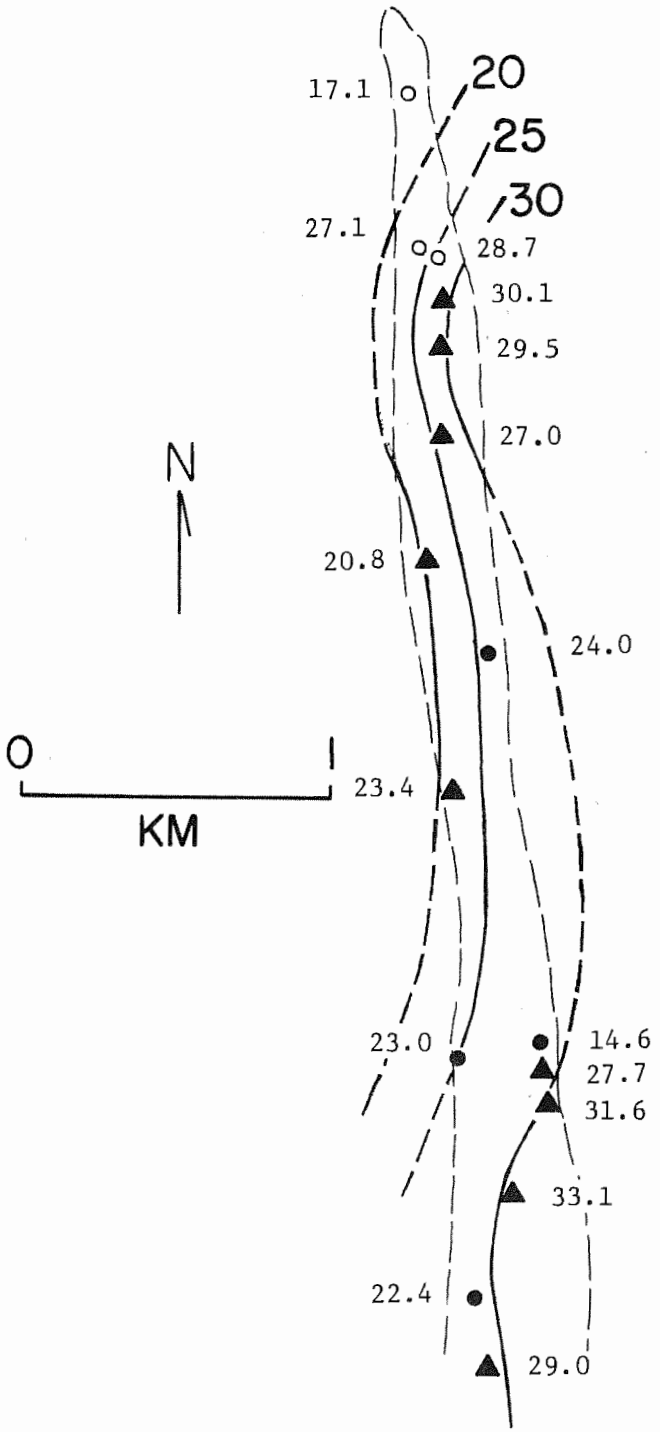

Fig. 35. Outline map of the Greenwich syncline at Quabbin Reservoir, with outcrop locations of analyzed samples. Triangles indicate the assemblage mus-or-sill-plag-qz; open circles are mus-sill-plag-qz rocks; closed circles are or-sill-plag-qz assemblages. Numbers beside each point are the An content of analyzed plagioclase. Contours are drawn on the basis of the triangular points, with some control from the other points, as noted in the text.

been drawn for the area using standard logical contouring techniques. Ideally, these contours are contours of equal metamorphic grade or, with slight simplification, of equal temperature. The increase in An content of contours from W to E is indicative of increasing temperature.

The experimental data in Figure 27 make it possible to quantify the contours. The temperature difference between invariant points (An) and (Ab) is about 55°C, which is the limit on temperature difference for 100% variation of Ca/Ca+Na. Assuming linear or nearly linear change of reaction curves with changing composition between the two invariant points, the range of plagioclase composition in qz-plag-mus-or-sill assemblages of about An 15 suggests that the temperature difference across the transition zone at Quabbin is about 10°C, or a gradient perpendicular to contours of 20 - 30°C/Km. This gradient seems rather low and is evidence that the present erosional surface intersects the metamorphic gradient at a low angle, as also appears to be the case in western Maine (Evans and Guidotti, 1966) and southeastern Connecticut (Lundgren, 1966). In Figure 36 the An contours are superimposed on the geologic map of the Quabbin Reservoir area (Robinson, 1967b). They are consistent with the general west to east trend to increasingly higher-grade metamorphic zones.

The systematic compositional behavior of coexisting minerals provides evidence that heterogeneous equilibrium was reached during metamorphism and that the variation in intensive variables was regional rather than local. This is an important implication in the contrast it provides between the Quabbin area and the Bryant Pond quadrangle and adjacent area in Maine (Evans and Guidotti, 1966). In Maine,

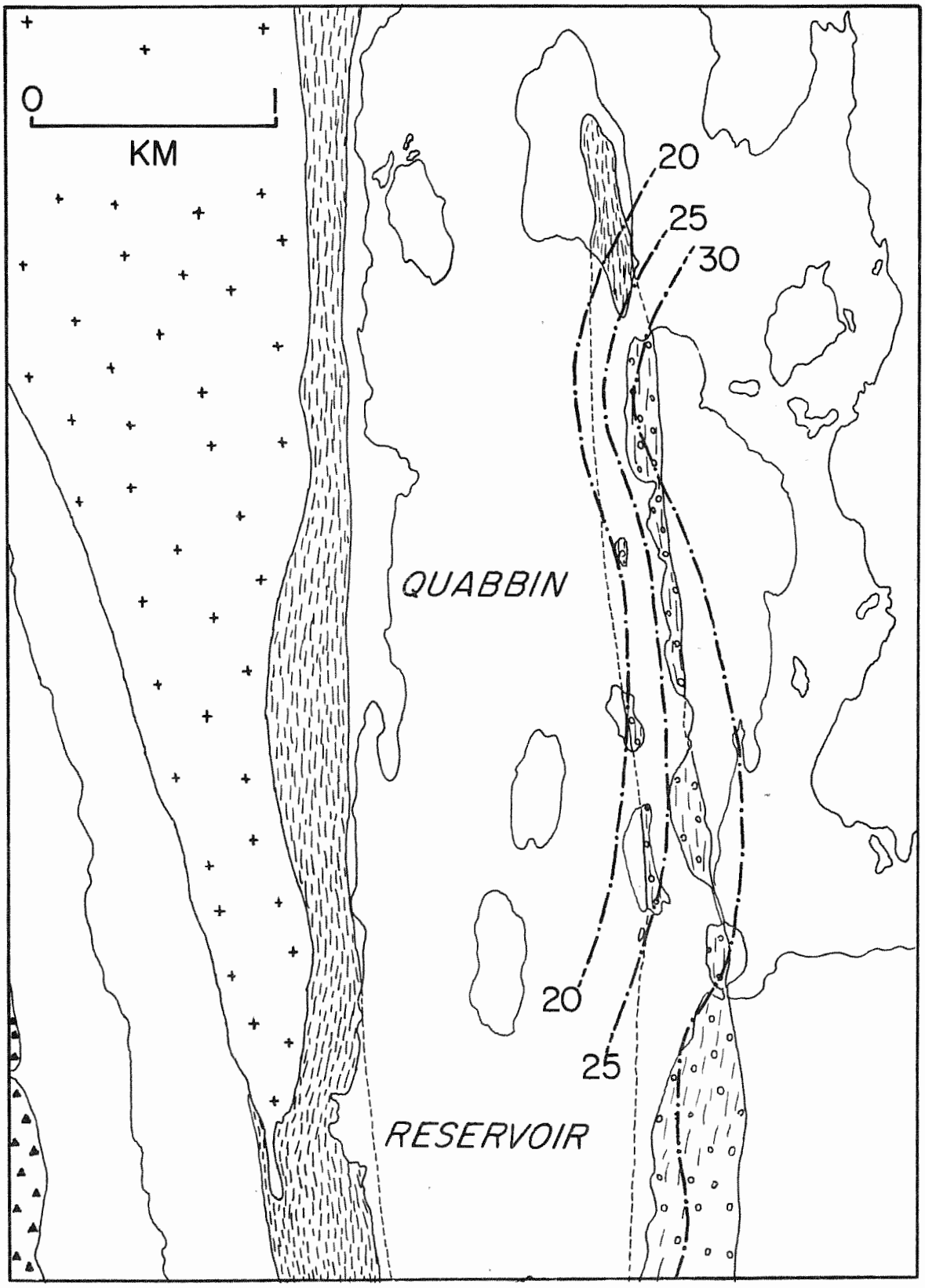

Fig. 36. Geologic map of the Quabbin Reservoir area showing distribution of assemblages in pelitic rocks (symbols the same as in Figure 2), with superimposed isopleths of plagioclase composition in the assemblage mus-or-sill-plag-qz. Note that the isopleths agree with the west to east progression to higher-grade metamorphic zones.

plagioclase composition in the assemblage qz-plag-mus-sill-or behaves randomly and has been interpreted by Evans and Guidotti as indicating local control of μH_2O. This may be caused, at least in part, by the contact-metamorphic nature of the metamorphism in Maine. The Quabbin area seems to display fairly pure regional metamorphism, in which regional control of intensive variables is more to be expected.

Evidence for Retrograde Metamorphism

The schists at Quabbin only rarely show evidence of major retrograde effects. Cross-cutting quartz veins and late pegmatites cause retrogression of sillimanite to muscovite aggregates in adjacent schists, but these effects are always quite local. Some schists contain chlorite of uncertain origin. Occurrence of chlorite is sporadic and none of the samples of this study showed any evidence of chloritization.

Garnet zoning, however, appears to be inconsistent with equilibration at highest metamorphic temperatures. High-grade garnets are typically homogeneous and other authors have suggested that Fe and/or Mn enrichment in garnet rims indicates re-equilibration at lower temperatures through either cooling or remetamorphism (Hess, 1971; Richardson, 1974). It has been noted in an earlier section of this paper that garnet rim compositions must be interpreted with caution. Continuous reactions which consume garnet will cause Fe-enrichment in the rims as a prograde effect. A better measure of prograde or retrograde nature of garnet zoning is the fractionation of Fe and Mg between garnet and biotite. Prograde compositional change will be reflected by both garnet and biotite, resulting in appropriate fractionation of Fe

and Mg. The K_D and temperature values in Table 14 suggest that the equilibrium between biotite and garnet edges reflects lower temperatures than biotite-garnet core pairs. Since biotite is homogeneous within any sample, it appears to have totally re-equilibrated. In the re-equilibration process, biotite will change Fe/Mg ratio much less than the garnet because there is much more modal biotite than garnet. This argument leads to the interpretation that garnet core - biotite pairs will be an accurate indicator of peak metamorphic temperatures while garnet rim - biotite pairs will give fractionation values indicative of lower-temperature compositional readjustment. If it is indeed valid to consider biotite composition as unchanged, then both sets of K_D values should be valid.

The retrograde process is illustrated in Figure 37, an AFM Ksp-projection. High-grade garnet and biotite compositions are indicated by A and A' and K_D is reflected by the length of the tie-line between them. A prograde reaction consuming garnet would produce garnet and biotite compositions B and B' and preserve a K_D similar to that between A and A'. Retrograde readjustment of garnet rim composition, however, will produce the tie-line from B to A', characterized by a lower K_D and indicative of lower temperature.

It is unclear whether the proposed lower-temperature re-equilibration is an effect of cooling (as suggested for rocks from Phillipston, Mass., by Richardson, 1974) or caused by a later, lower-grade metamorphic event, possibly Alleghenian, as suggested by Lundgren (1966). In any event, it appears that the only minerals which have demonstrably been affected are garnet and biotite. Muscovite and feldspar compositions seem to reflect peak metamorphic conditions.

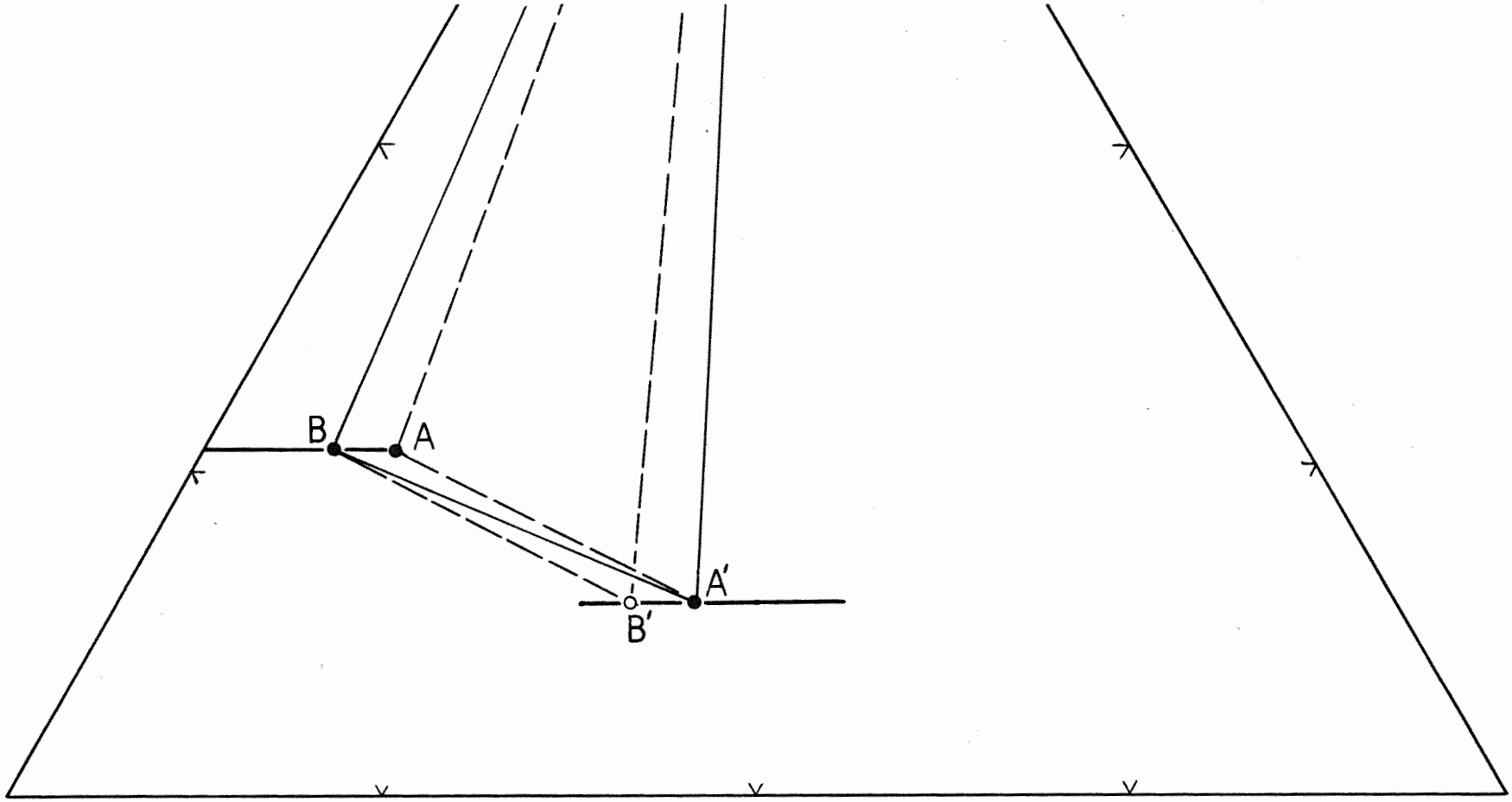

Fig. 37. Enlarged AFM (Ksp) projection showing postulated prograde and retrograde compositional relations between garnet and biotite. Gar-bio pair A-A' reflect high-grade conditions. A hypothetical prograde reaction consuming garnet would result in gar-bio pair B-B'. But in a rock with a minor amount of garnet relative to biotite, retrograde compositional readjustment will affect the garnet (probably only the rim) much more than the biotite, resulting in biotite-garnet rim Fe/Mg fractionation given by B-A'. The calculated K_D for this pair will yield a lower temperature.

REFERENCES

Albee, A.L. (1965) Phase equilibria in three assemblages of kyanite-zone pelitic schists, Lincoln Mountain quadrangle, central Vermont. J. Petrology 6, 246-301.

_____ (1972) Metamorphism of pelitic schists: reaction relations of chloritoid and staurolite. Geol. Soc. Am. Bull. 83, 3249-3268.

_____ and L. Ray (1970) Correction factors for electron probe microanalysis of silicates, oxides, carbonates, phosphates and sulfates. Anal. Chem. 42, 1408-1414.

Althaus, Egon, E. Karotke, K.H. Nitsch and H.G.F. Winkler (1970) An experimental reexamination of the upper stability limit of muscovite plus quartz. N. Jahrb. Mineral. Monatsh Jahrg. 7, 325-336.

Bambauer, H.V., M. Corlett, E. Eberhard, R. Gubser, F. Laves, H.-U. Nissen and K. Viswanathan (1965) Variations in X-ray powder patterns of low structural state plagioclase. Schweiz Mineral. und Petrogr. Mitt. 45, 327-330.

Barker, Fred (1962) Cordierite-garnet gneiss and associated microcline-rich pegmatite at Sturbridge, Massachusetts and Union, Connecticut. Am. Mineral. 47,907-918.

Bell, P.M. and G.L. Nord (1974) Microscopic and electron diffraction study of fibrolitic sillimanite. Carnegie Inst. Wash. Yearbook 73, 444-448.

Bence, A.E. and A.L. Albee (1968) Empirical correction factors for the electron microanalysis of silicates and oxides. J. Geol. 76, 382-403.

Cameron, W.E. and J.R. Ashworth (1972) Fibrolite and its relationship with sillimanite. Nature, Phys. Sci. 235, 134-136.

Carmichael, D.M. (1969) On the mechanism of prograde metamorphic reactions in quartz-bearing pelitic rocks. Contrib. Mineral. Petrology 20, 244-267.

Chatterjee, N.D. (1971) Preliminary results of the synthesis and upper stability of margarite. Naturwissenschaften 58, 147.

_____ (1972) The upper stability limit of the assemblage paragonite + quartz and its natural occurrences. Contrib. Mineral. Petrology 34, 288-303.

Chinner, G.A. (1965) The kyanite isograd in Glen Clova, Angus, Scotland. Min. Mag. 34, 132-143.

Currie, K.L. (1971) The reaction 3 cordierite = 2 garnet + 4 sillimanite + 5 quartz as a geological thermometer. Contrib. Mineral. Petrology 33, 215-226.

Day, H.W. (1973) The high temperature stability of muscovite plus quartz. Am. Mineral. 58, 255-262.

Deer, W.A., R.A. Howie and J. Zussman (1962) Rock Forming Minerals. Vol. 1, Ortho- and Ring Silicates. John Wiley and Sons, Inc., New York.

Donnay, G., J. Wyart and G. Sabatier (1960) The catalytic nature of high-low feldpsar transformations. Carnegie Inst. Wash. Yearbook 59, 173-174.

Eggler, D.H., B.O. Mysen and M.G. Seitz (1974) The solubility of CO_2 in silicate liquids and crystals. Carnegie Inst. Wash. Yearbook 73, 226-228.

Emerson, B.K. (1898) Geology of Old Hampshire County, Massachusetts. U.S. Geol. Survey Monograph 29, 790 p.

Ernst, W.G. (1963) Significance of phengitic micas from low-grade schists. Am. Mineral. 48, 1357-1373.

Eskola, Pentti (1915) On the relations between the chemical and mineralogical composition in the metamorphic rocks of the Orijarvi region. (In Norwegian with English summary). Bull. Comm. Geol. Finlande 44, 145 p.

Eugster, H.P., A.L. Albee, A.E. Bence, J.B. Thompson, Jr. and D.R. Waldbaum (1972) The two-phase region and excess mixing properties of paragonite-muscovite crystalline solutions. J. Petrology 13, 147-178.

Evans, B.W. (1965) Application of a reaction rate method to the breakdown equilibria of muscovite and muscovite + quartz. Am. J. Sci. 263, 647-667.

_____ and C.V. Guidotti (1966) The sillimanite-potash feldspar isograd in western Maine, U.S.A. Contrib. Mineral. Petrology 12, 25-62.

Field, M.T. (1975) The Bedrock Geology of the Ware area, west-central Massachusetts. Ph.D. Thesis, University of Massachusetts, Amherst, Massachusetts.

French, B.M. (1966) Some geological implications of equilibrium between graphite and a C-H-O gas at high temperatures and pressures. Rev. Geophysics 4, 223-253.

Guidotti, C.V. (1963) Metamorphism of the pelitic schists in the Bryant Pond quadrangle, Maine. Am. Mineral. 48, 772-791.

_____ (1970) The mineralogy and petrology of the transition from the lower to upper sillimanite zone in the Oquossoc Area, Maine. J. Petrology 11, 277-336.

_____ (1973) Compositional variation of muscovite as a function of metamorphic grade and assemblage in metapelites from N. W. Maine. Contrib. Mineral. Petrology 42, 33-41.

_____, H.H. Herd and C.L. Tuttle (1973) Composition and structural state of K-feldspars from K-feldspar + sillimanite grade rocks in northwestern Maine. Am. Mineral. 58, 705-716.

Hall, D.J. (1970) Compositional Variations in Biotites and Garnets from Kyanite and Sillimanite Zone Mica Schists, Orange Area, Massachusetts and New Hampshire. M.S. Thesis, University of Massachusetts, Amherst, Massachusetts, 110 p.

Heald, M.T. (1950) Structure and petrology of the Lovewell Mt. quadrangle, New Hampshire. Geol. Soc. Am. Bull. 61, 43-89.

Hess, P.C. (1969) The metamorphic paragenesis of cordierite in pelitic rocks. Contrib. Mineral. Petrology 24, 191-207.

_____ (1971) Prograde and retrograde equilibria in garnet-cordierite gneisses in south-central Massachusetts. Contrib. Mineral Petrology 30, 177-195.

Hietanen, Anna (1969) Distribution of Fe and Mg between garnet, staurolite and biotite in aluminum-rich schist in various metamorphic zones north of the Idaho Batholith. Am. J. Sci. 267, 422-456.

Holdaway, M.J. (1971) Stability of andalusite and the aluminum-silicate phase diagram. Am. J. Sci. 271, 97-131.

Hollister, L.S. (1966) Garnet zoning: an interpretation based on the Rayleigh Fractionation Model. Science 154, 1647-1651.

Hounslow, A.W. and J.M. Moore, Jr. (1967) Chemical petrology of Grenville schists near Fernleigh, Ontario. J. Petrology 8, 1-28.

James, R.S. and D.L. Hamilton (1969) Phase relations in the system $NaAlSi_3O_8$-$KAlSi_3O_8$-$CaAl_2Si_2O_8$-SiO_2 at 1 kilobar water vapor pressure. Contrib. Mineral. Petrology 21, 111-141.

Kerrick, D.M. (1972) Experimental determination of muscovite + quartz stability with $P_{H_2O} < P_{Total}$. Am. J. Sci. 272, 946-958.

Kretz, Ralph (1961) Some applications of thermodynamics to coexisting minerals of variable composition. Examples: orthopyroxene-clinopyroxene and orthopyroxene-garnet. J. Geology 69, 361-387.

Kwak, T.A.P. (1968) Ti in biotite and muscovite as an indication of metamorphic grade in almandine amphibolite facies rocks from Sudbury, Ontario. Geochim. Cosmochim. Acta 32, 1222-1229.

Lundgren, L.W. (1966) Muscovite reactions and partial melting in southeastern Connecticut. J. Petrology 7, 421-453.

Luth, W.C., R.H. Jahns and O.F. Tuttle (1964) The granite system at pressures of 4 to 10 kilobars. J. Geophys. Res. 69, 759-773.

Lyons, J.B. and S.A. Morse (1970) Mg/Fe partitioning in garnet and biotite from some granitic, pelitic and calcic rocks. Am. Mineral. 55, 231-245.

Morse, S.A. (1970) Alkali feldspars with water at 5 kb pressure. J. Petrology 11, 221-253.

Naylor, R.S., G.M. Boone, E.L. Boudette, D.D. Ashenden and Peter Robinson (1973) Pre-Ordovician rocks in the Bronson Hill and Boundary Mountain anticlinoria, New England, U.S.A. Trans. Am. Geophys. Union 54, 495.

Newton, R.C. and J.R. Goldsmith (1973) "Hydrothermal" reactions with traces of H_2O at high pressures. Trans. Am. Geophys. Union 54, 482.

Peper, J.D. (1967) Stratigraphy and structure of the Monson area, Massachusetts and Connecticut. In: New England Intercollegiate Geological Conference, 59th Ann. Mtg., Guidebook, 105-113.

Peto, Peter and A.B. Thompson (1974) Wet and dry melting of white mica - alkali feldspar assemblages. Am. Geophys. Union Trans. 55, 479.

Richardson, S. M. (1974) Cation exchange reactions and metamorphism of high-grade pelites in central Massachusetts. Geol. Soc. Am., Abstracts with Programs for 1974, 1059

Richardson, S.W., M.C. Gilbert and P.M. Bell (1969) Experimental determination of kyanite-andalusite and andalusite-sillimanite equilibria: the aluminosilicate triple point. Am. J. Sci. 267, 259-272.

Robinson, Peter (1963) Gneiss Domes of the Orange Area, Massachusetts and New Hampshire. Ph.D. Thesis, Harvard University, Cambridge, Massachusetts, 253 p.

_____ (1967a) Gneiss domes and recumbent folds of the Orange area, west-central Massachusetts. In: New England Intercollegiate Geological Conference, 59th Ann. Mtg., Guidebook, 17-47.

_____ (1967b) Geology of the Quabbin Reservoir area, central Massachusetts. In: New England Intercollegiate Geological Conference, 59th Ann. Mtg., Guidebook, 114-127.

Saxena, S.K. and N.B. Hollander (1969) Distribution of iron and magnesium in coexisting biotite, garnet and cordierite. Am. J. Sci. 267, 210-216.

Shaw, D.M. (1956) Geochemistry of pelitic rocks III: Major elements and general geochemistry. Geol. Soc. Am. Bull. 67, 919-934.

Smith, J.V. (1972) Critical review of synthesis and occurrence of plagioclase feldspars and a possible phase diagram. J. Geology 80, 505-525.

Stewart, D.B. and P.H. Ribbe (1969) Structural explanation for variations in cell parameters of alkali feldspar with Al/Si ordering. Am. J. Sci. 267A, 444-462.

Sturt, B.A. (1962) The composition of garnets from pelitic schists in relation to the grade of metamorphism. J. Petrology 3, 181-191.

Thompson, A.B. (1974) Calculation of muscovite-paragonite-alkali feldspar phase relations. Contrib. Mineral. Petrology 44, 173-194.

Thompson, J.B., Jr. (1955) Thermodynamic basis for the mineral facies concept. Am. J. Sci. 253, 65-103.

_____ (1957) The graphical analysis of mineral assemblages in pelitic schists. Am. Mineral. 42, 842-858.

_____ (1961) Mineral facies in pelitic schists. In: G.A. Sokolov, Ed., Physicochemical Problems in the Formation of Rocks and Mineral Deposits. Akad. Nauk, SSSR, Moscow, 313-325 (In Russian with English Summary).

_____, Peter Robinson, T.N. Clifford and N.J. Trask (1968) Nappes and gneiss domes in west-central New England. In: Zen, E-An, W.S. White, J.B. Hadley and J.B. Thompson, Jr., Eds., Studies of Appalachian Geology: Northern and Maritime. John Wiley and Sons, Inc, New York, 203-218

_____ and D.R. Waldbaum (1969) Mixing properties of sanidine crystalline solutions: III. Calculations based on two-phase data. Am. Mineral 54, 811-838.

Tuttle, O.F. and N.L. Bowen (1958) Origin of Granite in Light of Experimental Studies. Memoir 74, Geol. Soc. Am., New York, 153 p.

Velde, B. (1965) Phengite micas: synthesis, stability and natural occurrence. Am. J. Sci. 263, 886-913.

Winkler, H.G.F. (1967) Petrogenesis of Metamorphic Rocks. Springer-Verlag, New York, 237 p.

Wright, T.L. and D.B. Stewart (1968) X-ray and optical study of alkali feldspar: I. Determination of composition and structural state from refined unit cell parameters and 2V. Am. Mineral. 53, 38-87.

Zen, E-An (1969) The stability relations of the polymorphs of aluminum silicate: a survey and some comments. Am. J. Sci. 267, 297-309.

APPENDIX

Garnets from two samples, 933B and T12A, have been analyzed in considerable detail with the microprobe. Profiles were analyzed on each garnet, and the results were presented graphically in Figure 10. Maps for the two garnets are shown in Figures A-1 and A-2 with the locations of all analyses indicated. The numbers refer to the analyses tabulated in Tables A-1 and A-2.

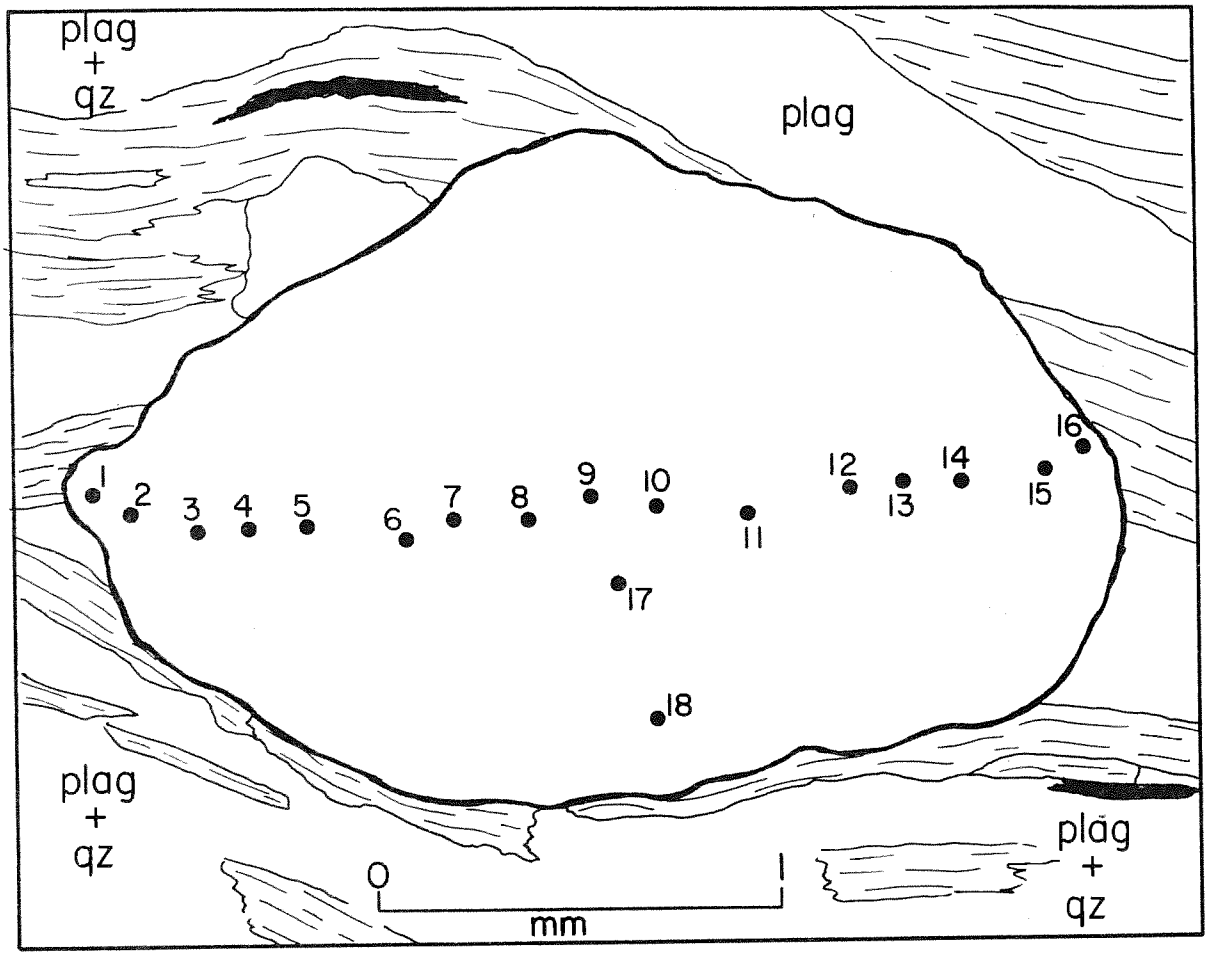

Fig. A-1. Sketch of garnet from T12A. Spots are locations of microprobe analyses tabulated in Table A-1. Analyses 1 to 16 are shown as the profile in Fig. 10.

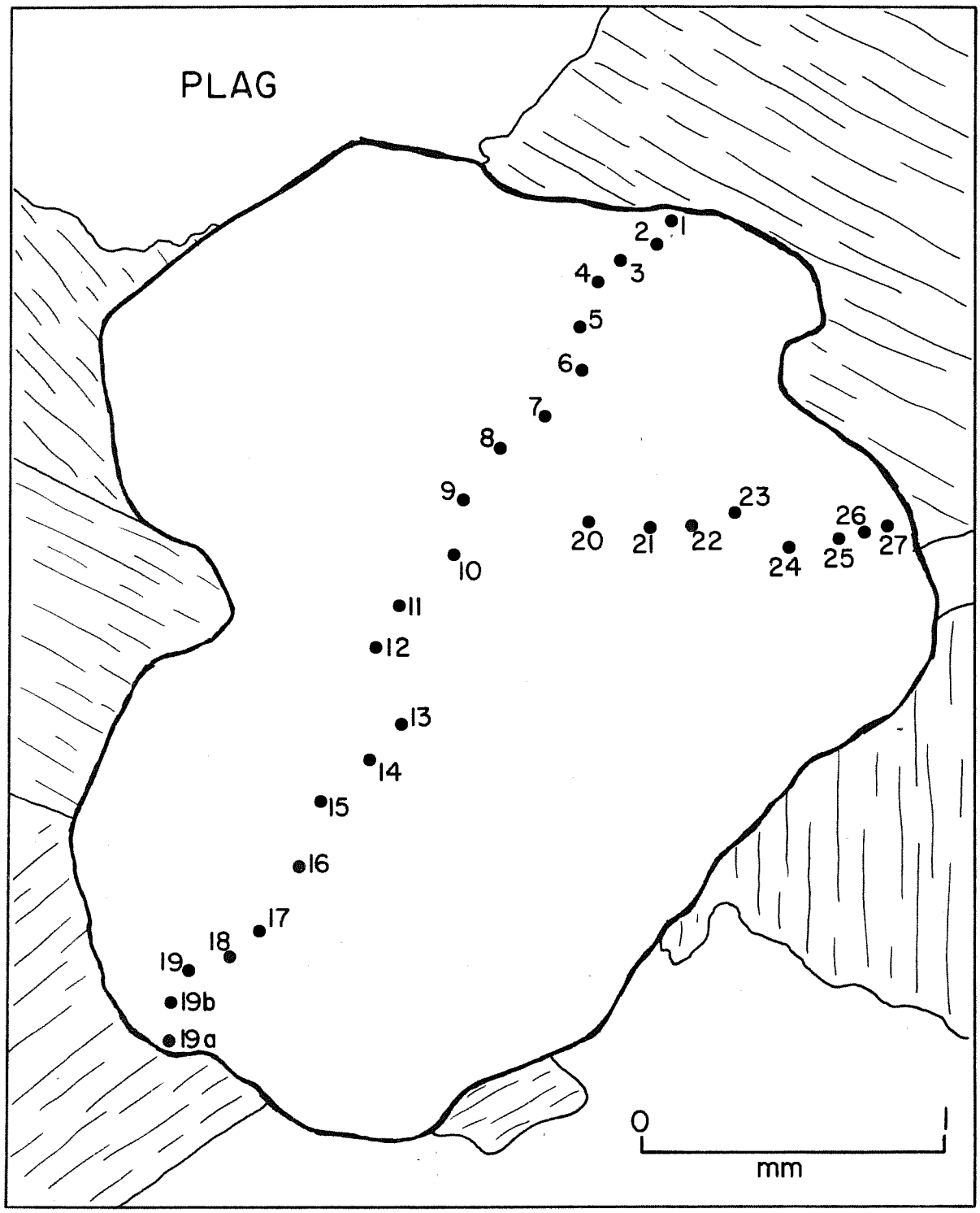

Fig. A-2. Sketch of garnet from 933B. Spots are locations of microprobe analyses tabulated in Table A-2. Analyses 1 to 19a constitute the profile shown in Fig. 10.

TABLE A-1. MICROPROBE ANALYSES OF GARNET PROFILE, SAMPLE T12A.

	1	2	3	4	5	6	7	8
SiO_2	36.97	37.59	37.26	37.38	37.51	37.49	37.13	37.28
TiO_2	.12	.11	.16	.08	.12	.09	.09	.09
Al_2O_3	20.16	21.12	20.68	20.67	20.55	20.05	20.53	20.18
Cr_2O_3	.08	.06	.13	.08	.09	.09	.05	.10
FeO	35.32	35.45	34.32	33.92	33.98	33.83	33.86	33.78
MnO	1.79	1.72	1.60	1.57	1.52	1.41	1.46	1.57
MgO	3.22	3.27	3.71	4.30	4.30	4.22	4.42	4.38
CaO	1.07	1.04	1.10	1.23	1.33	1.38	1.22	1.29
BaO	.11	.13	.10	.10	.12	.11	.10	.11
Na_2O	.00	.00	.10	.00	.00	.00	.00	.00
K_2O	.02	.03	.02	.03	.04	.02	.02	.01
Total	98.86	100.51	99.18	99.36	99.54	98.69	98.88	98.78
Formulas based on 12 oxygens								
Si	3.016	3.008	3.013	3.010	3.016	3.039	3.005	3.022
Al								
	3.016	3.008	3.013	3.010	3.016	3.039	3.005	3.022
Al	1.938	1.990	1.971	1.962	1.948	1.916	1.959	1.928
Ti	.004	.004	.010	.005	.007	.004	.005	.005
Cr	.003	.002	.008	.005	.006	.004	.003	.006
	1.945	1.996	1.989	1.972	1.961	1.924	1.967	1.939
Fe	2.409	2.372	2.321	2.285	2.285	2.294	2.292	2.290
Mn	.122	.116	.110	.107	.104	.094	.100	.108
Mg	.390	.390	.447	.516	.515	.508	.533	.529
Ca	.093	.087	.095	.106	.115	.118	.106	.112
Ba	.001	.001	.003	.003	.004	.001	.003	.003
Na	.000	.000	.016	.000	.000	.000	.000	.000
K	.001	.001	.002	.003	.004	.000	.002	.001
	3.016	2.967	2.994	3.020	3.027	3.015	3.036	3.043
Alm	79.9	80.0	78.1	75.8	75.7	76.1	75.6	75.4
Py	12.9	13.2	15.0	17.1	17.1	16.9	17.6	17.4
Gr	3.1	2.9	3.2	3.5	3.8	3.9	3.5	3.6
Sp	4.1	3.9	3.7	3.6	3.4	3.1	3.3	3.6

9	10	11	12	13	14	15	16	17	18
37.23	37.42	37.44	37.86	37.43	37.33	37.28	37.23	37.38	37.64
.12	.09	.12	.09	.13	.10	.12	.06	.14	.11
20.50	20.47	20.55	20.52	20.36	20.32	21.08	20.79	20.51	21.33
.04	.13	.09	.07	.04	.06	.08	.09	.10	.08
33.63	33.68	33.41	33.88	33.65	34.19	34.05	35.16	33.88	34.05
1.45	1.43	1.44	1.38	1.50	1.53	1.59	1.63	1.39	1.47
4.13	4.18	4.08	4.16	4.19	4.30	3.79	3.54	4.26	3.80
1.26	1.27	1.35	1.21	1.09	1.00	1.03	1.00	1.32	1.29
.11	.07	.17	.12	.09	.12	.09	.06	.10	.07
.00	.00	.00	.00	.00	.00	.00	.02	.00	.10
.02	.02	.02	.00	.02	.02	.04	.03	.03	.02
98.51	98.75	98.68	99.29	98.50	98.96	99.16	99.60	99.11	99.96
3.021	3.027	3.030	3.044	3.035	3.022	3.007	3.006	3.017	3.010
3.021	3.027	3.030	3.044	3.035	3.022	3.007	3.006	3.017	3.010
1.961	1.952	1.961	1.945	1.946	1.939	2.005	1.979	1.951	2.008
.007	.005	.007	.005	.008	.006	.007	.004	.008	.004
.003	.008	.006	.004	.003	.004	.005	.006	.006	.004
1.971	1.965	1.974	1.954	1.957	1.949	2.017	1.989	1.965	2.016
2.283	2.279	2.261	2.278	2.282	2.315	2.297	2.374	2.287	2.276
.100	.098	.099	.094	.103	.105	.109	.111	.095	.098
.500	.504	.492	.498	.506	.519	.456	.426	.512	.450
.110	.110	.117	.104	.095	.087	.089	.087	.114	.110
.003	.002	.002	.004	.003	.004	.003	.002	.003	.000
.000	.000	.000	.000	.000	.000	.000	.003	.000	.000
.002	.002	.002	.000	.002	.002	.004	.003	.003	.001
2.998	2.995	2.976	2.978	2.991	3.032	2.958	3.006	3.014	2.935
76.3	76.2	76.2	76.6	76.4	76.5	77.8	79.2	76.0	77.6
16.7	16.8	16.6	16.7	16.9	17.1	15.5	14.2	17.0	15.3
3.7	3.7	3.9	3.5	3.3	2.9	3.0	2.9	3.8	3.7
3.3	3.3	3.3	3.2	3.4	3.5	3.7	3.7	3.2	3.4

TABLE A-2. MICROPROBE ANALYSES OF GARNET PROFILE, SAMPLE 933B.

	1	2	3	4	5	6	7	8
SiO_2	35.92	35.64	35.78	35.92	35.85	36.18	36.77	38.70
TiO_2	.01	.02	.04	.04	.04	.00	.01	.00
Al_2O_3	21.14	21.23	21.72	21.75	21.64	22.10	21.70	21.30
Cr_2O_3	.00	.00	.00	.04	.00	.00	.00	.04
FeO	33.97	33.50	33.57	33.32	33.27	32.40	32.59	32.98
MnO	3.25	2.58	2.34	2.34	2.19	2.08	1.98	2.10
MgO	3.00	3.80	4.14	4.25	4.54	4.66	4.54	4.57
CaO	1.29	1.35	1.31	1.34	1.39	1.50	1.55	1.55
BaO	.05	.03	.00	.05	.05	.03	.02	.01
Na_2O	.05	.00	.00	.03	.00	.00	.02	.12
K_2O	.00	.00	.00	.00	.00	.00	.00	.00
Total	98.68	98.25	98.90	99.10	99.10	98.95	99.18	101.37
Formulas based on 12 oxygens								
Si	2.945	2.924	2.906	2.908	2.901	2.916	2.955	3.034
Al	.055	.076	.094	.092	.099	.084	.045	
	3.000	3.000	3.000	3.000	3.000	3.000	3.000	3.034
Al	1.987	1.986	1.985	1.982	1.966	2.016	2.011	1.967
Ti	.000	.000	.002	.002	.002	.000	.001	.000
Cr	.000	.000	.000	.002	.000	.000	.000	.000
	1.987	1.986	1.987	1.986	1.968	2.016	2.012	1.967
Fe	2.329	2.298	2.279	2.254	2.252	2.184	2.190	2.162
Mn	.224	.178	.160	.159	.149	.142	.135	.138
Mg	.366	.462	.500	.513	.546	.560	.544	.534
Ca	.113	.118	.112	.116	.119	.130	.133	.128
Ba	.000	.000	.000	.000	.000	.000	.000	.000
Na	.007	.000	.000	.004	.000	.000	.003	.018
K	.000	.000	.000	.000	.000	.000	.000	.000
	3.039	3.056	3.051	3.046	3.066	3.016	3.005	2.980
Alm	76.8	75.2	74.7	74.1	73.4	72.4	73.0	73.0
Py	12.1	15.1	16.4	16.9	17.8	18.6	18.1	18.0
Gr	3.7	3.9	3.7	3.8	3.9	4.3	4.4	4.3
Sp	7.4	5.8	5.2	5.2	4.9	4.7	4.5	4.7

9	10	11	12	13	14	15	16	17
38.34	39.06	38.56	38.31	38.74	38.56	38.28	38.21	38.41
.00	.00	.02	.00	.00	.02	.01	.03	.00
20.84	20.16	20.93	20.95	20.30	20.65	20.46	20.45	20.87
.00	.01	.02	.00	.00	.00	.01	.00	.00
32.29	32.80	33.26	33.09	33.17	32.86	32.46	33.28	33.52
1.91	2.03	2.10	2.05	2.07	2.09	2.04	2.15	2.18
4.47	4.42	4.56	4.13	4.18	4.32	4.33	4.14	4.09
1.49	1.54	1.50	1.48	1.43	1.49	1.40	1.39	1.32
.00	.00	.03	.02	.00	.00	.03	.00	.04
.00	.00	.00	.00	.00	.00	.00	.15	.00
.00	.00	.00	.00	.00	.00	.00	.00	.00
99.35	100.02	100.96	100.03	99.90	99.99	99.02	99.80	100.44
3.057	3.099	3.042	3.044	3.085	3.065	3.070	3.056	3.048
3.057	3.099	3.042	3.044	3.085	3.065	3.070	3.056	3.048
1.959	1.884	1.945	1.962	1.905	1.934	1.935	1.927	1.951
.000	.000	.000	.000	.000	.000	.000	.000	.000
.000	.000	.000	.000	.000	.000	.000	.000	.000
1.959	1.884	1.945	1.962	1.905	1.934	1.935	1.927	1.951
2.153	2.177	2.193	2.200	2.208	2.184	2.178	2.225	2.224
.128	.135	.139	.137	.138	.140	.136	.146	.146
.531	.521	.535	.487	.495	.511	.515	.493	.482
.126	.130	.125	.126	.121	.126	.120	.117	.111
.000	.000	.000	.000	.000	.000	.000	.000	.000
.000	.000	.000	.000	.000	.000	.000	.023	.000
.000	.000	.000	.000	.000	.000	.000	.000	.000
2.938	2.963	2.992	2.950	2.962	2.961	2.949	3.004	2.963
73.2	73.5	73.3	74.6	74.5	73.8	73.8	74.7	75.1
18.1	17.6	17.9	16.5	16.7	17.2	17.5	16.5	16.3
4.3	4.3	4.2	4.3	4.1	4.3	4.1	3.9	3.7
4.4	4.6	4.6	4.6	4.7	4.7	4.6	4.9	4.9

TABLE A-2. MICROPROBE ANALYSES OF GARNET PROFILE, SAMPLE 933B (Continued)

	18	19	19a	19b	20	21	22	23
SiO_2	37.46	37.11	36.92	37.24	37.77	38.32	38.58	38.68
TiO_2	.00	.04	.03	.00	.00	.07	.11	.12
Al_2O_3	20.29	20.46	20.39	20.79	20.91	20.25	20.39	20.24
Cr_2O_3	.06	.00	.04	.04	.03	.00	.02	.00
FeO	33.36	33.00	34.23	33.75	32.74	32.79	32.89	32.88
MnO	2.38	2.33	3.05	2.82	1.96	1.97	2.01	2.10
MgO	4.25	3.79	3.05	3.56	4.00	4.30	4.05	4.18
CaO	1.30	1.21	1.18	1.17	1.38	1.29	1.24	1.20
BaO	.00	.00	.03	.00	.03	.00	.00	.00
Na_2O	.00	.00	.00	.00	.02	.00	.09	.03
K_2O	.00	.00	.00	.00	.00	.00	.00	.00
Total	99.10	97.95	98.91	99.37	98.83	98.99	99.39	99.43
Formulas based on 12 oxygens								
Si	3.025	3.028	3.014	3.007	3.041	3.077	3.083	3.089
Al								
	3.025	3.028	3.014	3.007	3.041	3.077	3.083	3.089
Al	1.932	1.965	1.960	1.979	1.984	1.916	1.922	1.905
Ti	.000	.002	.000	.000	.000	.002	.004	.007
Cr	.002	.000	.002	.002	.002	.000	.000	.000
	1.934	1.967	1.962	1.981	1.986	1.918	1.926	1.912
Fe	2.252	2.250	2.336	2.280	2.204	2.200	2.199	2.196
Mn	.161	.160	.208	.192	.134	.132	.136	.140
Mg	.512	.459	.371	.426	.480	.513	.481	.497
Ca	.111	.105	.101	.099	.119	.110	.105	.101
Ba	.000	.000	.000	.000	.000	.000	.000	.000
Na	.000	.000	.000	.000	.003	.000	.012	.004
K	.000	.000	.000	.000	.000	.000	.000	.000
	3.036	2.974	3.016	2.997	2.940	2.955	2.933	2.938
Alm	74.2	75.7	77.4	76.1	75.0	74.4	75.2	74.8
Py	16.9	15.4	12.3	14.2	16.3	17.4	16.4	16.9
Gr	3.6	3.5	3.4	3.3	4.1	3.7	3.7	3.5
Sp	5.3	5.4	6.9	6.4	4.6	4.5	4.7	4.8

24	25	26	27
38.27	37.57	37.90	38.00
.06	.07	.09	.11
20.19	20.23	20.61	20.21
.00	.00	.00	.00
32.97	33.16	33.43	33.57
2.13	2.34	2.47	2.92
3.74	3.65	3.44	2.94
1.16	1.20	1.09	1.07
.00	.00	.00	.00
.11	.12	.12	.05
.00	.00	.00	.00
98.63	98.34	99.13	98.88
3.089	3.053	3.056	3.080
3.089	3.053	3.056	3.080
1.919	1.937	1.959	1.931
.002	.002	.005	.007
.000	.000	.000	.000
1.921	1.939	1.964	1.938
2.225	2.254	2.254	2.276
.144	.160	.169	.201
.450	.441	.413	.355
.099	.103	.094	.093
.000	.000	.000	.000
.016	.019	.019	.008
.000	.000	.000	.000
2.934	2.977	2.949	2.933
76.2	76.2	76.2	77.8
15.4	14.9	14.0	12.1
3.5	3.5	3.2	3.2
4.9	5.4	5.6	6.9

Tracy, R.J., 1975, High grade metamorphic reactions and partial melting in pelitic schist, Quabbin Reservoir area, Massachusetts: Contrib. No. 20, Geology Dept., Univ. of Mass.

Errata:

p. 63 (Muscovite-Biotite Element Fractionation)

It is necessary to make the approximation that all the Fe and Mg in muscovite occurs as celadonite substitution (see section on Muscovite) and that it is legitimate to ignore the octahedral aluminum content of biotite in postulating an exchange reaction. The exchange reaction for Fe-Mg distribution is therefore written:

$$3\ KAlFe^{2+}Si_4O_{10}(OH)_2 + KMg_3AlSi_3O_{10}(OH)_2 =$$

(Fe-Celadonite) (Phlogopite)

$$3KAlMgSi_4O_{10}(OH)_2 + KFe_3^{2+}AlSi_3O_{10}(OH)_2$$

(Mg-Celadonite) (Annite)

The expression for the equilibrium distribution coefficient for iron and magnesium between the two phases is:

$$K_{D\ Mg\text{-}Fe}^{Mus\text{-}Bio} = \frac{\left(a_{Mg}^{Mus}\right)^3 \cdot \left(a_{Fe}^{Bio}\right)^3}{\left(a_{Fe}^{Mus}\right)^3 \cdot \left(a_{Mg}^{Bio}\right)^3}.$$

Assuming ideal solution behavior, this is rewritten:

$$K_{D\ Mg\text{-}Fe}^{Mus\text{-}Bio} = \frac{\left(X_{Mg}^{Mus}\right)^3 \cdot \left(X_{Fe}^{Bio}\right)^3}{\left(X_{Fe}^{Mus}\right)^3 \cdot \left(X_{Mg}^{Bio}\right)^3}.$$

p. 68 (Garnet-Biotite Element Fractionation)

Exchange reaction:

$$Fe_3Al_2Si_3O_{12} + KMg_3AlSi_3O_{10}(OH)_2 = Mg_3Al_2Si_3O_{12} + KFe_3AlSi_3O_{10}(OH)_2$$

(Almandine) (Phlogopite) (Pyrope) (Annite)

The equilibrium distribution of Fe and Mg is given by:

$$K_{D\ Mg\text{-}Fe}^{Gar\text{-}Bio} = \frac{\left(a_{Mg}^{Gar}\right)^3 \cdot \left(a_{Fe}^{Bio}\right)^3}{\left(a_{Fe}^{Gar}\right)^3 \cdot \left(a_{Mg}^{Bio}\right)^3},$$

with minor occupants of garnet and biotite exchange sites ignored in this treatment. The expression for K_D is rewritten:

$$K_{D\ Mg\text{-}Fe}^{Gar\text{-}Bio} = \frac{\left(X_{Mg}^{Gar}\right)^3 \cdot \left(X_{Fe}^{Bio}\right)^3}{\left(X_{Fe}^{Gar}\right)^3 \cdot \left(X_{Mg}^{Bio}\right)^3}.$$

TABLE 13. MUSCOVITE-BIOTITE Fe-Mg FRACTIONATION. (CORRECTED)

Sample		X_{Fe}	X_{Mg}	X_{Fe}/X_{Mg}	K_D Mus-Bio * Mg-Fe
C67	Mus	.535	.465	1.151	.874
	Bio	.571	.429	1.331	
890	Mus	.447	.553	.808	2.023
	Bio	.514	.486	1.057	
892U	Mus	.493	.507	.972	1.193
	Bio	.523	.477	1.096	
853A	Mus	.397	.603	.658	2.941
	Bio	.457	.543	.842	
849A	Mus	.354	.646	.548	3.889
	Bio	.388	.612	.634	
869	Mus	.504	.496	1.016	1.016
	Bio	.518	.482	1.075	
871	Mus	.500	.500	1.000	1.232
	Bio	.551	.449	1.227	
C26	Mus	.511	.489	1.045	.923
	Bio	.513	.487	1.053	
595C	Mus	.420	.580	.724	2.333
	Bio	.467	.533	.876	
B35	Mus	.396	.604	.656	3.375
	Bio	.491	.509	.965	
M34	Mus	.483	.517	.934	1.540
	Bio	.560	.440	1.273	

*Calculated using ideal mica stoichiometry.